049279

JPRS-CST-85-040

20 November 1985

# China Report

## SCIENCE AND TECHNOLOGY



FBIS FOREIGN BROADCAST INFORMATION SERVICE



2
103
AØ6

## NOTE

JPRS publications contain information primarily from foreign newspapers, periodicals and books, but also from news agency transmissions and broadcasts. Materials from foreign-language sources are translated; those from English-language sources are transcribed or reprinted, with the original phrasing and other characteristics retained.

Headlines, editorial reports, and material enclosed in brackets [] are supplied by JPRS. Processing indicators such as [Text] or [Excerpt] in the first line of each item, or following the last line of a brief, indicate how the original information was processed. Where no processing indicator is given, the information was summarized or extracted.

Unfamiliar names rendered phonetically or transliterated are enclosed in parentheses. Words or names preceded by a question mark and enclosed in parentheses were not clear in the original but have been supplied as appropriate in context. Other unattributed parenthetical notes within the body of an item originate with the source. Times within items are as given by source.

The contents of this publication in no way represent the policies, views or attitudes of the U.S. Government.

## PROCUREMENT OF PUBLICATIONS

JPRS publications may be ordered from the National Technical Information Service, Springfield, Virginia 22161. In ordering, it is recommended that the JPRS number, title, date and author, if applicable, of publication be cited.

Current JPRS publications are announced in Government Reports Announcements issued semi-monthly by the National Technical Information Service, and are listed in the Monthly Catalog of U.S. Government Publications issued by the Superintendent of Documents, U.S. Government Printing Office, Washington, D.C. 20402.

Correspondence pertaining to matters other than procurement may be addressed to Joint Publications Research Service, 1000 North Glebe Road, Arlington, Virginia 22201.

JPRS-CST-85-040

20 November 1985

# CHINA REPORT

## SCIENCE AND TECHNOLOGY

## CONTENTS

PEOPLE'S REPUBLIC OF CHINA

## FIRST BATCH OF CHINESE PATENTS TO BE ANNOUNCED IN SEPTEMBER

Tianjin JISHU SHICHANG BAO [TECHNOLOGY MARKET WEEKLY] in Chinese 3 Sep 85 p 1

[Article by special-assignment reporter Shen Jiajian [3947 0857 1670]: "The First Batch of Chinese Patents Will be Announced Within the Month; After the Inventions are Announced They Will Enter the Objection Stage and Receive Temporary Legal Protection, with Uncompensated Use Not Permitted."

[Text] Director of the Chinese Patent Bureau Huang Kunyi [7806 0981 4135] announced at the recently assembled first national patent documentation conference that the first batch of Chinese patents would be announced in September, to let the public carry out discussion (the period for objections being 3 months), and that more patents would be announced each month. The implementation of our country's patent law will enter a new stage. Huang Kunyi said the major work of this stage is to announce how to treat the objection process and the openness under legal protection. The objection process is an examination by the masses, weighing the inventions on the scales of international standards, so that only the inventions that really pass will be approved. Moreover, the public should know that the openness under legal protection is different from the former openness without legal protection. The temporary legal protection begins from the day of announcement, so no announced invention may be used without compensation. This sort of common knowledge must be well proclaimed from the standpoint of both law and morality.

The first batch of patents announced will be approved in December after going through mass discussion.

13044/12899
CSO: 4008/2001

NATIONAL DEVELOPMENTS

## CAS PATENT INSTITUTE OPENS TO OUTSIDERS

Beijing BEIJING KEJIBAO [BEIJING S&T WEEKLY] in Chinese 26 Aug 85 p 1

[Article by staff reporter Hao Meifang [6727 2734 3364]: "China Academy of Sciences Patent Institute Begins External Operations"]

[Text] The China Academy of Sciences (CAS) Patent Institute officially began external operations on 16 August at CAS and at (Kehai Gongsi) in Zhongguan Cun in Haidian District of Beijing.

This patent institute is composed of patent representatives and patent workers from each of the CAS institutes in the Beijing area. The great majority of them come from the first line of scientific research, a contingent with a broad coverage of topics and specialties, able to enter the ranks of those who engage in patent representation in patent and economic legal matters.

Since March of this year, the patent institute has on the one hand been using all forms of activities to enter government offices, research institutes and laboratories to publicize the meaning of the patent system established by our country, procedures for applying for patents, the method of selecting documents and conducting patent searches; they have also compiled all kinds of patent materials to introduce to scientific research personnel trade knowledge related to patents and patent permissions. On the other hand, they have actively helped CAS's own inventors handle applications, so that when the Chinese Patent Law took effect on 1 April, 78 applications were made to the Patent Bureau through them, making up about 2 percent of the whole country's applications in the same period.

At present, the patent institute cannot only take on patent representation and patent legal work for work units and individuals in the academy, but also fully possesses all the requirements for serving inventors from all segments of the public with application and consultation services. President of the CAS Lu Jiaxi [4151 0857 6932], CAS Secretary General Gu Yijian [7357 0110 0256], Patent Bureau Director Shen Yaozeng [3088 1031 2582], officials of various relevant ministries and commissions of the State Council, and comrades from the China Trade Promotion Association and the Beijing Patent Administration Bureau attended the opening ceremony.

13044/12899
CSO: 4008/2001

## SYSTEM OF ENGAGING S&T PERSONNEL DISCUSSED

Beijing BEIJING KEJIBAO [BEIJING S&T WEEKLY] in Chinese 2 Sep 85 p 1

[Article by staff reporter Zhi Qiang [1807 1730]: "The State Science and Technology Commission's Science and Technology Cadre Bureau's Responsible Person Indicated That Arranging the Implementation of the Appointment System for Personnel Must Be Cautiously Undertaken"]

[Text] Not long ago, at the seminar on the "appointment" work system for S&T assembled by the State Science and Technology Commission, a responsible person from the Science and Technology Cadre Bureau stressed that implementing the appointment system must be cautiously undertaken with reference to the problems of others and must be based on the positive effect of transferring each category of personnel.

The responsible person from the Science and Technology Cadre Bureau of the State Science and Technology Commission said to use a lifelong appointment system for those few famous experts with a reputation for good character and deep academic contributions, who are well known at home and abroad. For other experts suited to a retirement leave, carry out a retirement leave system. Those who are still healthy after retirement who can persist in work can, under conditions they agree to, continue fulfilling their function, ensuring that they will not only have something to rely on in their old age, but also something to do in old age, and something to delight in in old age. This embodies the spirit of honoring the old and respecting the wise, and is able to make even more middle-aged and young S&T personnel become academic leaders, or to be appointed to higher positions better suited to them.

This responsible person continued by saying that personnel who have not yet been appointed must be correctly treated and their appointments appropriately arranged. First they must have a correct understanding that they are mostly useful talents, not a burden, and at the same time conditions must be created to arrange for them to enter posts in which they are more able to fulfill their function. Secondly, the purpose of transferring personnel is to better fulfill the function of personnel and to adjust for surpluses and shortages, which is a direction of reform for the personnel system, and the outmoded idea must be destroyed that being transferred to another post in the same or a different work unit is a sign of "making a mistake" or "losing face." According to our understanding,

the personnel sent out from high-level schools, research institutes, or hospitals are science and technology personnel of above median ability, and not a few of them become backbones of the organization in their new posts, and some enter the leading echelons, fulfilling an even greater function than in the original work unit.

The responsible person of the Science and Technology Cadre Bureau of the State Science and Technology Commission also indicated that for individuals who had not performed well and who had not been appointed and were difficult to transfer, there should, based on their educational level, be assistance for their transfers supplemented by necessary administrative and economic measures. Some work units are strict in regard to these administrative and economic measures, some are lenient. We think that since it is all based on reeducation, using these methods is necessary, but they must be suitable. The Shenyang Metals Institute of the Chinese Academy of Sciences's method is to withhold 1 percent of the salary every month, which puts a certain pressure on a person, without intensifying contradictions. This method is worthy of study.

13044/12899
CSO: 4008/2001

NATIONAL DEVELOPMENTS

## FUJIAN SCIENCE AND TECHNOLOGY DEVELOPMENT PLAN DISCUSSED

Fuzhou FUJIAN RIBAO in Chinese 26 Aug 85 p 1

[Article by staff reporter Chen Minzhen [7115 2404 4176]: "To Work Out a Provincial Science and Technology Development Plan with Special Characteristics, Almost 100 Famous Experts and Professors Assembled in Fuzhou"]

[Text] From 21-23 August, almost 100 famous experts and professors from our province assembled at the Xihu Hotel in Fuxhou to discuss the question of provincial scientific and technological development strategy.

They mentioned that our province is located in the subtropics, has the advantages of "mountains, sea, overseas Chinese, and Special Economic Zones," and should work out a S&T development plan with the province's special characteristics. S&T and the economy are inseparably joined, and when the S&T development plan is worked out it should be adapted to economic development. They hoped to form leading "locomotive" industries among the numerous industries, and suggested placing the biotechnology, petrochemical, electronics, and new-materials industries in the leading position, to form a special characteristic of "having it when others lack it, and having it in superior form when others have it." Some suggested using Xiamen's advantages in oceanographic research to organize the 10-odd research units and schools together to begin comprehensive oceanographic development.

The provincial leaders Xiang Nan [7309 0589], Jia Qinglin [6328 1987 2651], and Cai Ninglin [5591 1337 2651] came to the meeting to hear the suggestions given by everyone for "locomotive" industries in our province's S&T development plan.

This project was begun last year under the leadership of the leaders' task force for provincial S&T planning. They divided into 24 specialized groups and organized the participation of more than 1,100 famous experts and scholars in discussions and working out plans. They forecast that at the end of this year they will have worked out a medium- and long-term S&T development plan for our province.

13044/12899
CSO: 4008/2001

APPLIED SCIENCES

## MC68000 MONITOR PROGRAM DISASSEMBLED

Chongqing WEIXING JISUANJI [MICROCOMPUTERS] in Chinese No 2, 14 Mar 85 pp 102-107

[Article by Yuan Hongchun [5913 1347 2504], Chengdu Academy of Electronic Communications Engineering: "A Monitor for the MC68000 Single Board Microcomputer"]

[Text] I. Preface

The Chengdu Academy of Electronic Communications Engineering [CAECE] Microcomputer Development and Training Center and the state run Factory 830, on the basis of selling the foreign MC68000 DEC (MC68000 Educational Computer Board) sample materials, have cooperatively developed the successful DJS-0600N 16-bit single board microcomputer, which underwent technical evaluation in early July 1984. It is now being produced in small quantities at Factory 830.

In the process of completing this research work, the author has disassembled and printed out the 16K byte monitor that is burned into the MC68000 DEC EPROM on this single board computer. Based on the program inventory so obtained, he has analyzed the operating processes of the 26 monitor commands in this monitor.

With the DJS-0600N single board computer as background, this paper briefly discusses the important contents of the monitor routines.

The author feels that if we are to further study and analyze microcomputer monitor programs, or if we hope to utilize or develop in our own work the same ideas in microcomputer software, then this paper can provide a certain amount of help and reference value.

My classmates Su Guoquan and Cheng Dongyang of the CAECE computer department joined in this monitor analysis, doing a great deal of work. I extend my heartfelt appreciation.

Due to my limitations, there will be certain errors and deficiencies, for which I ask instruction from my readers.

## II. Overview of the DJS-0600N

### 2.1 Important Technical Characteristics

The DJS-0600N single board microcomputer has at its core the MC68000 microprocessor chip, which with other LSI devices is packaged on a 30 cm x 24 cm two-sided printed circuit board.

Chief technical characteristics:

--4 MHz MC68000 16-bit MPU can provide to the user eight 32-bit data and address registers, respectively, a range of 16 megabytes directly addressable, 56 powerful instructions, 5 kinds of operations, and 6 basic types and 14 flexible addressing modes.

--Sixteen 16K bit dynamic RAM's (MCM4116), composing 32K bytes of user memory.

--Two 8K byte EPROM's (MCM68A764) making up 16K bytes of EPROM. The monitor program called "TUTOR" is burned into the EPROM, which can provide monitor, debugging, and assembly/disassembly functions.

--2 RS232C compatible serial input/output ports made up of MC6850ACIA's.

--One 16-bit parallel input/output interface with a 24-bit programmable timer, composed of an MC68230 (PI/T).

--1 audio-frequency tape input/output port.

--Fitted with RESET and ABORT function buttons, making it easier for the user to end a program under abnormal conditions, and to return again to the monitor status.

In use, the user need only connect an external CRT and a DC power source (+5 V, ±12 V) to form a basic system with reasonable capabilities. It is a powerful method and tool for the study and development of MC68000 applications.

### 2.2 Schematics

This schematic shows the main devices used in this single board computer and the logical connections between them.

We point out also at this time that on this single board computer, port No 1 is provided for CRT use. Port No 2 is for modem or mainfrane use. Port No 3 is for a line printer. Port No 4 is then for connecting a recorder to act as a peripheral storage device.

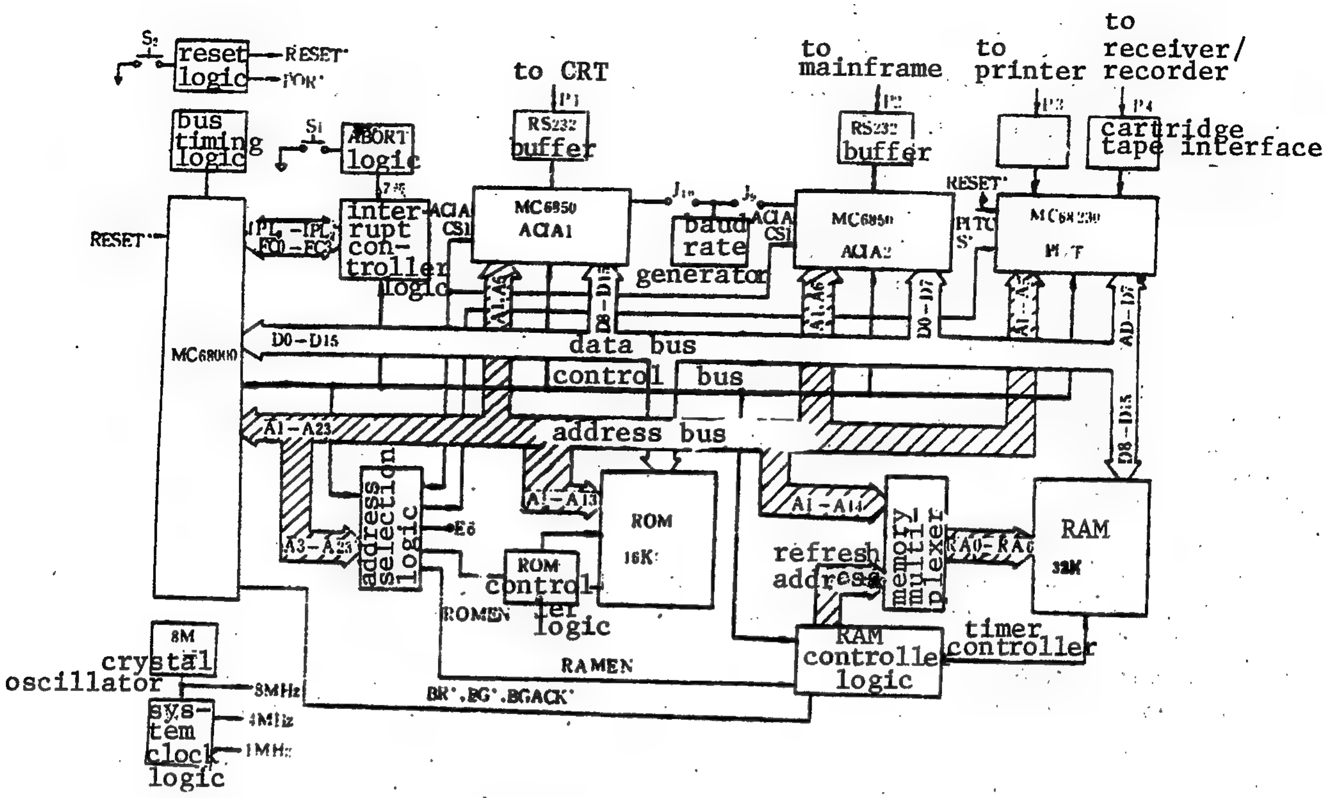


Figure 1.

## 2.3 Storage Area Address Allocation

| Function | | | Address |
|---|---|---|---|
| System storage | Store abnormal vector table | ROM/EPROM | \$000000-\$000007 |
| | | RAM | \$000008-\$0003FF |
| | Monitor program uses scratch area | RAM | \$000400-\$0008FF |
| User storage | | RAM | \$000900-\$007FFF |
| Monitor program (TUTOR) | | | |
| Firmware package | | ROM/EPROM | \$008000-\$00BFFF |
| Unused area | | | \$00C000-\$00FFFF |
| I/O equipment | RI/T parallel interface/timer | | \$010000-\$01003F |
| | $ACIA_2$ (low byte) | | \$010040-\$010043 |
| | and $ACIA_1$ (high byte) | | ↓ \$01FFFF |
| Unused area | | | \$020000-\$02FFFF |
| MC6800 page | | | \$030000-\$03FFFF |
| Unused area | | | \$040000-\$FFFFFF |

III. Monitor Program

This monitor program is called TUTOR, is written in MC68000 mnemonics, and occupies a total of 16K bytes.

TUTOR is chiefly composed of:

1. routines for system initialization
2. routines to enter the monitor
3. main routines to accomplish 26 command functions
4. various subroutines used by the main command routines
5. more than 20 basic common subroutines
6. byte string, byte table, data, working units, etc.
7. assembly routines
8. disassembly routines

Implementation of all routines uses the structured method of calling subroutine during the process of running the main routines, while subroutines themselves can be nested for calling.

The relations between TUTOR and the user are realized by the user typing certain commands on the CRT terminal keyboard. Those commands may be divided into four types:

1. allows user to display or modify memory
2. allows user to display or modify each internal register of the MC68000 MPU
3. allows user to run programs at various levels of control
4. control access to all I/O on the single board computer

There is yet another function in TUTOR, which is the so-called "TRAP14" handling routine. This allows the user's program to call certain subroutines in TUTOR directly.

The operation mode of TUTOR is as shown in the following diagram

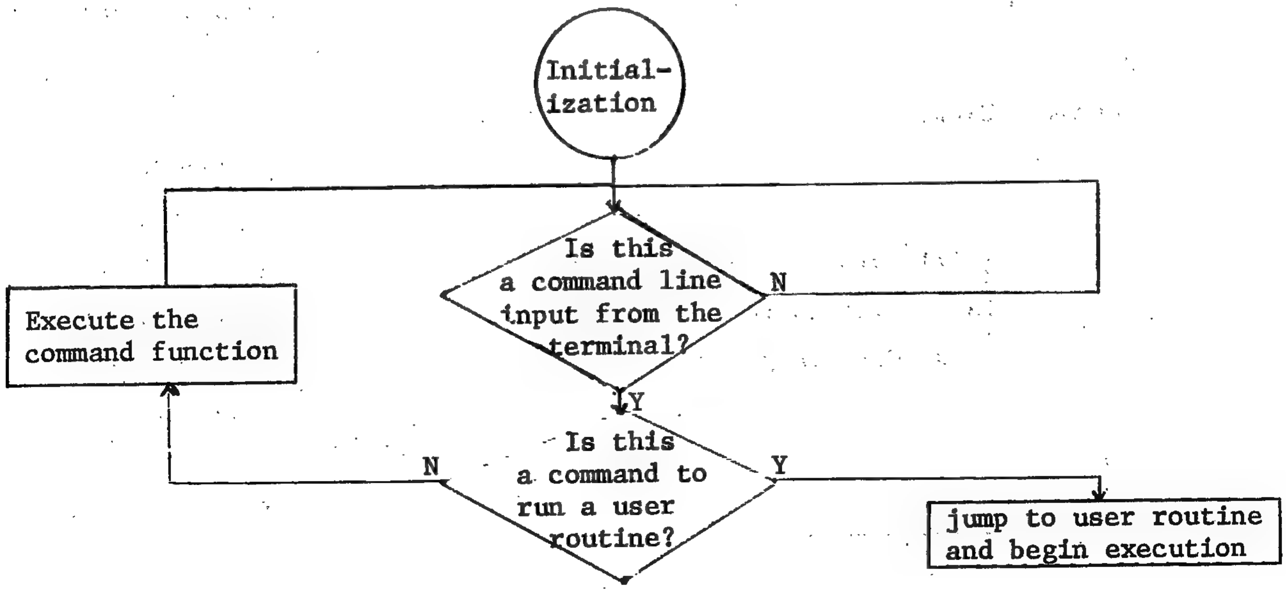

On power up or by pressing the RESET button, the single board computer will begin system initialization. The CPU is reset and the TUTOR program is called. After initialization, the terminal screen will print the following prompt:

TUTOR 1.X>

(where X is the software version number)

It then waits for a response. At this time, the user can then type in any command supported by the firmware package. While the user is still inputting the first line, the standard input subroutines in TUTOR will control the system, and only when a carriage return has been input, indicating completion of the line, will command processing begin.

## 3.1 TUTOR Initialization Routines and Entering the Monitor

When the system has been initialized, the MC68000 microprocessor will automatically fetch the beginning addresses of the system supervisor mode stack pointer and initialization routines from the eight cells from \$8000 to \$8007, and place them in SS and PC, respectively. It then begins execution of the initialization routines.

The routine flowchart is as shown below. Blocks that have addresses to the right indicate subroutines pertaining to that block, which address is then the entering address for the subroutine (the same with the rest).

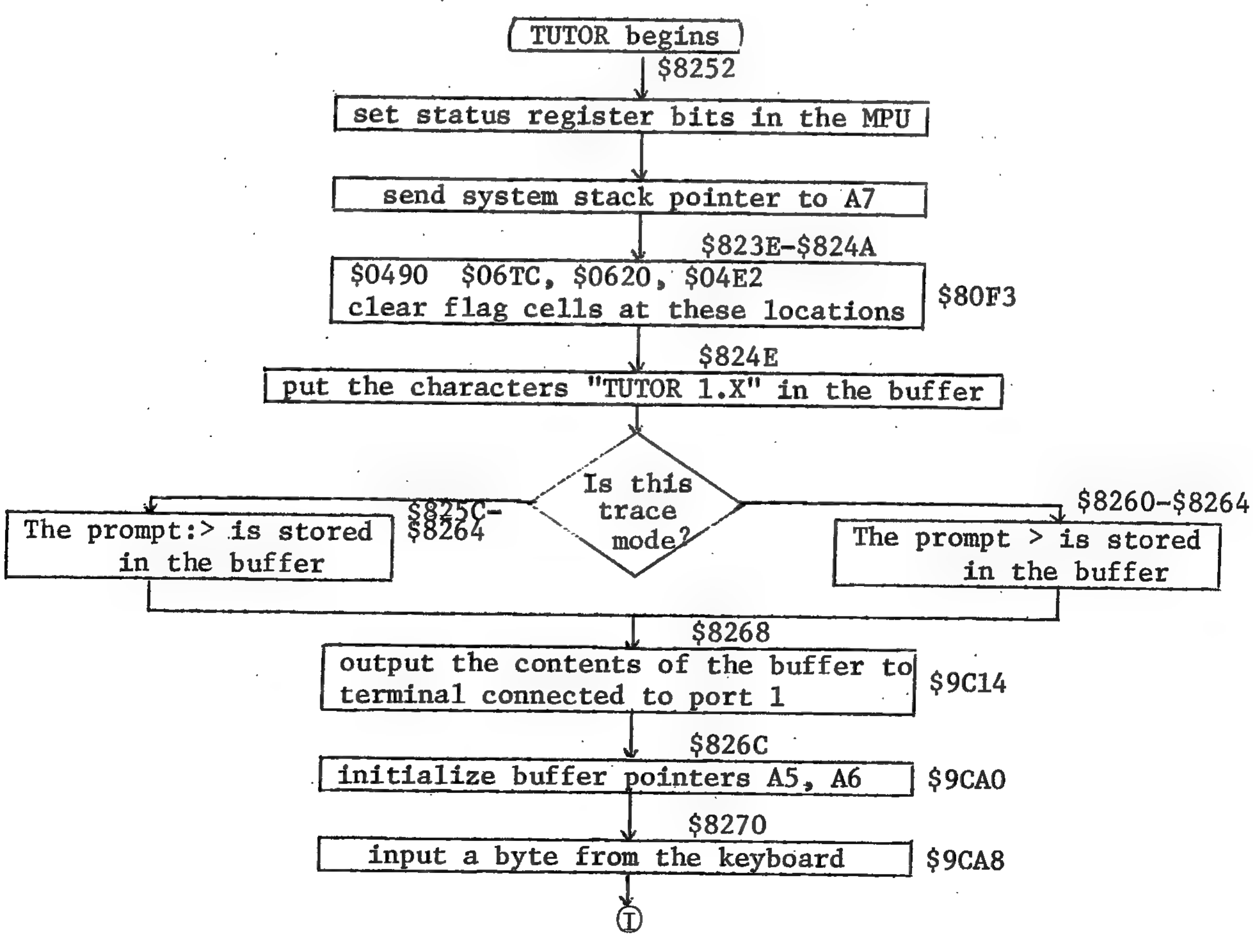


Figure 2.

| Command name | Meaning | Entry point |
|---|---|---|
| BF | memory block fetch | $84E8 |
| BM | block move | $8538 |
| BR | breakpoint set | $8654 |
| BS | block search | $871A |
| BT | block test | $8854 |
| DC | data conversion | $88A6 |
| DF | register group for display formatting | $8904 |
| DU | dump to memory | $8A22 |
| GD | direction execution | $8634 |
| GO | run a program | $8626 |
| GT | run to a breakpoint | $85DA |
| HE | help (display all command names) | $8E84 |
| LO | load | $8FC8 |
| MD | memory display | $9166 |
| MM | modify memory | $931E |
| MS | memory set | $94A2 |
| NOBR | clear breakpoints | $9650 |
| NOPA | printer disable | $A1C2 |
| OF | display offset value | $96C6 |
| PA | printer connect | $A1C6 |
| PF | port mode | $9744 |
| .RX | one register display/edit | $9596 |
| TM | transparent mode | $987A |
| TR | tracing | $858A |
| TT | temporary breakpoint tracing | $85A6 |
| VE | verify | $8FC2 |
| * | send data to port No 2 | |
| .A -.A | display/set address registers | |
| .D -.D | display/set data registers | |
| .R -.R | display/set corresponding shift registers | |
| .PC | display/set program data | |
| .SR | display/set status registers | |
| .SS | display/set sup. stack pointer | |
| .US | display/set user stack pointer | |

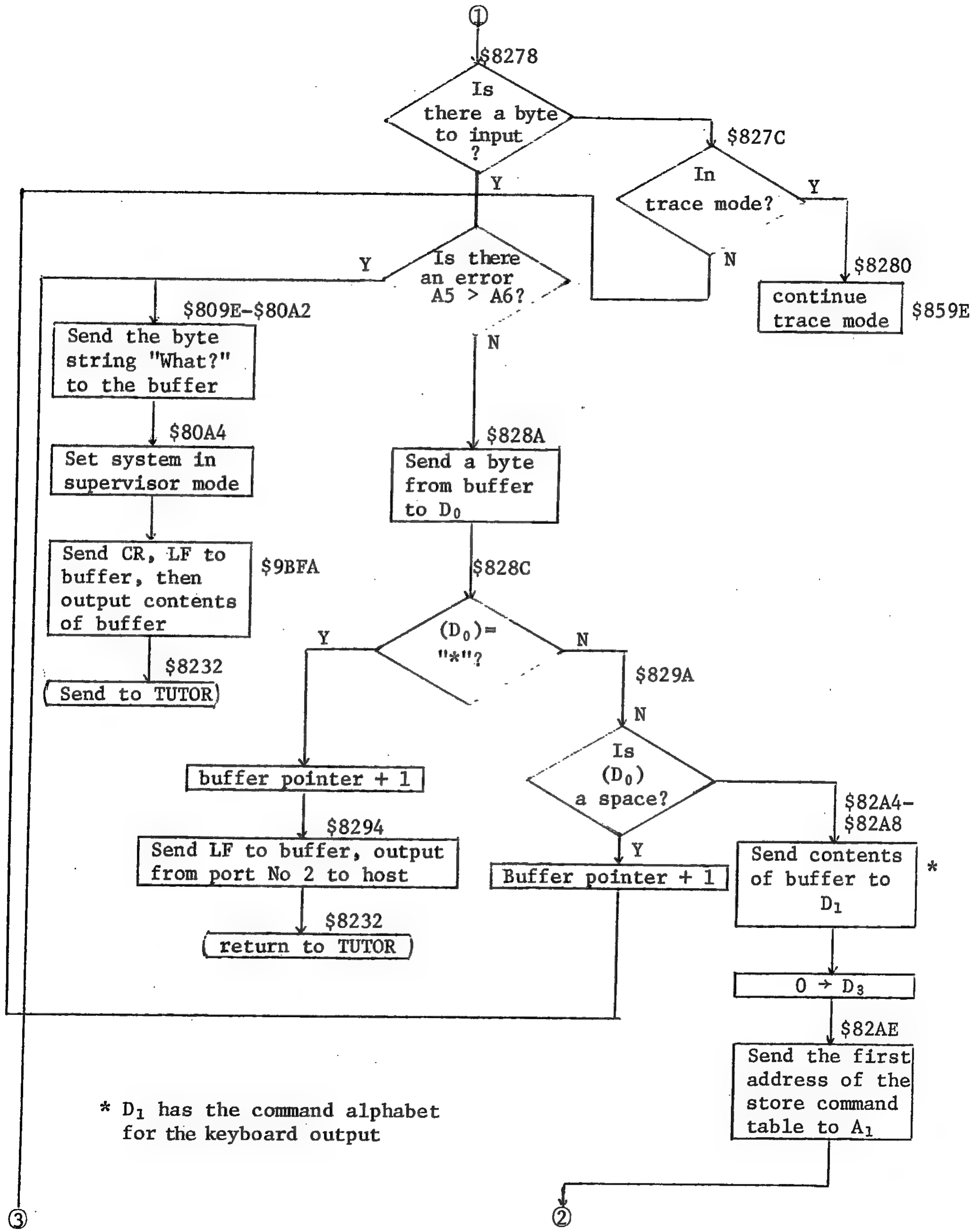

1
$8278
Is there a byte to input ?
Y
$827C
In trace mode?
Y
N
$8280
continue trace mode
$859E
Is there an error A5 > A6?
Y
N
$809E-$80A2
Send the byte string "What?" to the buffer
$80A4
Set system in supervisor mode
Send CR, LF to buffer, then output contents of buffer
$9BFA
$8232
Send to TUTOR
$828A
Send a byte from buffer to D0
$828C
(D0)= "*"?
Y
N
$829A
N
buffer pointer + 1
$8294
Send LF to buffer, output from port No 2 to host
$8232
return to TUTOR
Is (D0) a space?
Y
Buffer pointer + 1
$82A4-$82A8
Send contents of buffer to D1
*
0 → D3
$82AE
Send the first address of the store command table to A1
* D1 has the command alphabet for the keyboard output
3
2


Figure 3

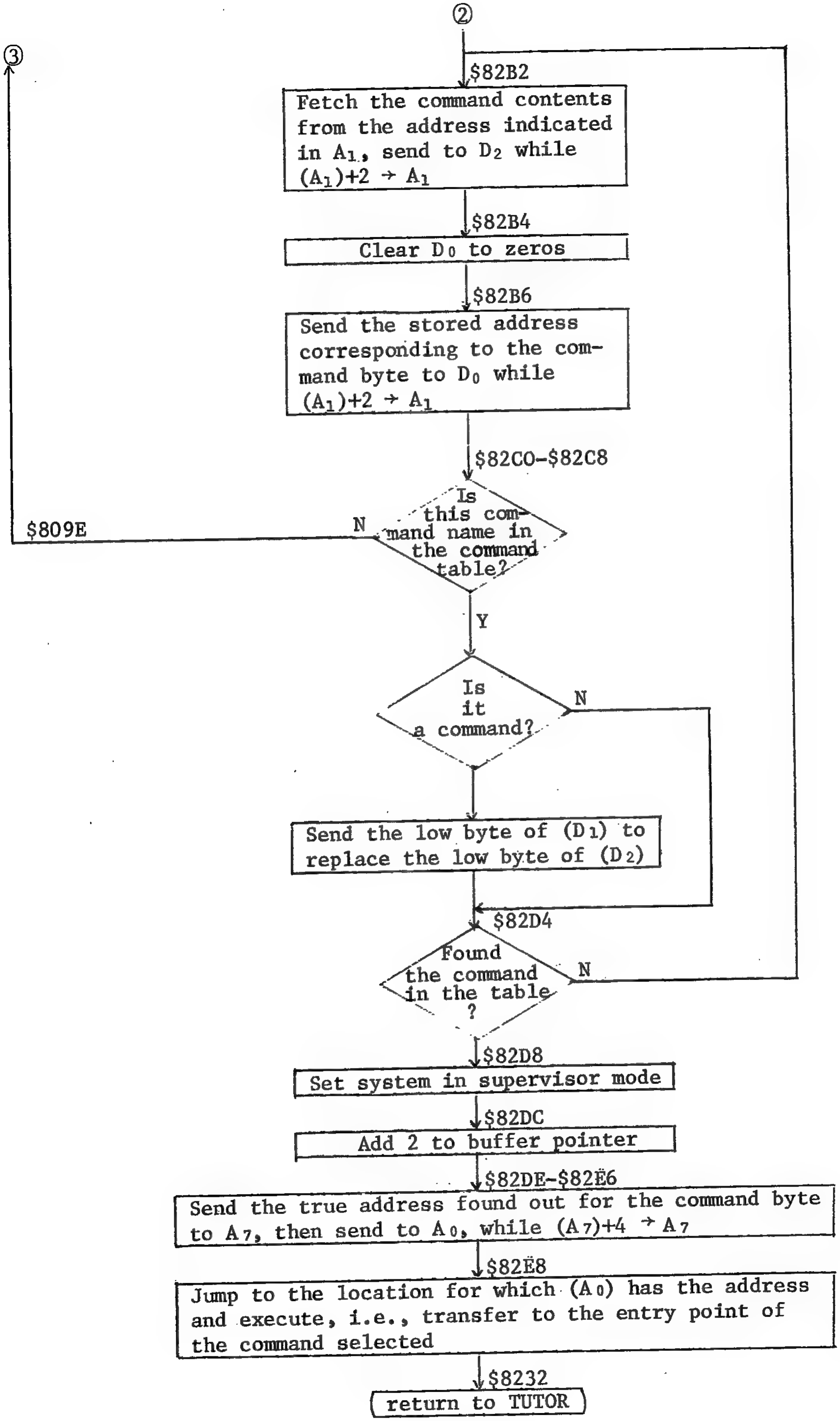
②
③
$82B2
Fetch the command contents from the address indicated in A1, send to D2 while (A1)+2 → A1
$82B4
Clear D0 to zeros
$82B6
Send the stored address corresponding to the command byte to D0 while (A1)+2 → A1
$82C0-$82C8
Is this command name in the command table?
N
$809E
Y
Is it a command?
N
Send the low byte of (D1) to replace the low byte of (D2)
$82D4
Found the command in the table ?
N
$82D8
Set system in supervisor mode
$82DC
Add 2 to buffer pointer
$82DE-$82E6
Send the true address found out for the command byte to A7, then send to A0, while (A7)+4 → A7
$82E8
Jump to the location for which (A0) has the address and execute, i.e., transfer to the entry point of the command selected
$8232
return to TUTOR

Figure 4

In these routines the user input is checked to see what command it is, which depends upon comparing the command input by the user against a command table set up in a section of the program memory. In this section of memory addresses, each four bytes is used by a command. The first two bytes store the command name and the latter two bytes store the difference between the command entry point and the $8000 location. When the user issued command corresponds to one in the command table, the routine jumps to the command entry point and executes the command.

### 3.2 The Names of Monitor Commands and Entry Points

The names and entry points of the TUTOR commands are shown in the table.

The last eight commands in the table, having to do with displaying or setting registers, are not just commands provided with entry points, but are derived from the .RX command.

### 3.3 Analysis and Examples of Monitor Command Routines

We already know that the principle for writing any command routine lies in accomplishing the function belonging to the command, step by step. The underlying design philosophy for this monitor program is the same. In the TUTOR monitor program, the command routine structure uses levels of subroutine nesting, as well as the method of having the main program call subroutines.

Routine flowcharts for two commands have been appended to this article as examples.

#### 3.3.1 The BM (Block Move) Command

The function of this command is to move the contents of a clock of memory to another block.

The instruction syntax is as follows:

    BM <address 1>  <address 2>  <address 3>

where <address 1> is the first address for the source block, <address 2> is the last address of the source block, and <address 3> is the first address of the object block.

#### 3.3.2 The TR (Trace) Command

This command is used to trace instructions during execution.

The command syntax is as follows:

    TR (<counter value>)

The counter value in this command is the number of instructions to trace at one time. If no value is provided with the command, this means that each command

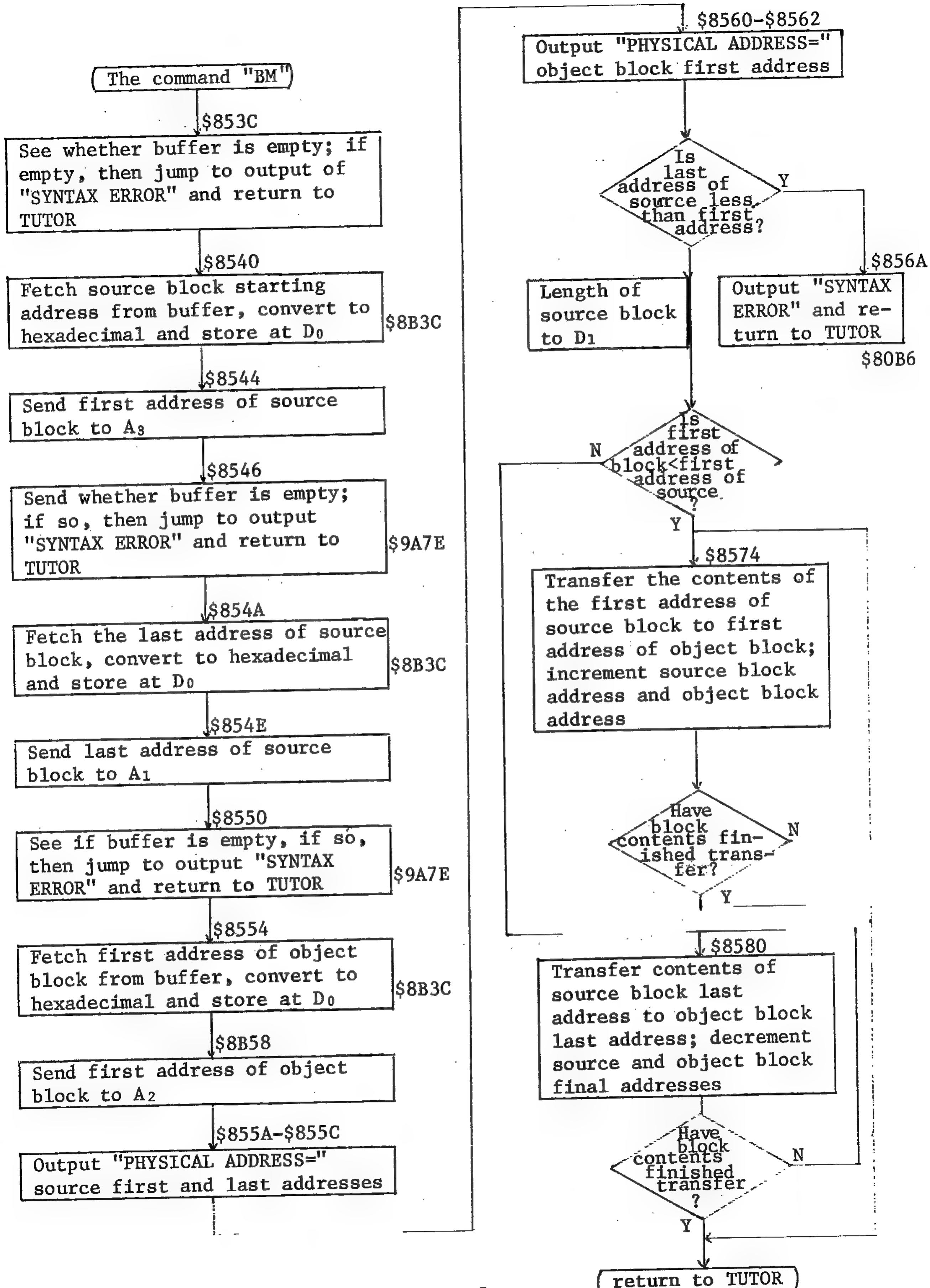
The command "BM"
$853C
See whether buffer is empty; if empty, then jump to output of "SYNTAX ERROR" and return to TUTOR
$8540
Fetch source block starting address from buffer, convert to hexadecimal and store at D0
$8B3C
$8544
Send first address of source block to A3
$8546
Send whether buffer is empty; if so, then jump to output "SYNTAX ERROR" and return to TUTOR
$9A7E
$854A
Fetch the last address of source block, convert to hexadecimal and store at D0
$8B3C
$854E
Send last address of source block to A1
$8550
See if buffer is empty, if so, then jump to output "SYNTAX ERROR" and return to TUTOR
$9A7E
$8554
Fetch first address of object block from buffer, convert to hexadecimal and store at D0
$8B3C
$8B58
Send first address of object block to A2
$855A-$855C
Output "PHYSICAL ADDRESS=" source first and last addresses
$8560-$8562
Output "PHYSICAL ADDRESS=" object block first address
Is last address of source less than first address?
Y
$856A
Output "SYNTAX ERROR" and return to TUTOR
$80B6
Length of source block to D1
Is first address of block<first address of source?
N
Y
$8574
Transfer the contents of the first address of source block to first address of object block; increment source block address and object block address
Have block contents finished transfer?
N
Y
$8580
Transfer contents of source block last address to object block last address; decrement source and object block final addresses
Have block contents finished transfer?
N
Y
return to TUTOR

Figure 5

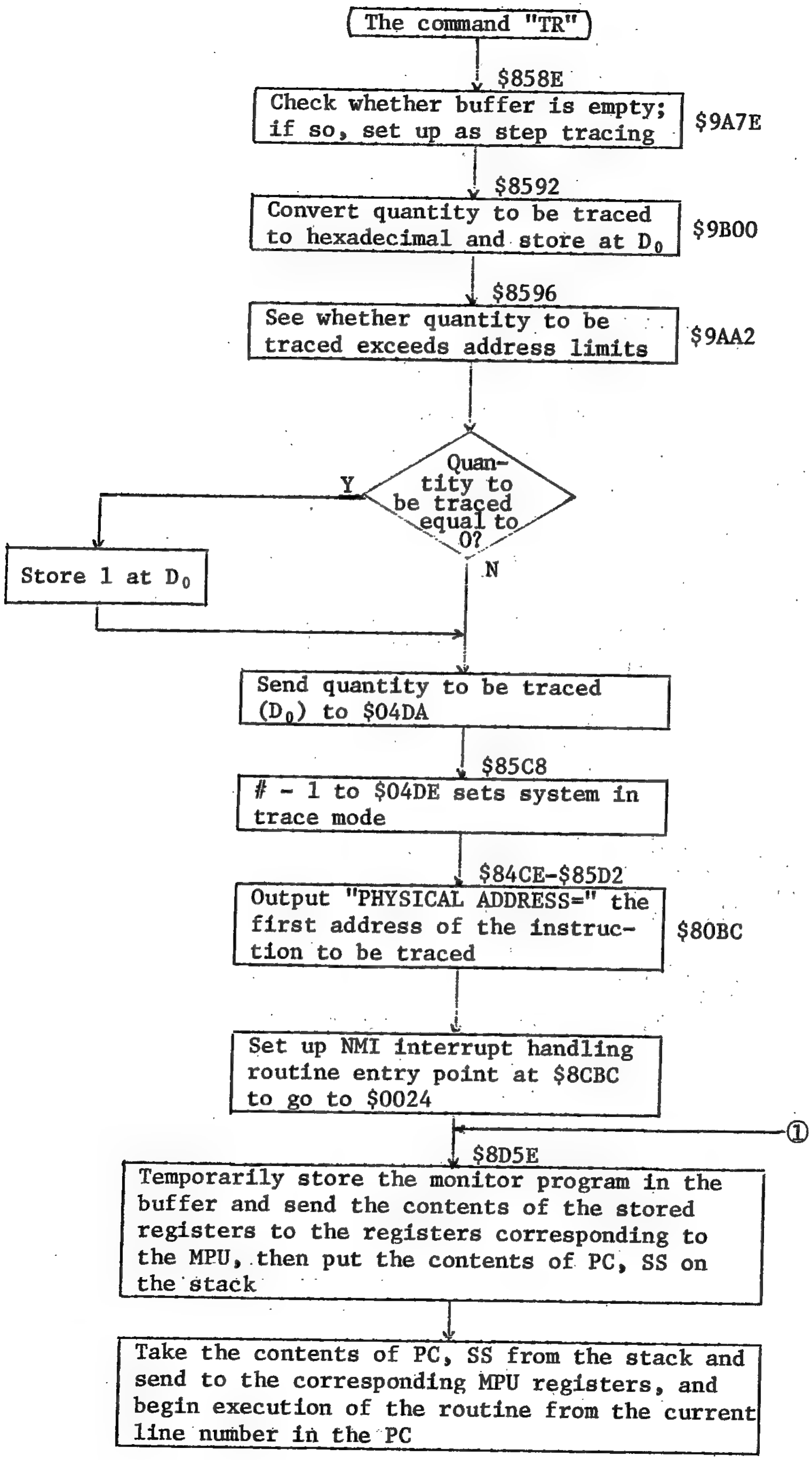
The command "TR"
$858E
Check whether buffer is empty; if so, set up as step tracing
$9A7E
$8592
Convert quantity to be traced to hexadecimal and store at $D_0$
$9B00
$8596
See whether quantity to be traced exceeds address limits
$9AA2
Quantity to be traced equal to 0?
Y
N
Store 1 at $D_0$
Send quantity to be traced ($D_0$) to $04DA
$85C8
# - 1 to $04DE sets system in trace mode
$84CE-$85D2
Output "PHYSICAL ADDRESS=" the first address of the instruction to be traced
$80BC
Set up NMI interrupt handling routine entry point at $8CBC to go to $0024
①
$8D5E
Temporarily store the monitor program in the buffer and send the contents of the stored registers to the registers corresponding to the MPU, then put the contents of PC, SS on the stack
Take the contents of PC, SS from the stack and send to the corresponding MPU registers, and begin execution of the routine from the current line number in the PC

Figure 6

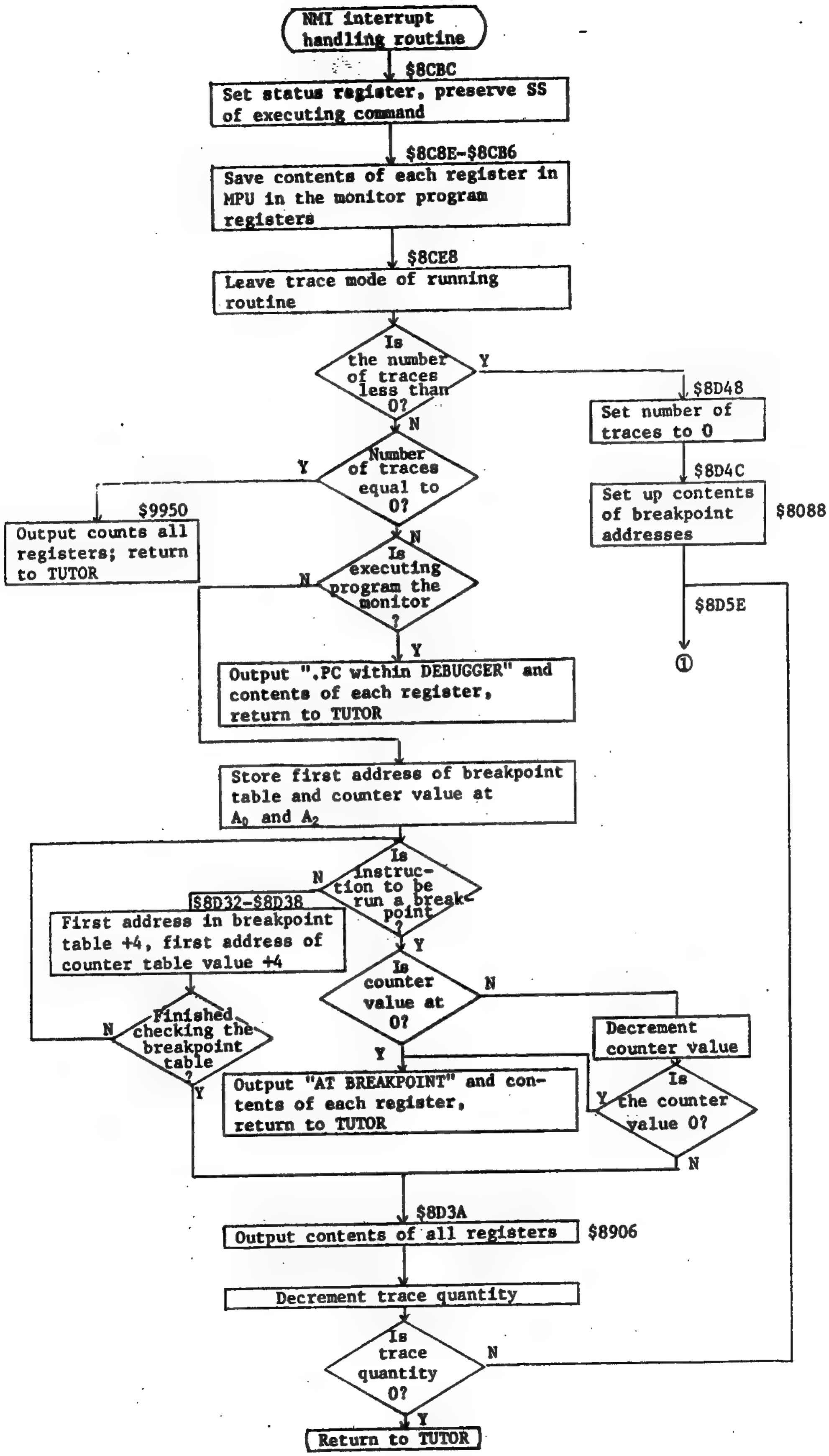
NMI interrupt handling routine
$8CBC
Set status register, preserve SS of executing command
$8C8E-$8CB6
Save contents of each register in MPU in the monitor program registers
$8CE8
Leave trace mode of running routine
Is the number of traces less than 0?
Y
N
$8D48
Set number of traces to 0
$8D4C
Set up contents of breakpoint addresses
$8088
$8D5E
①
Number of traces equal to 0?
Y
N
$9950
Output counts all registers; return to TUTOR
Is executing program the monitor?
N
Y
Output ".PC within DEBUGGER" and contents of each register, return to TUTOR
Store first address of breakpoint table and counter value at $A_0$ and $A_2$
Is instruction to be run a breakpoint?
N
Y
$8D32-$8D38
First address in breakpoint table +4, first address of counter table value +4
Finished checking the breakpoint table?
N
Y
Is counter value at 0?
N
Y
Decrement counter value
Is the counter value 0?
Y
N
Output "AT BREAKPOINT" and contents of each register, return to TUTOR
$8D3A
Output contents of all registers
$8906
Decrement trace quantity
Is trace quantity 0?
N
Y
Return to TUTOR

Figure 7

is to trace one execution. The initial address of the instruction to be executed is given by the value of the program counter (PC). After each instruction has run, this command will also display on the CRT screen the contents of the microprocessor's internal registers at this time (PC, SR, US, SS, $D_0$-$D_7$, $A_0$-$A_7$) for the user to analyze and use. At the same time, it will disassemble and display the instruction at the address pointed to by the PC.

## 3.4 Examples of Common Subroutines

In the TUTOR monitor program there are also more than 20 commonly used subroutines, as for example: an input subroutine that inputs a byte from any port to the single board computer, an output subroutine that outputs a byte to any port, a conversion subroutine that converts 1, 2, 4, 6, or 8 hexadecimal data to ASCII code or that converts ASCII code to hexadecimal data, as well as several subroutines that accomplish other functions.

In addition to providing command routine calls, in this program common subroutines may be called directly by the user by calling the "TRAP14" handling routine.

For an example, we will here use only the input routine that sends data from the keyboard to a memory buffer to analyze the operating process of this subroutine.

As we said before, we know that there are four ports in this single board computer. Two serial ports connect a CRT and a host computer, respectively, (or a modem), while the other two ports are used to connect a line printer and a tape cartridge recorder. Therefore, there are four I/O subroutines. The entry points to these subroutines are as in the following table:

| Port No | Routine entry point stored at | Routine entry point | I/O |
|---|---|---|---|
| Port 1 | \$062C<br>\$0630 | \$9CC8<br>\$9C14 | input<br>output |
| Port 2 | \$0634<br>\$0638 | \$9FDE<br>\$9C34 | input<br>output |
| Port 3 | \$063C<br>\$0640 | \$9CC8<br>\$9D70 | input<br>output |
| Port 4 | \$0644<br>\$0648 | \$A0A6<br>\$9EA6 | input<br>output |

12586/9365
CSO: 4008/1073

APPLIED SCIENCES

# MICROPROCESSOR APPLICATION IN ERROR CODE CORRECTION

Beijing DIANZI KEXUE JISHU [ELECTRONIC SCIENCE AND TECHNOLOGY] in Chinese
Vol 15, 10 Feb 85 pp 2-8

[Article by Zhou Dahua [6650 1129 5478] and Liu Yuqin [0491 3768 3830]: "Application of Microprocessor in Error Code Correction"]

[Text] In this paper, microprocessor software is used to correct error codes. Hamming code and cyclic code are interwoven to correct 8 bits of burst error. Thus, the use of complicated equipment required in the conventional interweaving method can be avoided.

## Hamming Code

A universal monitoring matrix H is chosen to be a (7,4) Hamming code

$$H = \begin{bmatrix} 0 & 1 & 1 & 1 & 1 & 0 & 0 \\ 1 & 0 & 1 & 1 & 0 & 1 & 0 \\ 1 & 1 & 0 & 1 & 0 & 0 & 1 \end{bmatrix}$$

The code length is 7. There are 4 information bits and 3 monitoring bits. It is capable of correcting any single random error in a string of codes. Let us assume that the information sequence is $C_0$, $C_1$, $C_2$, $C_3$ and the monitoring sequence is $C_4$, $C_5$, $C_6$, then the code block ($C_0$, $C_1$, $C_2$, $C_3$, $C_4$, $C_5$, $C_6$) satisfies the following:

$$\begin{bmatrix} 0 & 1 & 1 & 1 & 1 & 0 & 0 \\ 1 & 0 & 1 & 1 & 0 & 1 & 0 \\ 1 & 1 & 0 & 1 & 0 & 0 & 1 \end{bmatrix} \cdot \begin{pmatrix} C_0 \\ C_1 \\ C_2 \\ C_3 \\ C_4 \\ C_5 \\ C_6 \end{pmatrix} = \begin{bmatrix} 0 \\ 0 \\ 0 \end{bmatrix} \tag{1}$$

i.e., $HC^T = 0^T$ (2)

where $0 = [0\ 0\ 0]$

It can be expressed by the following equations:

$$\begin{cases} C_4 = C_1 \oplus C_2 \oplus C_3 \\ C_5 = C_0 \oplus C_2 \oplus C_3 \\ C_6 = C_0 \oplus C_1 \oplus C_3 \end{cases} \tag{3}$$

Let us assume that the error pattern created when the code block is transmitted in a channel is $E = (E_0E_1E_2E_3E_4E_5E_6)$. If there is an error in the ith bit, then $E_i = 1$, otherwise, it is zero. If the code block received is $C' = C+E = (C_0'\ C_1'\ C_2'\ C_3'\ C_4'\ C_5'\ C_6')$, where $C_i' = C_i + E_i$, based on equation (2) we get

$$HC'^T = H\ (C+E)^T = HC^T + HE^T = HE^T \tag{4}$$

Let $S^T = HE^T$, or $S = EH^T$, where S is the conjugate transpose. We get equation (5)

$$\begin{bmatrix} S_2 \\ S_1 \\ S_0 \end{bmatrix} = \begin{bmatrix} 0 & 1 & 1 & 1 & 1 & 0 & 0 \\ 1 & 0 & 1 & 1 & 0 & 1 & 0 \\ 1 & 1 & 0 & 1 & 0 & 0 & 1 \end{bmatrix} \cdot \begin{pmatrix} E_0 \\ E_1 \\ E_2 \\ E_3 \\ E_4 \\ E_5 \\ E_6 \end{pmatrix} \tag{5}$$

In transmission, if there is only an error at $C_2$, then $E = (0010000)$. Substituting it into equation (5), we get $S = [S_2S_1S_0] = [110]$. Therefore, we can see that if only $E_i$ is 1 in E, $S^T$ is the ith column in the matrix H. Table 1 is tabulated based on equation (5).

In equation (4), $S^T = HC'^T$, i.e.

$$\begin{bmatrix} S_2 \\ S_1 \\ S_0 \end{bmatrix} = \begin{bmatrix} 0 & 1 & 1 & 1 & 1 & 0 & 0 \\ 1 & 0 & 1 & 1 & 0 & 1 & 0 \\ 1 & 1 & 0 & 1 & 0 & 0 & 1 \end{bmatrix} \cdot \begin{pmatrix} C_0' \\ C_1' \\ C_2' \\ C_3' \\ C_4' \\ C_5' \\ C_6' \end{pmatrix}$$

Then, the decoding equations are:

$$\begin{cases} S_2 = C_1' \oplus C_2' \oplus C_3' \oplus C_4' \\ S_1 = C_0' \oplus C_2' \oplus C_3' \oplus C_5' \\ S_0 = C_0' \oplus C_1' \oplus C_3' \oplus C_6' \end{cases} \tag{7}$$

By using the coding equations in (3), decoding equations in (7) and Table 1, error correction can be carried out by software.

Table 1. Relation Between Error Location and Conjugate Transpose

| Error location | S | | | Error location | S | | |
|---|---|---|---|---|---|---|---|
| | $S_2$ | $S_1$ | $S_0$ | | $S_2$ | $S_1$ | $S_0$ |
| | 0 | 0 | 0 | $C_3$ | 1 | 1 | 0 |
| $C_0$ | 0 | 1 | 1 | $C_4$ | 1 | 0 | 0 |
| $C_1$ | 1 | 0 | 1 | $C_5$ | 0 | 1 | 0 |
| $C_2$ | 1 | 1 | 0 | $C_6$ | 0 | 0 | 1 |

Because there are numerous I/O interfaces and transmission modes, we will not discuss this issue in this paper. We will only introduce code compiling process using a Z80 microprocessor or a single board computer software. In order to accelerate the code compiling rate, assembly language is used.

1. Encoding

In Figure 1, the front half byte ($a_0$-$a_3$) of the first address of the input data is coded and transmitted to the first output address. Then the latter half byte ($a_4$-$a_7$) is coded and sent to the second byte. The same process is repeated for the second input byte until all the data are coded. The coding process is shown in Figure 2. In equation (3), because the value of Ci in the information and monitoring bits is in the GF92) domain, the addition of the module 2 of $C_1$, $C_2$, and $C_3$ is equivalent to the ordinary addition among themselves; which is 1 for odd numbers and 0 for even numbers. The latter is adopted to simplify the program significantly. In the program, registers C, D, and E are assigned to represent the values of the monitoring bits $C_4$, $C_5$, and $C_6$, respectively.

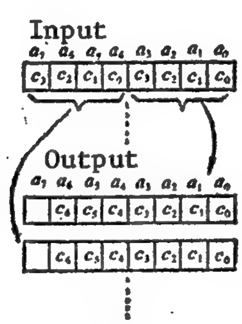


Figure 1.

In Figure 2, RRA is the cyclic right shift of the contents of the accumulator A and the carry marker. From the carry marker, we can determine whether the 0th bit of A, $C_0$, is 0 of 1. If it is 1, then $B_0$ is set to be 1. Otherwise, $B_0$ is set to be 0. $B_0$ is the 0th bit in the B register. Based on equation (3), if $C_0$ is 1, then 1 is added to both registers D and E. The immediate RRA to follow is to process $C_1$. After four such RRA, the content in register A, $C_0$ - $C_3$, is first entered into $a_0$ - $a_3$ in register B and then used to evaluate

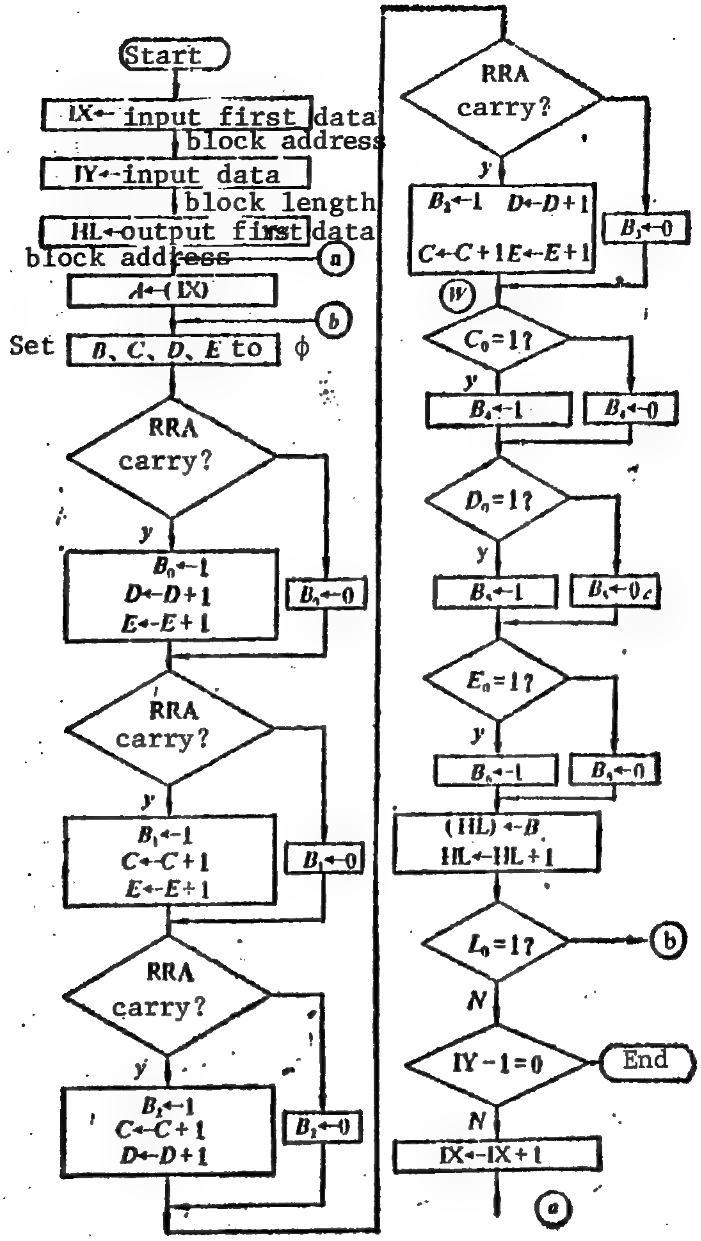


Figure 2.

registers C, D, and E in order to ascertain the contents in monitoring bits $C_4$, $C_5$, and $C_6$ and send them to $a_4$–$a_7$ in B. The next cycle is to code the latter half byte of the input data and send it to the second byte of the output data until the entire coding process is completed. In Figure 2, the address of the first data block should be an even number to allow the program to proceed as shown in Figure 1.

## 2. Decoding

Based on equation (7), decoding is done at the receiving end. We only correct errors in information bits $C_0$ - $C_3$ and ignore monitoring bit errors. The decoding process is schematically shown in Figure 3. Table 2 is the Hamming code error correction table. If an error occurs at $C_2'$, its conjugate S = (110) appears as 06H in a register. This number is called the conjugate number. Its corresponding error pattern is $E_2$ = 1 and the remaining $E_1$ = 0. In the corresponding register, an error occurs at $C_2'$ and the register value is 04H, which is called the correction number. In the program, 04H is used to correct the error in $C_2'$. In Figure 4 the symbol CORREC is used to represent the first addresses of the conjugate number and the correction number (CORREC: DB03, 05, 06, 07, 01, 02, 03, 04, 08).

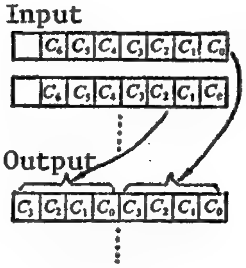


Figure 3.

Table 2.

| Error location | Conjugate $S_2$ | $S_1$ | $S_0$ | Conjugate number | Error correction number |
|---|---|---|---|---|---|
| $C_0'$ | 0 | 1 | 1 | 03H | 01H |
| $C_1'$ | 1 | 0 | 1 | 05H | 02H |
| $C_2'$ | 1 | 1 | 0 | 06H | 04H |
| $C_3'$ | 1 | 1 | 1 | 07H | 08H |

In Figure 4 the values of $S_2$, $S_1$, and $S_0$ in equation (7) are stored in registers B, C, and D, respectively, from the start to the point W where decoding of equation (1) is completed. The conjugate transpose is obtained at W. It is compared to conjugate number of the first address of CORREC. If $C_2'$ is wrong, the conjugate transpose in A is 110, which is equal to the conjugate number 06 in HL. Then, HL plus 3 is 04 (the correction number). The error in $C_2'$ is corrected by using the XORB command. The following program is used to complete the program shown in Figure 3 with the first address of the data block being even. This process continues until data processing is completed.

## Cyclic Code

Let us choose the generating polynomial g(x) to be:

$$g(x) = x^3 + x^2 + 1 \tag{8}$$

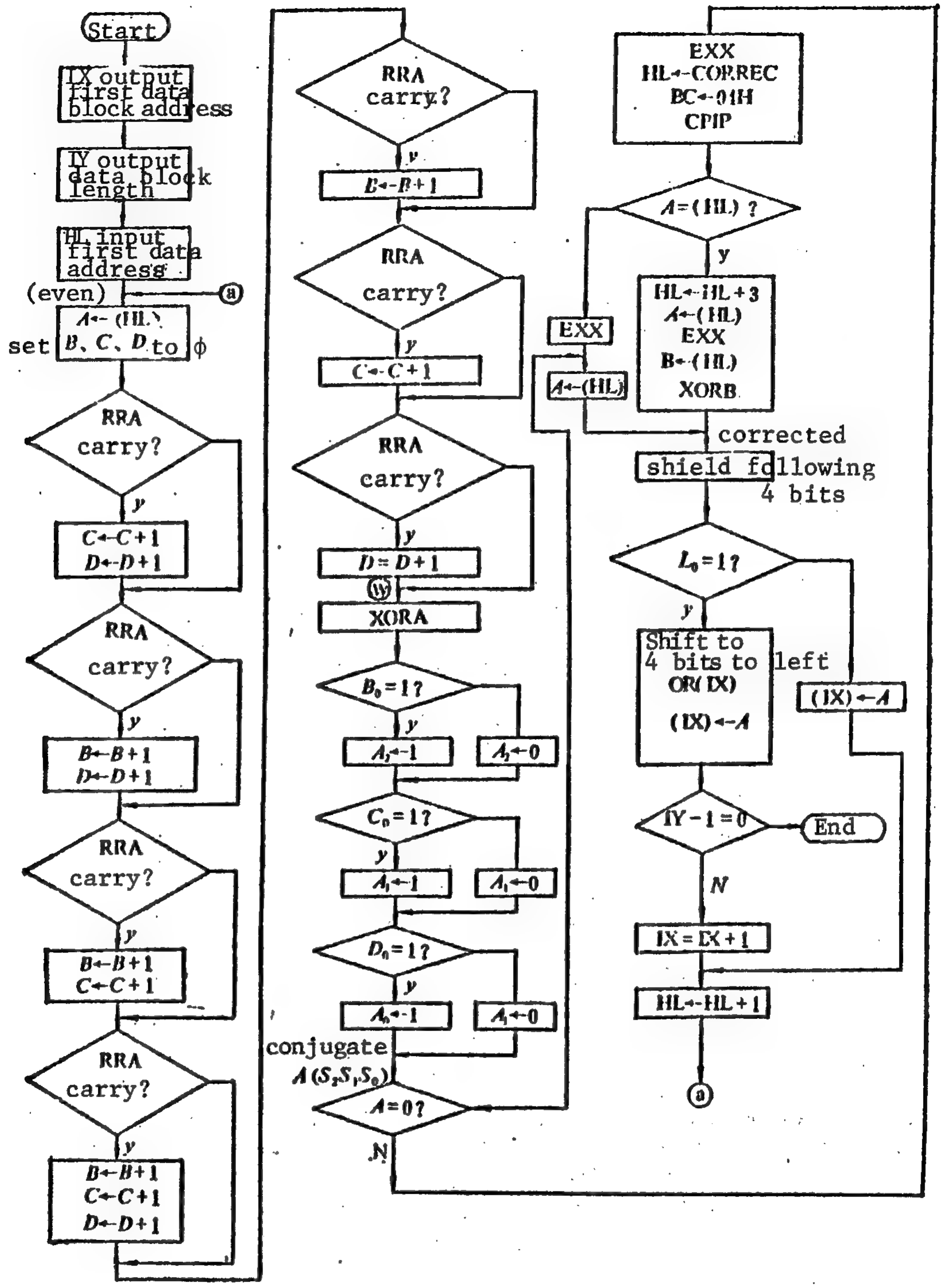
Start
IX output first data block address
IY output data block length
HL input first data address
(even)
A← (HL)
set B、C、D to ϕ
RRA carry?
y
C←C+1
D←D+1
RRA carry?
y
B←B+1
D←D+1
RRA carry?
y
B←B+1
C←C+1
RRA carry?
y
B←B+1
C←C+1
D←D+1
RRA carry?
y
B←B+1
RRA carry?
y
C←C+1
RRA carry?
y
D=D+1
XORA
B0=1?
y
A2←1
A2←0
C0=1?
y
A1←1
A1←0
D0=1?
y
A0←1
A0←0
conjugate A (S2S1S0)
A=0?
N
EXX
HL←CORREC
BC←01H
CPIP
A=(HL)?
y
HL←HL+3
A←(HL)
EXX
B←(HL)
XORB
EXX
A←(HL)
corrected
shield following 4 bits
L0=1?
y
Shift to 4 bits to left
OR(IX)
(IX)←A
(IX)←A
IY−1=0
End
N
IX=IX+1
HL←HL+1

Figure 4.

Then, the generating matrix G is:

$$G=\begin{bmatrix} 1 & 0 & 0 & 0 & 1 & 1 & 0 \\ 0 & 1 & 0 & 0 & 0 & 1 & 1 \\ 0 & 0 & 1 & 0 & 1 & 1 & 1 \\ 0 & 0 & 0 & 1 & 1 & 0 & 1 \end{bmatrix} \tag{9}$$

Thus, a (7,4) cyclic code for correcting a 1 bit random error can be totally defined. In order to facilitate encoding and decoding, it is necessary to make the generating matrix G be a universal monitoring matrix H:

$$H=\begin{bmatrix} 1 & 0 & 1 & 1 & 1 & 0 & 0 \\ 1 & 1 & 1 & 0 & 0 & 1 & 0 \\ 0 & 1 & 1 & 1 & 0 & 0 & 1 \end{bmatrix} \tag{10}$$

The encoding equations are:

$$\begin{cases} C_4=C_0\oplus C_2\oplus C_3 \\ C_5=C_0\oplus C_1\oplus C_2 \\ C_6=C_1\oplus C_2\oplus C_3 \end{cases} \tag{11}$$

and the decoding equations are

$$\begin{cases} S_2=C_0'\oplus C_2'\oplus C_3'\oplus C_4' \\ S_1=C_0'\oplus C_1'\oplus C_2'\oplus C_5' \\ S_0=C_1'\oplus C_2'\oplus C_3'\oplus C_6' \end{cases} \tag{12}$$

Equation (11) is similar to (3) and equation (12) is similar to (7), therefore, the code compiling program is also similar.

1. Encoding

The encoding scheme is shown in Figure 1. Figure 5 shows the cyclic code compiling program. Registers C, D, and E are used to represent the values of $C_4$, $C_5$, and $C_6$ in equation (11), respectively.

2. Decoding

The decoding scheme is shown in Figure 3. Figure 6 shows the flow chart of the cyclic code decoding program. Registers B, C, and E represent $S_2$, $S_1$, and $S_0$ in equation (12), respectively. The error correction table is shown in Table 3, using CORREC to represent the conjugate number and the first correction number address (CORREC: DB06, 03, 07, 05, 01, 02, 04, 08).

Table 3. Cyclic Code Correction Table

| Error location | Conjugate $S_2$ | $S_1$ | $S_0$ | Conjugate number | Error correction number |
|---|---|---|---|---|---|
| $C_0'$ | 1 | 1 | 0 | 06H | 01H |
| $C_1'$ | 0 | 1 | 1 | 03H | 02H |
| $C_2'$ | 1 | 1 | 1 | 07H | 04H |
| $C_3'$ | 1 | 0 | 1 | 05H | 08H |

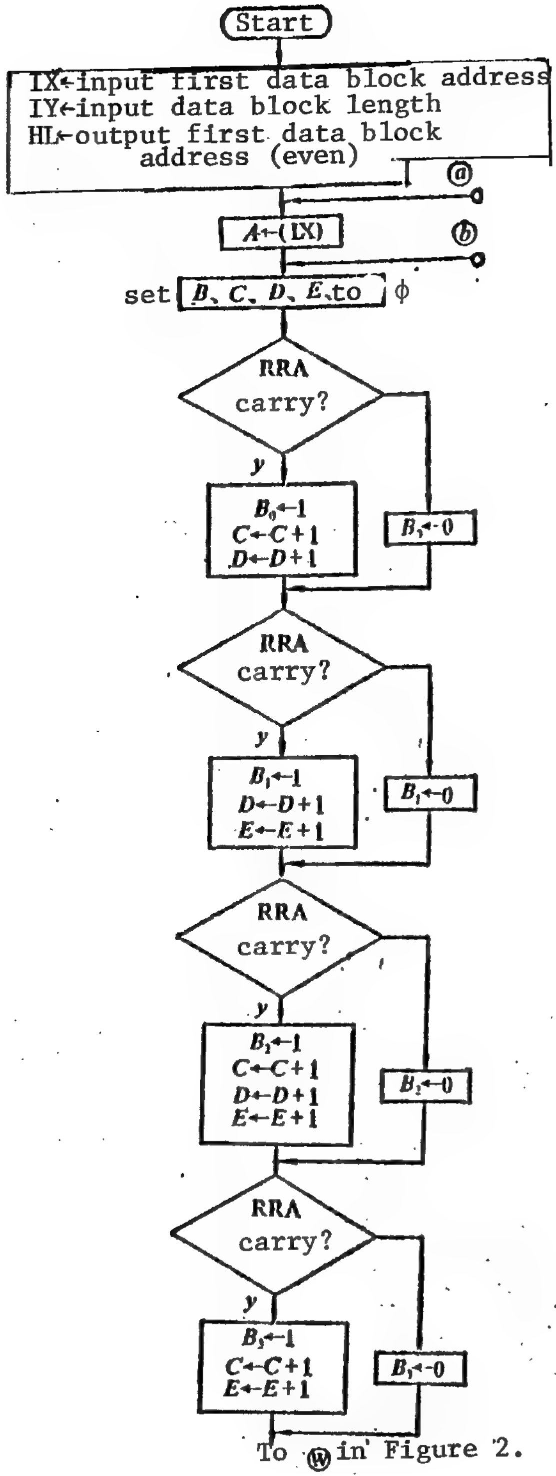

Start
IX←input first data block address
IY←input data block length
HL←output first data block address (even)
ⓐ
A←(IX)
ⓑ
set B、C、D、E to ϕ
RRA carry?
y
B0←1
C←C+1
D←D+1
B0←0
RRA carry?
y
B1←1
D←D+1
E←E+1
B1←0
RRA carry?
y
B2←1
C←C+1
D←D+1
E←E+1
B2←0
RRA carry?
y
B3←1
C←C+1
E←E+1
B3←0
To Ⓦ in Figure 2.


Figure 5.

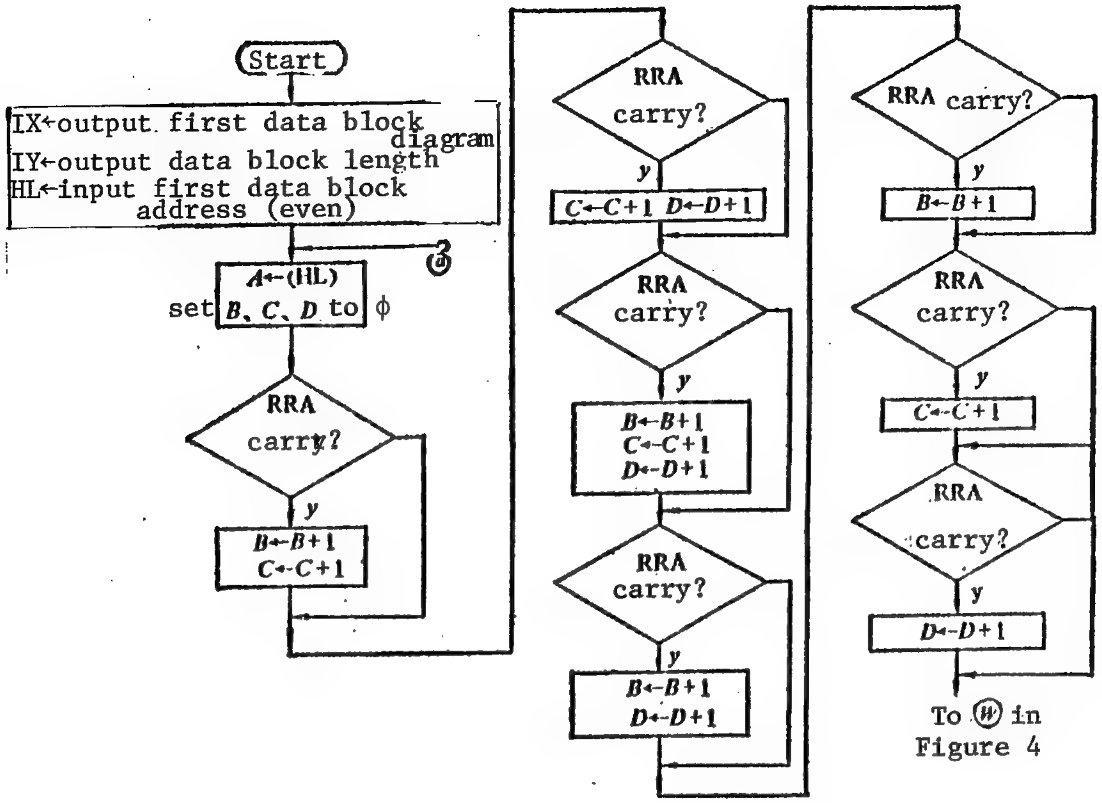


Figure 6.

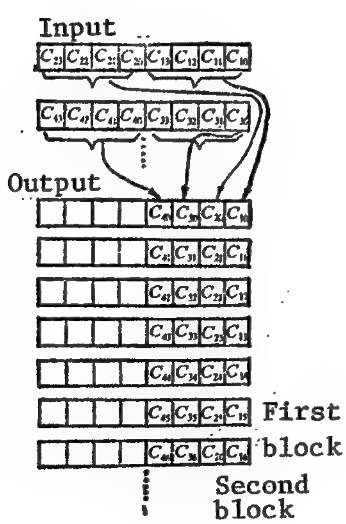


Figure 7.

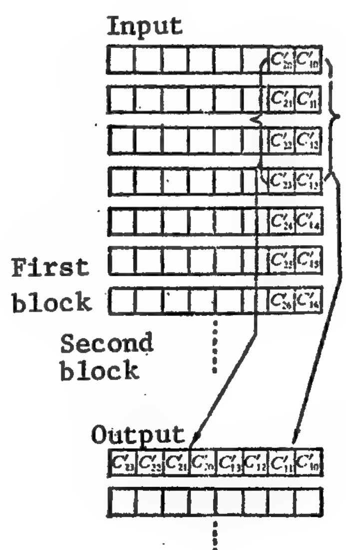


Figure 8.

## Interwoven Hamming Code

As shown in Figure 7, at the sending end, the first half input data byte $C_{10}$ - $C_{13}$ is Hamming coded to $C_{10}$ - $C_{16}$ and transmitted to the 9th bit of each corresponding byte in the first output data block (each data block contains 7 bytes). Then, the latter half of the first input byte, $C_{20}$ - $C_{23}$, is similarly treated until 4 input bytes are processed and sent to fill the first output data block. Then, the next block is similarly processed. This is the encoding process of the interwoven code at the sending end.

At the receiving end, the 0th bit of each byte in the first input block is decoded into $C_1'{}_0$ - $C_1'{}_6$. After correcting the errors, $C_1'{}_0$ - $C_1'{}_3$ is sent to the front half of the first byte, as shown in Figure 8. It proceeds in this manner until the first input block is Hamming decoded and sent to the output. Then the next block is processed. This is the interwoven decoding process at the receiving end.

Based on the above, 8 (7,4) Hamming codes form an interwoven code matrix. The degree of interweaving is 8. Each byte contains the first bit of every (7,4) code. In the transmission process, if the burst length is 8 bits, then it is equivalent to having a 1 bit error in each (7,4) code at the receiving end during decoding. Each (7,4) code, however, can correct 1 bit of error. Thus, these 8 bits of burst errors can also be corrected.

### 1. Interwoven Encoding

Figure 9 is the encoding flow chart. Equation (3) is used to encode. Let registers C, D, and E represent the values of $C_4$, $C_5$, and $C_6$, respectively. Shifting (HL) to the right by 1 bit is done by using the RRC(HL) command. Based on the scheme shown in Figure 7, a block is encoded before the next block is processed until the entire job is completed.

### 2. Interwoven Decoding

Figure 10 is the decoding flow chart. Equation (7) is used for decoding. Let registers B, C, and D represent the values of $S_2$, $S_1$, and $S_0$, respectively. With the exception that its error correction numbers are 10, 20, 30, and 40, the rest of the error correction table is the same as Table 2. Therefore, CORREC: DB03, 05, 06, 07, 10, 20, 40, and 80.

## The Cyclic Interwoven Code

The interweaving process of the cyclic interwoven code is the same as those in Figures 7 and 8. Encoding and decoding, however, are done based on equations (11) and (12). Figures 11 and 12 are the flow charts for encoding and decoding cyclic interwoven codes. The registers are set as that for the Hamming interwoven code. With the exception that the error correction numbers are 10, 20, 40, and 80, the rest of the error correction table is the same as Table 3. Therefore, CORREC: DB06, 03, 07, 05, 10, 20, 40, and 80.

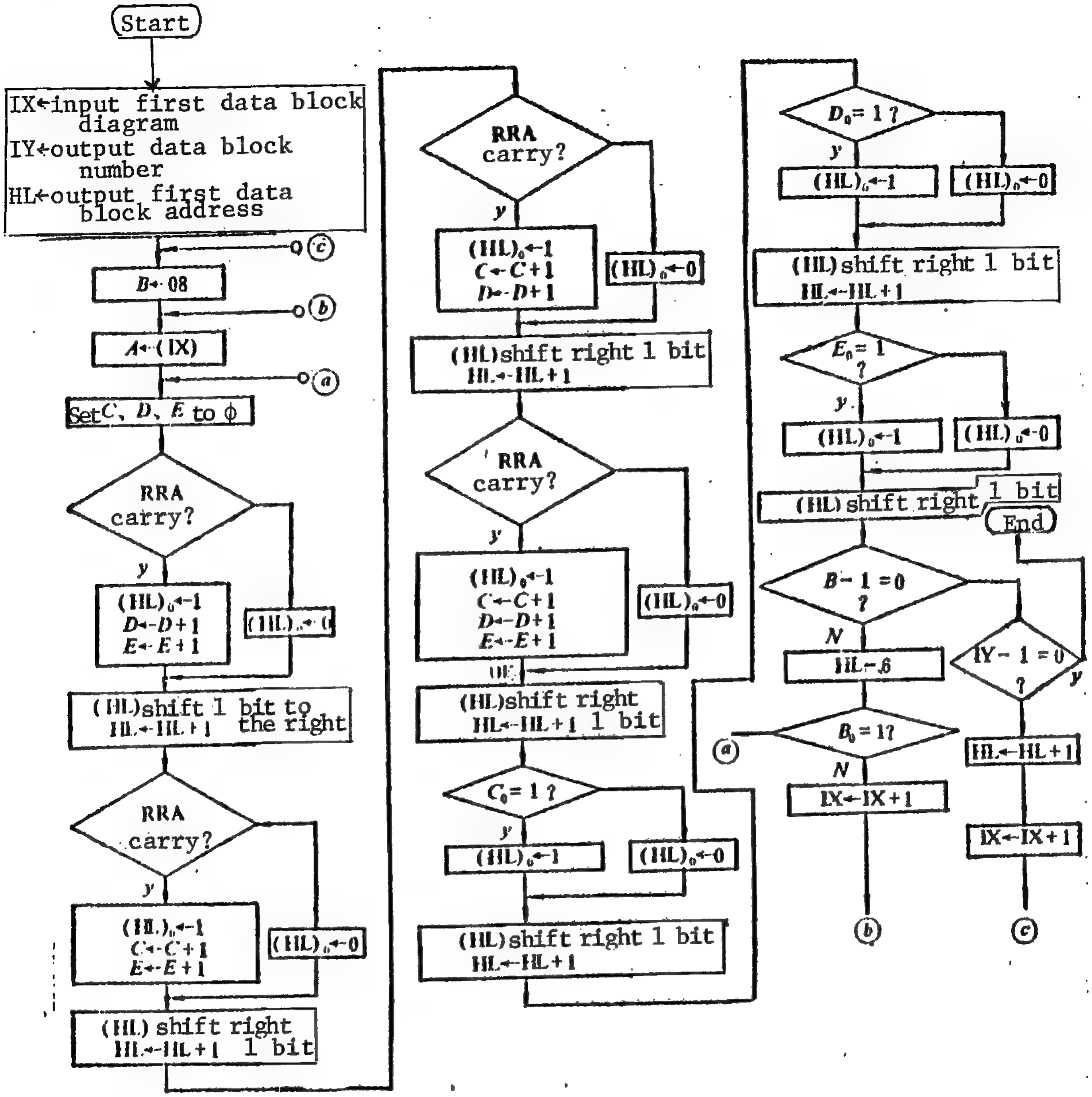
Start
IX←input first data block diagram
IY←output data block number
HL←output first data block address
B←08
A←(IX)
Set C, D, E to φ
RRA carry?
y
(HL)₀←1
D←D+1
E←E+1
(HL)₀←0
(HL)shift 1 bit to the right
HL←HL+1
RRA carry?
y
(HL)₀←1
C←C+1
E←E+1
(HL)₀←0
(HL) shift right 1 bit
HL←HL+1
RRA carry?
y
(HL)₀←1
C←C+1
D←D+1
(HL)₀←0
(HL)shift right 1 bit
HL←HL+1
RRA carry?
y
(HL)₀←1
C←C+1
D←D+1
E←E+1
(HL)₀←0
(HL)shift right 1 bit
HL←HL+1
C₀=1?
y
(HL)₀←1
(HL)₀←0
(HL)shift right 1 bit
HL←HL+1
D₀=1?
y
(HL)₀←1
(HL)₀←0
(HL)shift right 1 bit
HL←HL+1
E₀=1?
y
(HL)₀←1
(HL)₀←0
(HL) shift right 1 bit
End
B−1=0?
N
HL←6
IY−1=0?
y
B₀=1?
N
IX←IX+1
HL←HL+1
IX←IX+1
a
b
c

Figure 9.

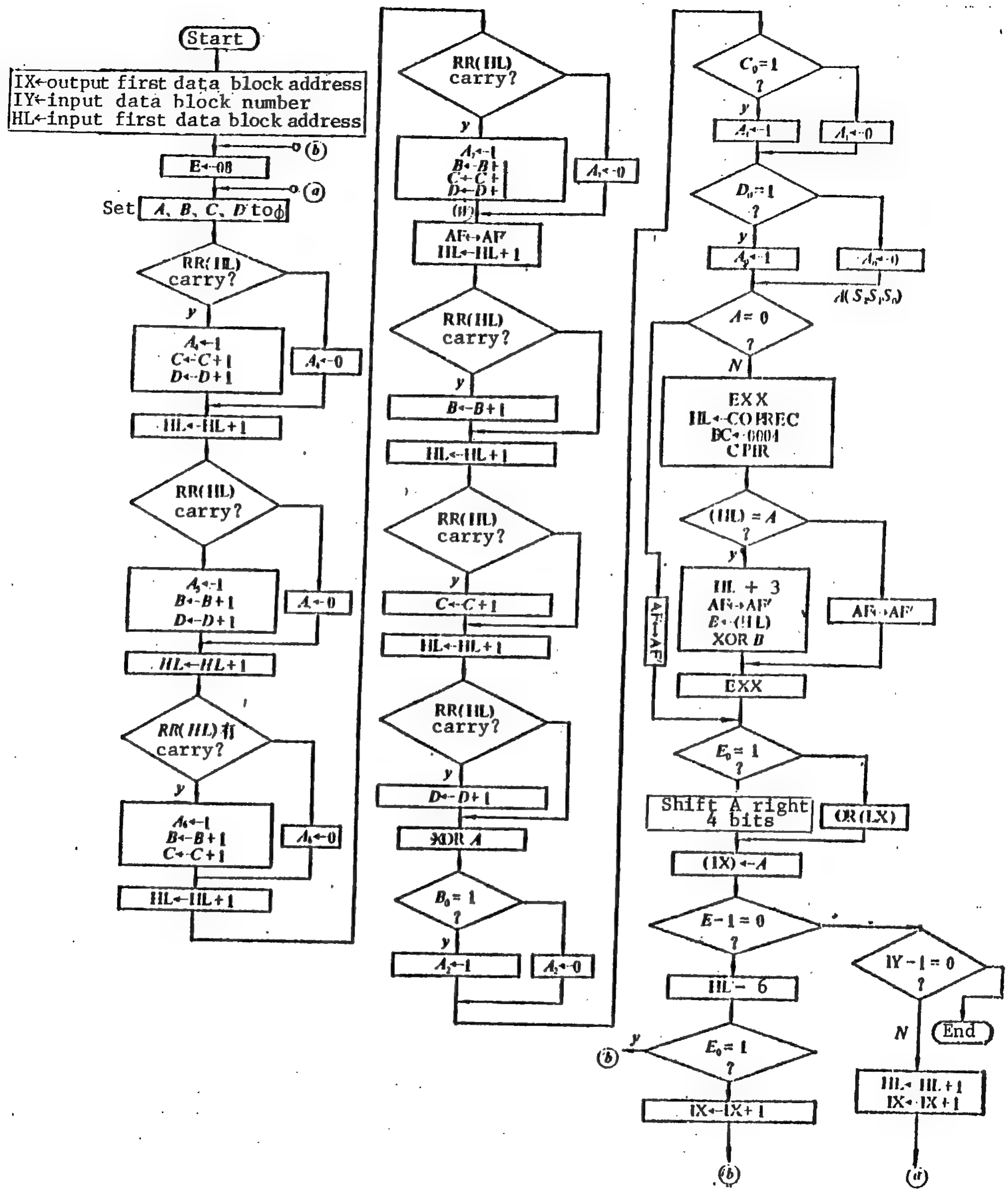
Start
IX←output first data block address
IY←input data block number
HL←input first data block address
E←08
Set A, B, C, D to 0
RR(HL) carry?
RR(HL) carry?
carry?
AF↔AF'
HL←HL+1
EXX
EXX
Shift A right 4 bits
(IX)←A
E−1=0 ?
IY−1=0 ?
End
IX←IX+1
HL←HL+1
IX←IX+1

Figure 10.

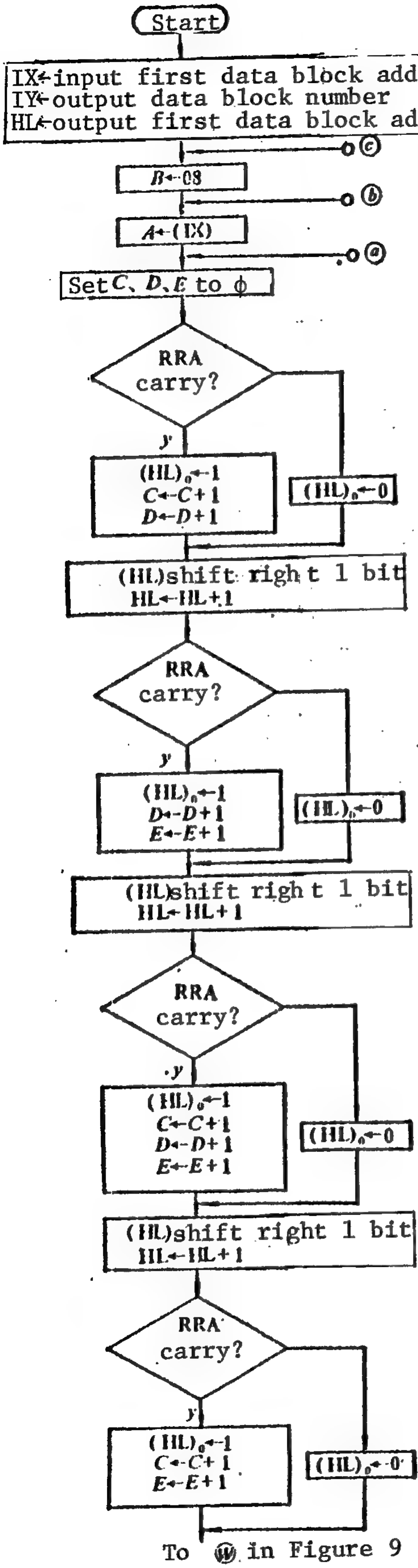


Figure 11.

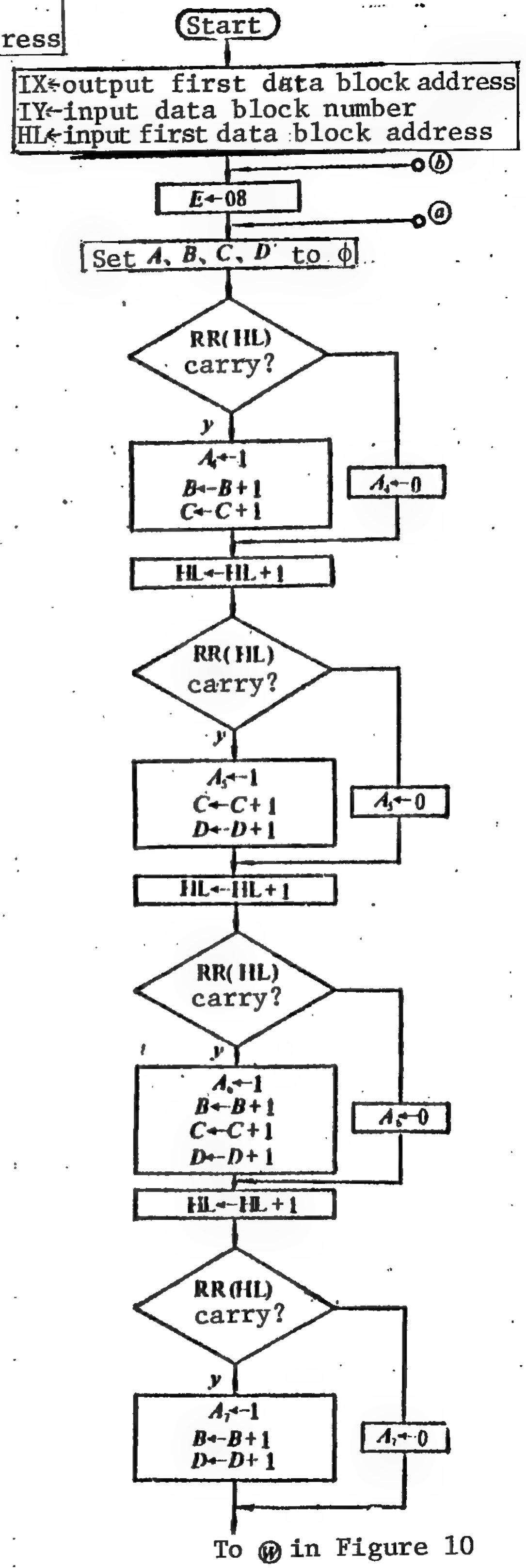


Figure 12.

Based on the above, the main portion between the cyclic code and the Hamming code, as well as between the cyclic interwoven code and Hamming interwoven code, is identical. Therefore, it is possible to set up subroutines to handle them.

## Conclusions

In the coding process, we should first consider fast speed, i.e. less T states. Then, we should conserve the internal storage elements. For example, the command XORA is three state number less than that of LD A, OOH. LDBC, nnH is 4 T less than that of LDB, nH and LD C, nH. RRA is 4 T less than that of BITO, A. JP is 2 T less than JR, however, there is one extra internal storage element.

The data processing rates of common data transmitters and demodulators are 1.2 kb/s, 2.4 kb/s and 4.8 kb/s. Using 4.8 kb/s as an example, it takes 11.667 ms to transmit a block of data (a total of 7 bytes in 56 bits). The execution time required for a 2 MHz microprocessor using a encoding program with 4,522 states is 2.261 ms. The execution time of a decoding program with 6,325 states is 3.163 ms. If the primary frequency of the microprocessor is 4 MHz, then the execution time could be cut in half. Thus, at a data transmission rate of 4.8 kb/s, microprocessor coding has no effect. It can be considered transparent. An interrupt mode may be used at both the receiving and sending end to perform data input and output simultaneously.

## REFERENCES


1. Macwilliams, F.J. and Sloane, N.J.A., "The Theory of Error-Correcting Codes," North-Holland, 1977.

2. Wan Zhexian [5502 0772 0341], ALGEBRA AND CODING, Science Publishing Co., 1976.

3. Kong Xianzheng [1313 2009 2973], "Basic Principle of Digital Information Transmission," Defense Industry Publishing Co., 1976.



12553/9365
CSO: 4008/1057

APPLIED SCIENCES

## NOVEL CONTROL CIRCUIT FOR PROXIMITY FOCUSED MICROCHANNEL PLATE IMAGE INTENSIFIERS

Beijing DIANZI KEXUE XUEKAN [JOURNAL OF ELECTRONICS] in Chinese Vol 6 No 6, Nov 84 pp 473-480

[Article by Zhou Xuan [6650 2467] of the Institute of Semiconductor of the Chinese Academy of Sciences, manuscript received on 20 May 1983 and revised manuscript received on 9 September 1983: "A Novel Control Circuit for Proximity Focused Microchannel Plate Image Intensifiers"]

[Text] Abstract: Because of its high temporal and spatial resolution, wide spectral and dynamic input intensity range, high gain, and ability to record transient single events, the proximity focused microchannel plate (MCP) image intensifier can be used as a super high-speed optical shutter.

A microchannel plate image intensifier and a gating pulse generator, which controls its shutter effect, constitute a super high-speed camera with high gain and fast response. In this paper, a comparison of three pulse control modes for a typical second generation image intensifier (18 mm, Model ITT-F4111 image intensifier) is made. Based on the comparison, a novel control circuit for gating the photocathode of the image intensifier, as well as capable of generating high amplitude nanosecond pulses, is introduced. It was experimentally determined that the exposure time of the camera could reach approximately 2 ns by using this control generator. In addition, the paper also discusses the match between the generator and the image intensifier. Furthermore, a simple and effective method is introduced to eliminate multiple exposures which must absolutely be avoided in single shot photography.

### I. Introduction of the Problem

The proximity focused microchannel plate image intensifier is a novel optoelectronic device. In addition to being used as an optical shutter alone, it also

has a significant light intensifying effect.[1] The combination of a microchannel plate image intensifier shutter and high-speed, high-voltage pulse generator to control the optical shutter can constitute a super high-speed camera; capable of capturing single instantaneous events with an extremely short exposure time and high optical gain. This camera has a wide range of applications, involving many important technical areas such as high-voltage gas discharge and laser nuclear fusion

Without any doubt, the performance of the camera is mainly determined by the image converter tube itself. There is, however, the problem of how to more effectively utilize the image converter tube. Particularly, two major performance specifications--exposure time and optical gain--of the image converter tube of the microchannel plate image intensifier shutter depend directly on the width and amplitude of the control pulse. Therefore, the generation of large amplitude narrow pulses to control the optical shutter is a key technical issue in the development of an image converter tube for a super high-speed shutter camera.

In this paper, a typical second generation image intensifier, the Model ITT-F4111 proximity focused microchannel plate image intensifier, is used as an example to illustrate the pulse control of a high-speed image intensifier optical shutter.

## II. Three Control Modes for an Image Intensifier

The Model ITT-F4111 image intensifier is a compact specialized image converter tube and its external dimensions are shown in Figure 1.[2] The image intensifier is a circular plate whose external diameter is 45 mm. The effective diameter of the photocathode and the optical screen is 18 mm. The total thickness is approximately 22 mm.

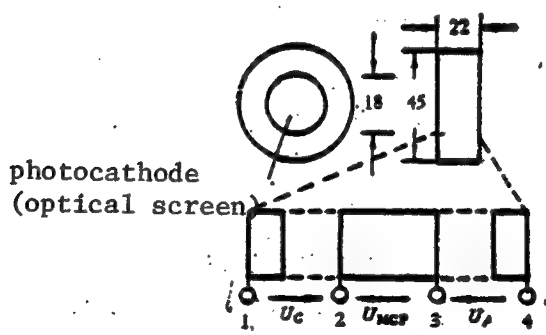


Figure 1. External Dimensions of the ITT-F4111 Image Intensifier

In order to control the operation of this image intensifier, the following three voltages are necessary:

(1) the cathode voltage $U_C$ between the photocathode (terminal 1) and the input end of the microchannel plate (terminal 2); (2) the microchannel plate voltage $U_{MCP}$ between the input of the microchannel plate and its output

(terminal 3); and (3) the anode voltage $U_A$ between the output of the microchannel plate and the anode (optical screen, terminal 4).

When the image intensifier is used as a high-speed optical shutter, one of the three voltages mentioned above must be supplied as pulses, while the other two remain as dc voltages. Thus, we have three pulse control modes:

(1) applying control pulses between the photocathode and the microchannel plate input; (2) applying control pulses between the input and the output of the microchannel plate; and (3) applying control pulses between the output of the microchannel plate and the anode.

Because of varying resistance between electrodes and also because pulses of different amplitudes and polarities may be required, the difficulties involved in implementing these control modes are also different.

The input resistance $R_i$ and input characteristics $C_i$ between various electrodes of the ITT-F4111 image intensifier are measured to be

between photocathode and microchannel plate input: $R_i = 4 \times 10^{10}\Omega$, $C_i = 23$pF;

between input and output of the microchannel plate: $R_i = 3.3 \times 10^{8}\Omega$, $C_i = 72$pF;

between microchannel plate output and anode: $R_i = 3.3 \times 10^{10}\Omega$, $C_i = 7$pF.

Based on the data, the resistance and capacitance between various electrodes of the image intensifier are very high. Even if a nearly ideal rectangular pulse can be obtained from a purely resistive low impedance circuit, it will be seriously distorted after it is impressed across the relevant electrodes of image intensifier. In this case, not only the desired short exposure time cannot be obtained because the edge of the control pulse is slowed down by the large time constant of the input end of the image intensifier, but also, due to resonance caused by the distribution of parameters, the optical gate is opened many times, leading to multiple exposures.

Table 1 shows a comparison of the three pulse control modes of the ITT-F4111 image intensifier.

Table 1. Comparison of Three Control Modes of the ITT-F4111 Image Intensifier

| | Pulse amplitude to reach maximum optical gain | Polarity of control pulse | Ground | Capacitance load (pF) | Usage |
|---|---|---|---|---|---|
| Control pulse at photocathode | 180 | negative | microchannel plate input | 23 | most common |
| Control pulse at microchannel plate input | 800 | negative | microchannel plate output | 72 | usually not used |
| Control pulse at photoanode | 5200 | positive | microchannel plate output | 7 | sometimes used |

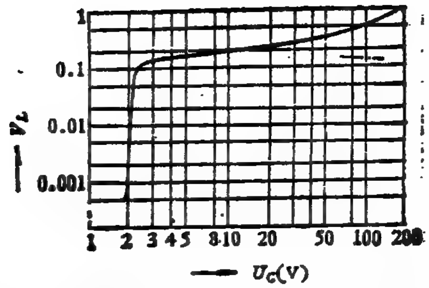


Figure 2. Relative Optical Gain $V_L$ vs Photocathode Voltage $U_C$ of the ITT-F4111 Image Intensifier

Obviously, the second control mode is usually not adopted due to the high capacitance load. The third control mode requires the largest amplitude for the control pulse. It is relatively difficult to generate and transmit high-speed, high-voltage pulses. This method is still used sometimes, however, because the capacitance load of this control mode is small. In an ITT-F4111 image intensifier, the variation of the relative optical gain $V_L$ with cathode voltage $U_C$ is shown in Figure 2.[2] Based on this figure, several dozen volts of voltage change at the cathode is sufficient to cause the optical gain to vary by several magnitudes. Only a 180V voltage pulse is required to reach the maximum optical gain (i.e. $V_L = 1$). In other words, it is most sensitive to control the photocathode. Because the first mode requires pulses of much lower amplitude as compared to those of the other two modes, it is thus possible to make the control pulse narrower. Therefore, it may be possible to get the shortest exposure time. It is the most commonly used control mode.

## III. Generation of Large Amplitude Narrow Pulses To Control the Photocathode of the Image Intensifier

### 1. Limitation of the Basic Avalanche Transistor Trigger Circuit

In order to turn the optical gating circuit into solid state, usually an avalanche transistor is used to generate large amplitude pulses with steep leading edges. It is very difficult, however, to obtain the desired electrical control pulses for the optical gate based on the basic circuit comprising a single transistor, as shown in Figure 3, due to the following reasons.

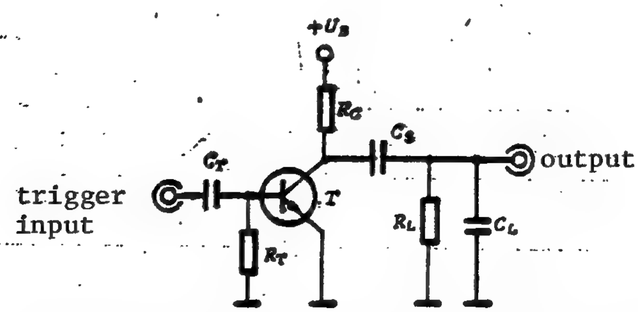


Figure 3. The Basic Avalanche Transistor Trigger Circuit

First, the wave form of the output pulse of the basic circuit is strongly dependent on the discharge time constant of the avalanche tube, $\tau_a = (C_S + C_L) R_L$. We selected a relatively good Model 2N5551 avalanche tube in our experiment. All the data reported in this paper were obtained with this type of tube. Figure 4 shows the output pulse wave forms at various capacitance values $C_S$ ($R_L = 50\Omega$). We can see that the amplitude of the pulse increases with increasing $C_S$. The rise and fall time of the pulse, however, also increase. Furthermore, $C_S$ has a larger effect on the trailing edge of the pulse than on the leading edge. When $C_S$ reaches 40 pF, the pulse amplitude no longer increases noticeably with $C_S$. The rise and fall time, however, continue to increase. Therefore, in order to get pulses of steeper edges, it is preferred to choose a small $C_S$. The price to pay, however, is to sacrifice some amplitude. When $C_S$ = 36 pF, pulses at 70-100 V can be obtained by using a selected 2N5551 tube on a 50Ω load. It is obvious that it is impossible to get the pulse amplitude required to control an optical gate with a basic circuit consisting of one avalanche tube.

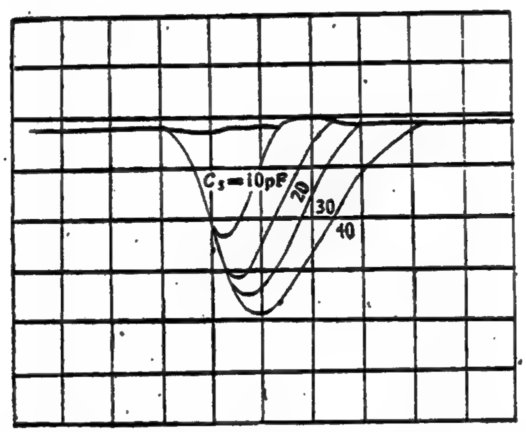


Figure 4. Output Pulse Wave Forms of the Basic Circuit at Various $C_S$'s (10, 20, 30, 40 pF) at $R_L$ = 50Ω; Y:20V/div; X:2 ns/div

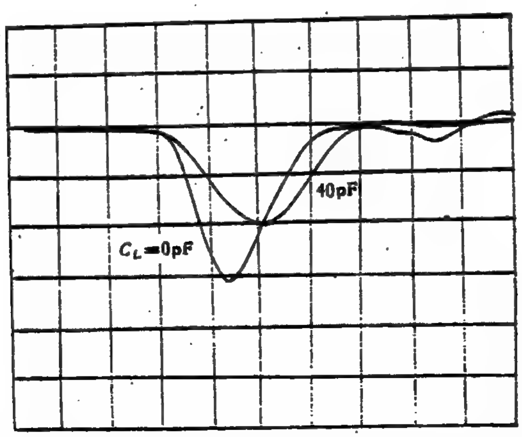


Figure 5. Output Pulse Wave Forms of the Basic Circuit at Various $C_L$'s (0, 40 pF) at $C_S$ = 20 pF and $R_L$ = 50Ω; Y:20V/div; X:2 ns/div

Next, the pulse wave form of the basic circuit is easily affected by capacitance load because the load capacitance $C_L$ will directly affect the discharge time constant of the avalanche tube. Figure 5 shows the effect of the load capacitance $C_L$ on the output wave form. Based on this figure, when $C_L = 40$ pF, the pulse amplitude drops to two-thirds of that at zero capacitive load. Furthermore, the half height width of the pulse increases to 4 ns. It is obvious that the basic circuit shown in Figure 3 cannot be directly used to drive an image intensifier with a high input capacitance.

In order to eliminate these two disadvantages, a new combination circuit is introduced. Through the use of two avalanche tubes operating in parallel, the avalanche currents are superpositioned on a common load to result in a pulse almost twice in amplitude as that obtained in the basic circuit (corresponding to the same $C_S$). The difficulty of choosing an appropriate avalanche tube is thus greatly reduced. In order to minimize the effect of the capacitance between the electrodes of the image intensifier on the pulse generated by the control pulse generator, a special pulse shaping network consisting of step diodes is introduced.

## 2. Basic Principle of the Combination Circuit

Figure 6 shows the schematic diagram of the control pulse generator. Through the simultaneous triggering of two avalanche tubes, their currents are superimposed on a common equivalent load. Thus, the resulting pulse amplitude is almost twice that of a single tube. The leading edge of the output pulse is determined by the difference between the rise time of the two tubes and the switching time. The trailing edge of the pulse is mainly determined by the stepping time $T_f$ of the step diode used for pulse shaping. By adjusting the positive current $I_f$ of the step diode and changing the storage time $T_S$, we can obtain almost symmetric sharp pulses. The basic principle of the combination circuit is explained in the following based on the diagram shown in Figure 7.

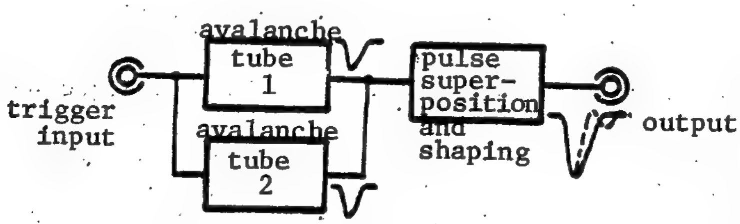


Figure 6. Diagram of the Control Pulse Generator

In the static state (without trigger signal input), diodes $D_1$ and $D_2$ are biased at $+U_1$ and $-U_2$ so that $D_1$ is on and $D_2$ is off. The forward current $I_f$ passing through $D_1$ can be adjusted by the bias $+U_1$:

$$I_f = \frac{+U_1}{R_{D1} + R_{D3} + R_S + r_f} \tag{1}$$

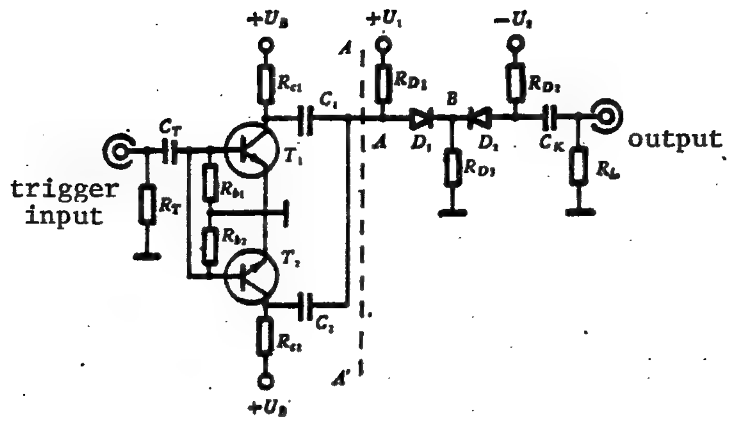


Figure 7. Principle of the Control Pulse Generator

where $r_f$ is the forward resistance of $D_1$ and $R_S$ is the serial resistance of $D_1$. The circuit on the right side of the dotted line AA' in Figure 7 can be expressed by an equivalent resistance $R_E$

$$R_E = R_{D1} // (R_s + r_f + R_{D3}) \tag{2}$$

Thus, an equivalent circuit of the generator such as the one shown in Figure 8 is obtained.

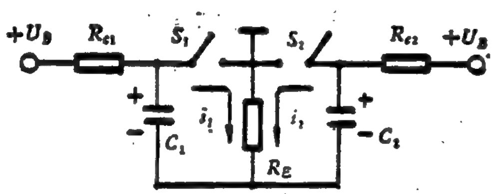

Figure 8. Equivalent Circuit of the Generator

The energy storage capacitors $C_1$ and $C_2$ in Figure 8 are charged by the power source $+U_B$ through a large resistance to a voltage slightly lower than the breakdown voltage $BV_{CBO}$ of the transistor across the collector and the base. The prerequisite condition is that the breakdown voltage of various transistors cannot vary too much. This can be ensured by adding a small resistor between the base and the collector of each transistor and by choosing the appropriate transistors. The two avalanche tubes are expressed by two ideal switches, $S_1$ and $S_2$, respectively.

If both avalanche tubes are simultaneously triggered by a positive pulse, then switches $S_1$ and $S_2$ in Figure 8 will close. Capacitors $C_1$ and $C_2$ will discharge through switches $S_1$ and $S_2$ and the equivalent resistance $R_E$. A voltage pulse $V_{RE} = (i_1 + i_2) R_E$ is generated on $R_E$. Of course, the rise time of the pulse generator on $R_E$ is equal to the avalanche rise time $T_a$ of a single transistor only when both tubes have the same characteristics. If the two avalanche tubes

have different rise times or there is a difference in their on times, the leading edge of the composite pulse will be slowed down. A "twist" effect, such as the one shown in Figure 9, may even result. Therefore, we must select the avalanche tubes used in the combination circuit.

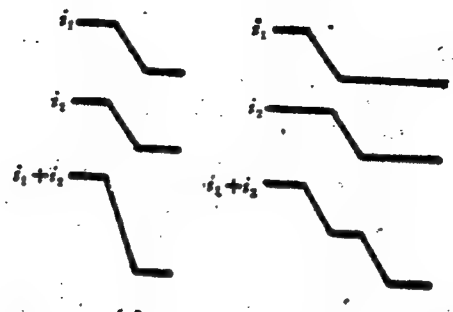


Figure 9. Superposition of Two Avalanche Pulses

Now, let us explain the operating principle of the circuit on the right side of the dotted line AA' in Figure 7. As described before, in the static state, the diode $D_1$ is biased forward and its forward resistance $r_f$ is very small. Therefore, points Ⓐ and Ⓑ in the figure can be considered as a short circuit. The diode $D_2$, on the other hand, is cut off in the inverse direction. When both avalanche tubes are simultaneously triggered, a large amplitude negative pulse will appear near point Ⓐ. Due to the charge storage effect of the step diode, the diode $D_1$ is still conducting within the storage period $T_S$ which is determined by the forward current $I_f$. Therefore, the negative pulse will also reach point Ⓑ. At this time, the reverse current $I_r$ is the step diode $D_1$ will continue to flow until the minority carriers stored near the junction is totally depleted. After the storage period $T_S$, the diode $D_1$ will rapidly enter a reverse cutoff state. Thus, the reverse current will steeply reach its saturation limit (within the stepping time $T_f$). Figure 10 shows the pulse shaping effect of the step diode on the trailing edge of the pulse. Figure 10(a) shows an avalanche pulse prior to being shaped. Its trailing edge is much slower than its leading edge. Figure 10(b) shows the current wave forms corresponding to diodes with various $T_S$. In the figure, Curve 2 is the optimum case where the storage time $T_S$ is over once the avalanche pulse amplitude reaches its maximum. In this case, the amplitude of the output pulses, the maximum and the base width of the pulse is equal to the sum of the avalanche rise time $T_a$ and the step time $T_f$. The following relation exists for $T_S$, $I_f$ and $I_r$[3]:

$$T_s = \tau \ln\left(1 + \frac{I_f}{I_r}\right) \tag{3}$$

where $\tau$ is the lifetime of the minority carrier. Because it involves the shaping of large amplitude pulses, the reverse current $I_r$ in equation (3) is very large. In order to have a certain storage time $T_S$ (which is necessary

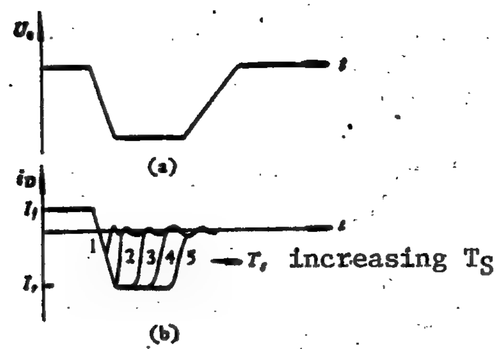


Figure 10. Using Step Tube To Improve the Trailing Edge of the Pulse

to shape the trailing edge of the pulse), we have to increase $I_f$ or $\tau$. In addition, the diode $D_1$ must have a high breakdown voltage and be able to sustain high power pulses. This is actually too critical a requirement for the step diode. To this end, the step diode used for pulse shaping has been specially designed.[4] Suitable tubes may also be chosen from high reverse voltage microwave variable capacitance step power tubes.

The high-speed Schottky diode $D_2$ is used to further shape the pulses. A reverse bias $U_{D2}$ is applied on the diode $D_2$ to regulate the adjustment of $-U_2$ in order to eliminate the oscillation at the bottom of the pulses. Furthermore, it can reduce the effective width of the output pulses, as shown in Figure 11.

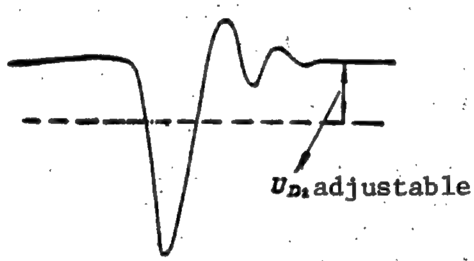


Figure 11. Shaving the Wave by Using a Schottky Diode

## 3. Results of Measurements

The output wave forms of the control pulse generator developed at various loads are shown in Figures 12 and 13. The wave form generated on a pure resistive load (50Ω) is fairly symmetric with negligible oscillation (see Figure 12). When it is triggered by a 5 ns, 5 V pulse, the delay time of the generator is 5 ns. If a trigger pulse with a steeper leading edge is used, then the delay will be even shorter. When a 40 pF capacitor is connected parallel to the output load (50Ω), the effect on the output wave form is not significant (see Figure 13).

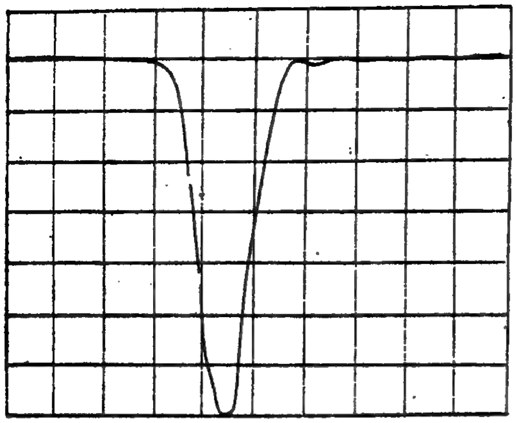

Figure 12. Wave Form of the Generator on a Pure Resistive Load (50Ω); Y:25V/div and X:2 ns/div

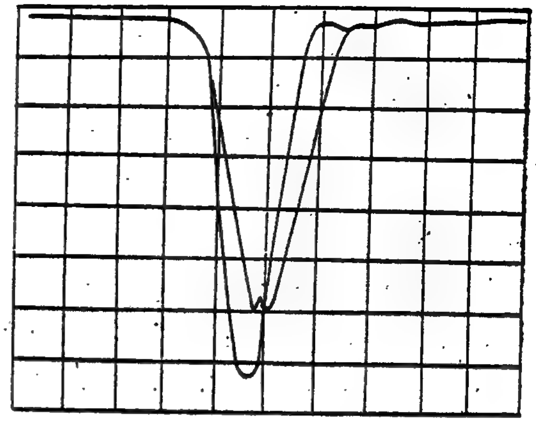

Figure 13. Effect of Capacitive Load on the Wave Form of the Pulse Generator; Y:25V/div and X:2 ns/div

4. Connecting the Pulse Generator to the ITT-F4111 Image Intensifier

If the pulse generator is directly connected to the ITT-F4111 image intensifier as shown in Figure 7, the result is still not satisfactory because the load in this situation is no longer a purely resistive 50Ω load. Instead, it is the impedance between the photocathode and the microchannel plate input of the image intensifier. As we mentioned earlier, $R_i = 4 \times 10^{10}\Omega$ and $C_i = 23$ pF. In addition, based on the relative optical gain $V_L$ vs photocathode voltage $U_C$ curve shown in Figure 2, we know that the optical gate may be opened to various extent when only a few volts is applied to the photocathode. If the wave form of the control pulse is not an ideal triangle, then the oscillation superimposed to the bottom of the pulse may lead to the continuous opening of the optical gate, resulting in multiple exposures. This must absolutely be avoided. To this end, another pulse shaping and dc bias circuit is introduced between the pulse generator and the image intensifier to result in the complete circuit for a photocathode controlled image intensifier, as shown in Figure 14.

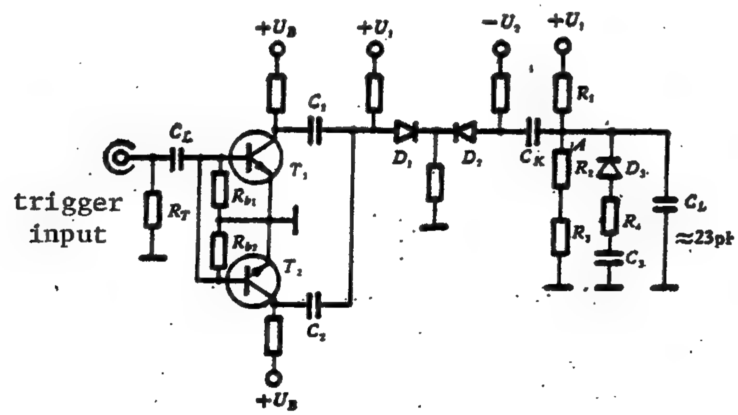


Figure 14. Complete Circuit of a Photocathode Controlled Image Intensifier

This circuit has the following functions. On one hand, for direct current, resistors $R_1$, $R_2$ and $R_3$ constitute a dc voltage divider which is used to shift the reference voltage (i.e., to change the voltage at point A in Figure 14) of the pulse output. Consequently, the reference voltage of the output pulse is $+U_A$, instead of 0. The function of the voltage biasing circuit is shown in Figure 15. Figure 15(a) shows that the oscillating amplitude at the bottom of the pulse is sufficient to cause the optical gate to open many times when the reference voltage of the pulse output is 0V. In Figure 15(b), with the aid of the voltage divider, the reference voltage is made to be $+U_A$. As long as $U_A$ is sufficiently large, it is possible to reliably prevent the opening of the optical gate due to the oscillation at the bottom of the control pulses. On the other hand, in terms of alternating current, the right side of the coupled capacitor of the pulse generator ($C_K$ in Figure 14) is an ac load. Therefore, the output pulse is not affected by the large dc resistance between the electrodes in the image intensifier. The nonlinear circuit consisting of the diode $D_3$ and $R_4$ and $C_3$ is used to further shape up the pulse. $D_3$ is a Schottky diode with an extremely low capacitance. The optimal values of $R_4$ and $C_3$ are determined experimentally.

Another function of the voltage biasing circuit is to adjust the effective width of the output pulse, resulting in a shorter exposure time. Of course, it is done at the expense of some optical gain because the effective amplitude of the pulse is also decreased with decreasing effective pulse width.

The super-high-speed camera, comprised of a control pulse generator and an image intensifier as the optical shutter, which is capable of capturing faint instantaneous single events with a response in the nanosecond range, has already been used in the study of high-speed physical phenomena.[5]

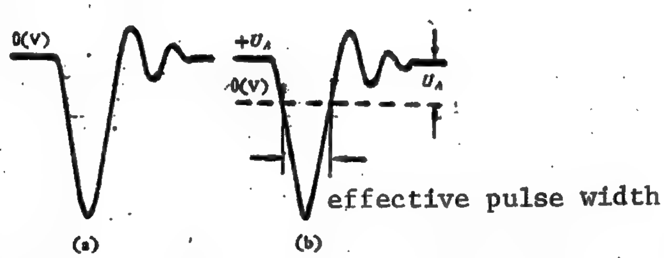


Figure 15. Function of the Voltage Biasing Circuit

This work was performed at the Institute of Electrical Measurement of Darmstadt Polytechnical University in West Germany.

REFERENCES


1. Hallock, F.S., SMPTE JOURNAL, Vol 89, 1980 p 709.

2. "Generation II Proximity Focused Channel Intensifier Tubes," ITT-Druckschrift F-4111.

3. Moll, J.L., et al., PROC. IRE, Vol 50, 1962 p 43.

4. Zhang Zhizhong [1728 1013 0022] and Zhou Xuan, WULI XUEBAO [CHINESE JOURNAL OF PHYSICS], Vol 30, 1981 p 84

5. Zhou Xuan, Volker, P., Forschungsberict des Fachgebietes Elektrische Meßtechnik, TH Darmstadt, 1980 pp 16-20.

12553/9365
CSO: 4008/1050

APPLIED SCIENCES

# DELAY EFFECT IN PULSED AVALANCHE DISCHARGE OF AN XeCl LASER AT HIGH GAS PRESSURE

Beijing WULI XUEBAO [ACTA PHYSICA SINICA] in Chinese Vol 34, No 7, Jul 85 pp 960-963

[Article by Lou Qihong [2869 4388 3163], Shanghai Institute of Optics and Precision Mechanics, CAS; manuscript received 28 August 1984]

[Text] Abstract. The pulsed avalanche discharge process in an XeCl laser at pressures up to 10 atm is analyzed and the effect of the delay phase on discharge formation time is discussed. By a comparison with experimental results for a pulsed avalanche discharge in an XeCl laser, a critical avalanche track length of about 1 mm is derived.

Avalanche/Self-sustained discharges are extensively used in excimer lasers; analysis of the physical principles of this type of discharges at high gas pressures. Palmer [1] established a simple physical model for estimating the minimum preionization density for uniform glow discharges at high gas pressures, in which the pulse voltage is applied at both edges of the discharge electrodes as a stepwise increasing function; shortly thereafter Levatter and Lin [2] considered the effect of finite voltage rise time on the discharge process, using working gas pressures below 3 atm. Below we analyze the pulsed avalanche discharge process at pressures up to 10 atm and discuss the effect of the delay phase on the discharge formation time; through a comparison with experimental results for a pulse avalanche discharge in an XeCl excimer laser we derive a critical track length of about 1 mm for the avalanche discharge.

## I. Pulse Avalanche Discharge Experiments at High Gas Pressures

In our experiments we used a small discharge apparatus driven by an X-ray preionization pulse forming network, whose construction and voltage measurement technique are described in Ref 3.

We first used a Rogowski coil to determine the discharge voltage waveform at a total gas pressure of 5 atm. The pulse forming network consisted of four high-voltage coaxial cables with characteristic resistances of 50 ohms, connected in parallel to give a characteristic resistance of 12.5 ohms. The gas discharge area was 2 $cm^2$ and the electrode spacing was 1 cm. Discharge circuit analysis indicated that when the load resistance R(t) was less than

Figure 1.

Voltage waveform of pulsed avalanche discharge in XeCl laser, showing impedance matching effect (time scale 50 ns per division; vertical scale 6 kV per division)


the characteristic resistance Z of the pulse shaping network, the voltage waveform consisted of damped oscillations whose second peak amplitude $U_2$ was related to its first peak amplitude $U_1$ by the ratio

$$-\frac{U_2}{U_1}=\frac{R-Z}{R+Z}. \qquad (1)$$

The negative sign on the left side of this equation indicates that $U_2$ and $U_1$ are of opposite sign. Figure 1 shows the discharge voltage waveform for an Ne:Xe:HCl ratio of 989:10:1. From the ratio of $U_2$ to $U_1$ we can determine the average value of R, 0.67Z = 8.4 ohms; this is rather close to the steady-state resistance of 7.6 ohms that we reported in Ref 3. The above result indicates that the line mismatch is not serious.

Under the working conditions described above, we determined the voltage waveform for a total gas pressure of 2-10 atm. It can be seen in Figure 2 that at 5 atm or less the voltage waveform agrees with the analysis in Ref 2: when the pulse voltage has risen linearly to a certain value, the laser medium rapidly becomes conductive and passes over to a pseudo-steady-state discharge. If we define the time elapsing between the maximum voltage and the steady state as the discharge buildup time $t_p$, then for $P \geq 5$ atm, $t_p \geq 20$ ns, while when $P>5$ atm the voltage waveform changes: there is a delay phase between the time that the voltage applied to the discharge gap rises rapidly and the phase during which the gas is conductive; the delay becomes more pronounced as the gas pressure is increased. When this delay phenomenon occurs, $t_p$ also increases with increasing gas pressure. Figure 2 also shows the range of $t_p$ for certain gas pressures; for clarity, $t_p$ is given only for total gas pressures of 2, 6 and 10 atm. Because the discharge process is somewhat random, the values presented in Figure 2 are a group of typical values. It will be seen below that the experimental data are obtained by averaging the values from 5 or more experimental photographs.

In addition, our experimental results also indicated that the delay phenomenon is inversely related to the initial voltage of the pulsed discharge source, decreasing when the source voltage rises. But if an excessively high initial voltage issued, the laser efficiency may be extremely low. In ordinary transverse-discharge excimer lasers, the usual initial voltage is 20-30 kV per centimeter of gap width in order to keep the laser in relatively high-efficiency operation. Since we studied the delay phenomenon under the conditions described above, we kept the initial discharge voltage constant and studied the delay phenomenon under these constant-voltage conditions.

Figure 2.

Voltage waveform for pulsed avalanche discharge in XeCl laser at 10 atm (vertical scale, 13 kV per division).

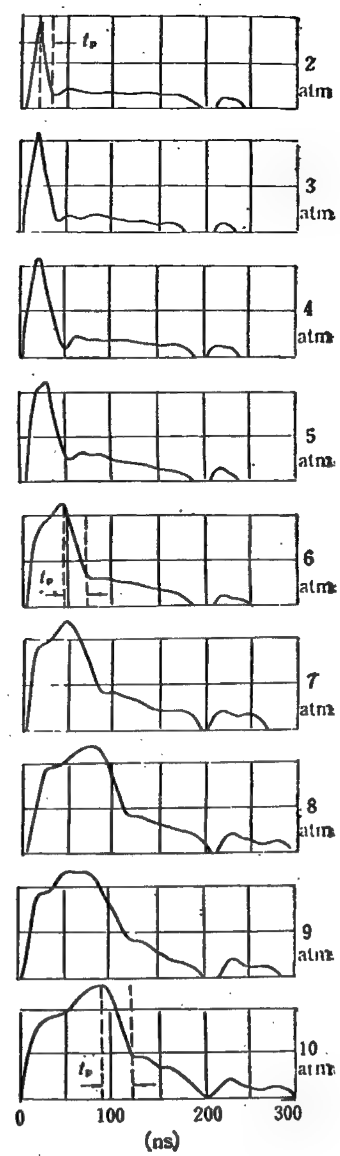


The above experimental results indicate that as the working gas pressure of the laser is increased, the pulsed avalanche discharge process acquires new characteristics.

## II. Analysis of the Discharge Formation Process at High Gas Pressure

According to the general theory of gas discharges, there are two discharge mechanisms: the slow process, also called the Towsend mechanism, which does not take account of the space charge field produced by charged particles, and the fast, streamer process, also called the channel mechanism, which takes account of a strong space charge field and passes over directly from a primary electron avalanche into a streamer discharge; if this discharge is not controlled, it readily becomes a spark channel. In order to suppress the development of a spark channel, the preionization technique can be used.

Based on the analysis in Ref 2, when the applied voltage rises linearly, the electron avalanche head radius $r_c$ at the initial breakdown is approximately

$$r_c \cong (40\xi_c \bar{\lambda}_e)^{1/2}, \qquad (2)$$

where $\xi_c$ is the critical discharge track length and $\bar{\lambda}_e$ is the electron mean free path. In order to obtain a uniform discharge, the streamer discharge must develop uniformly in each part of the discharge area, which requires that the average initial electron density $n_{e0}$ in the cathode surface layer satisfy the condition $n_{e0}>(r)-3$.

As the total gas pressure is increased, the electron mean free path $\bar{\lambda}_e$ decreases, so that $r_e$ falls as the gas pressure rises. In the present approximation, we ignore the change in $n_{eo}$ with gas pressure; then the discharge buildup time $t_p$ is given by

$$t_p \simeq \frac{\xi_c}{u_e}, \qquad (3)$$

where $u_e$ is the electron drift velocity in the discharge. According to Boltzmann coding calculations for XeCl excimer lasers, $u_e$ is a function of E/n, such that when E/n increases from $10^{-16}$ to $5 \times 10^{-16}$ V-cm$^2$, $u_e$ rises from $8 \times 10^6$ to $3.2 \times 10^7$ cm/sec; the relationship can be expressed described by an approximately linear formula. In our experiments, as the gas pressure was increased the number of particles n per unit volume rose; in addition, because the breakdown voltage increased and the delay was lengthened, the average field intensity E in the working gas before breakdown increased as a function of the gas pressure, but the rate of increase of E was much less than the rate of increase of n, so that E/n fell as the gas pressure rose, further lowering the electron drift velocity in the avalanche process.

For an Ne:Xe:HCl ratio of 989:10:1, we found the change in $t_p$ as a function of at different gas pressures from Figure 2. For the sake of accuracy, we averaged the results from five similar experimental photographs. These results are shown in Figure 3 by the dotted line. However, when we calculated the values of E/n and $u_e$ for different gas pressures, we obtained the interesting result that the product of $t_p$ and $u_e$ was essentially unchanged at different gas pressures, which means that the critical track length $\xi_c$ was not sensitive to changes in gas pressure (under our experimental conditions as described above). The values of $t_p$ calculated for various gas pressures from equation (3) with $\xi_c$ = 1 mm are shown in Figure 3; the agreement is excellent.

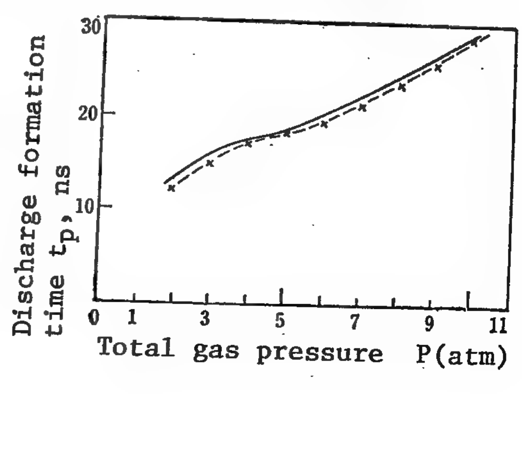


Figure 3.

Discharge formation time vs total gas pressure. Solid line gives theoretical calculated value, dotted line gives experimental results

## III. Conclusions

The analysis above indicates that when the total gas pressure exceeds 5 atm, the delay in discharge initiation has a rather large effect on the discharge buildup time; this delay phenomenon is statistical in nature and the delay time is inversely proportional to the probability W that a primary electron will start an avalanche. W in turn increases as the gap overvoltage rises. In the experiments described above, in order to maintain a constant stored energy value, we maintained the power supply voltage constant. In order to decrease the effect of this delay phenomenon, the voltage must be increased at high gas pressures so that it operates in a good overvoltage state, but this greatly increases the stored energy in the power supply and decreases the laser efficiency. In order to overcome this conflict, the two-pulse technique can be used, in which a high-overvoltage pulse can be used to decrease the delay, immediately followed by a lower-overvoltage pulse to increase device efficiency. This approach has already been used successfully.

On the other hand, the above comparison of theory and experimental results gives a critical avalanche track length of about 1 mm for a pulsed avalanche discharge in an XeCl excimer laser. This result is in agreement with the value $\xi_c$ = 1-2 mm reported in Ref 2 for mixed gas in an XeF laser with a voltage rise time of between 10 and 20 ns and thus provides an indirect method of determining $\xi_c$.

Comrade He Qisheng [0149 7784 3932] took part in the experiments, and we express our thanks to him.

## BIBLIOGRAPHY

1. Palmer, A.J., J. APPL. PHYS. LETT., Vol 25 (1974), p 138.

2. Levatter, J.I., and Lin, S.C., J. APPL. PHYS., Vol 51 (1980) p 210.

3. Lou, Q.H.; He, Q.S.; and Lin, S.C., APPL. PHYS. LET, Vol 41 (1982) p 514.

8480/8918
CSO: 4008/408

APPLIED SCIENCES

# PSEUDOINVERSE RESTORATION OF BLURRED IMAGE IN UNIFORM MOTION

Chengdu SICHUAN UNIVERSITY (ZIRAN KEXUE BAN) [JOURNAL OF SICHUAN UNIVERSITY (NATURAL SCIENCE EDITION)] in Chinese No 2, 1985 pp 44-49

[Article by Si Xianyu [5685 7359 3254], Zhang Guanshen [1728 0385 3947], Zhang Shaoying [1728 1421 4481] and Li Yongguo [2621 3057 0948], manuscript received on 22 December 1983: "A Pseudoinverse Restoration Method for Blurred Image in Uniform Motion"]

[Text] Abstract: In this paper, the mistakes in the iteration formula for the restoration of blurred images in uniform motion in reference [1] are identified. The correct formula is given. In addition, a pseudoinverse restoration method, which adds a corrected image to a basic image, is introduced. Results obtained from the computer show that this method is effective.

## 1. Introduction

In the image forming process, due to various reasons, there is a relative motion between the recording device and the image. For example, if the camera moves relative to the scene, the photograph taken will become blurred. Restoration of blurred images due to uniform motion is one of the topics in image processing. An iteration formula for the restoration of blurred images in uniform motion was discussed in the literature.[1] Because of a mixup of variables, however, a wrong equation was derived. In this paper, the iterative restoration formula was re-derived. In addition, based on the concept of pseudoinverse restoration, a pseudoinverse restoration method involving adding a corrected image to the basic image was introduced. The feasibility of this method was proven by simulations performed on a microprocessor.

## 2. Re-derivation of the Iteration Formula

Let us assume that the original image f(x) is moving uniformly along a straight line in the x-direction, the length of the frame is L, and the image moves by a distance a within the exposure time T. Assuming L = ka and k is an integer, then the blurred image becomes

$$g(x)=\int_0^T f\left(x-\frac{a}{T}t\right)dt \qquad (1)$$

A discrete formula is used to express this blurring process. Let us choose the frame length to be L image elements and the distance of the image movement to be a image elements, then

$$g(x) = \frac{1}{a}\sum_{n=0}^{a-1} f(x-n), \quad x = 0,\ 1,\ \cdots\ L-1 \tag{2}$$

$$g'(x) = g(x) - g(x-1), \tag{3}$$

is used to represent the partial difference of the blurred image. By substituting equation (2) into (3) we get

$$f(x) = ag'(x) + f(x-a)$$

Let us introduce two variables: Z and m. x = Z + ma, and m is the integer part of x/a. Z = 0, 1, ••• a − 1. The above equation can be written as:

$$f(Z+ma) = ag'(Z+ma) + f[Z+(m-1)a] \tag{4}$$

Let $\phi(Z)$ be the portion moved into the frame from the outside during the exposure period, i.e. $\phi(Z) = f(Z - a)$. Hence

When m = 0, $f(Z) = ag'(Z) + \phi(Z)$

m = 1 $f(Z+a) = ag'(Z+a) + f(Z) = ag'(Z+a) + ag'(Z) + \phi(Z)$

By iteration, we get

$$f(Z+ma) = a\sum_{k=0}^{m} g'(Z+ka) + \phi(Z) \tag{5}$$

In the range $ka \leqslant x < (k+1)a$, both sides of equation (5) are calculated. In addition, k equations corresponding to m = 0, 1, ••• k − 1 are added on both sides to obtain

$$\sum_{m=0}^{k-1} f(K+ma) = a\sum_{m=0}^{k-1}\sum_{k=0}^{m} g'(Z+ka) + k\phi(Z)$$

i.e.

$$\phi(Z) = \frac{1}{K}\sum_{m=0}^{k-1} f(Z+ma) - \frac{a}{K}\sum_{k=1}^{k-1}(K-k)g'(Z+ka) \tag{6}$$

Substituting it into equation (5), we get

$$f(x) = \frac{1}{K}\sum_{m=0}^{k-1} f(Z+ma) + a\sum_{k=0}^{m} g'(Z+ka) - \frac{a}{K}\sum_{k=0}^{k-1}(K-k)g'(Z+ka) \tag{7}$$

The first summation on the right is also unknown. For large k's, it approaches the average of f(x). Thus, it is approximately a constant, A. Hence

$$f(x) \doteq A + a\sum_{k=0}^{m} g'(Z+k_a) - \sum_{k=0}^{k-1} (K-k)g'(Z+ka) \tag{8}$$

The result in reference [1] is mistaken because variables m and k were mixed up. This conclusion was confirmed experimentally.

3. The Psuedoinverse Restoration Method

The uniform motion blurring process described above can be calculated in an equivalent vector space. Let us assume that the initial image vector is f and its sample number is m, the blurred image vector is g and its sample number is n, and the displacement is a = m - n, then the uniform speed blurring process can be expressed by the following vector matrix:

$$\boldsymbol{g} = \boldsymbol{H}\boldsymbol{f} \tag{9}$$

where

$$\boldsymbol{f} = [f(0)\ f(1)\ \cdots\ f(m-1)]^T$$
$$\boldsymbol{g} = [g(0)\ g(1)\ \cdots\ g(n-1)]^T$$

$$\boldsymbol{H} = \begin{pmatrix} 1 & 1 & \cdots & 1 & & & & 0 \\ & 1 & 1 & \cdots & 1 & & & \\ & & 1 & 1 & \cdots & 1 & & \\ & & & \ddots & \ddots & & \ddots & \\ 0 & & & & \underbrace{1 \quad 1 \quad \cdots \quad 1}_{a+1} & & & \end{pmatrix}. \tag{10}$$

H is an n x m right shifting cyclic matrix. The restoration problem is reduced to solving the matrix equation. Because m > n, the number of unknowns is larger than that equations. Therefore, there are infinite number of solutions. Hence, it is difficult to restore accurately. Based on the concept of a generalized inverse matrix, the least modular solution $f_{min}$ of the image vector f can be determined.

$$\boldsymbol{f}_{min} = \boldsymbol{H}^T(\boldsymbol{H}\boldsymbol{H}^T)^{-1}\boldsymbol{g} \tag{11}$$

Because the original image does not necessarily have the least amount of energy, however, the least modular solution is not an accurate estimation of the original image.

Based on the concept of psuedoinverse restoration,[3] a method to add a corrected image to the basic image is introduced. The general solution to equation (9) can be expressed as

$$f = H^R g q (I_n - H^{RO} H) y \tag{12}$$

where $H^R$ is a right inverse matrix of H, $I_m$ is a unit vector, and y is an arbitrary m x 1 column vector. Let us denote the right inverse matrix of H whose first a rows of elements are zero to be $H^{RO}$, then equation (12) can be rewritten as

$$\begin{aligned} f &= H^{RO} g + (I_n - H^{RO} H) y \\ &= f_0 + f_y \end{aligned} \tag{13}$$

We can also prove that

$$H^{RO} = \begin{pmatrix}
0 & 0 & 0 & 0 & \cdots & \cdots & \cdots & \cdots & \cdots & \cdots & 0 & & \\
\vdots & & & & & & & & & & \vdots & & \\
\vdots & & & & & & & & & & \vdots & & \\
0 & 0 & 0 & 0 & \cdots & \cdots & \cdots & \cdots & \cdots & \cdots & 0 & & \\
1 & & & & & & & & & & & & \\
-1 & 1 & & & & & & 0 & & & & & \\
0 & -1 & 1 & & & & & & & & & & \\
\vdots & & & & & & & & & & & & \\
\vdots & 0 & -1 & 1 & & & & & & & & & \\
0 & & 0 & -1 & \ddots & & & & & & & & \\
1 & 0 & & 0 & \ddots & \ddots & & & & & & & \\
-1 & 1 & 0 & & \ddots & \ddots & \ddots & & & & & & \\
0 & -1 & 1 & 0 & & \ddots & \ddots & \ddots & & & & & \\
\vdots & & \ddots & \ddots & \ddots & \ddots & \ddots & \ddots & \ddots & & & & \\
\vdots & & & \ddots & \ddots & \ddots & \ddots & \ddots & \ddots & \ddots & & & \\
0 & & & & \ddots & \ddots & \ddots & \ddots & \ddots & \ddots & & & \\
\triangle & 0 & \cdots & \cdots & 0 & -1 & 1 & 0 & \ddots & \ddots & 0 & -1 & 1
\end{pmatrix} \tag{14}$$

Furthermore, we find

$$
I_m - H^{RO}H = \left(\begin{array}{ccccc:c}
1 & & & & 0 & \\
 & 1 & & & & \\
 & & \ddots & & & \\
 & & & \ddots & & 0 \\
 & & & & \ddots & \\
0 & & & & 1 & \\
-1 & -1 & \cdots & \cdots & -1 & \\
\hdashline
1 & & & & 0 & \\
 & 1 & & & & \\
 & & \ddots & & & \\
 & & & \ddots & & 0 \\
 & & & & \ddots & \\
0 & & & & 1 & \\
-1 & -1 & \cdots & \cdots & -1 & \\
\hdashline
1 & & & & 0 & \\
 & 1 & & & & \\
 & & \ddots & & & 0 \\
 & & & \ddots & & \\
\multicolumn{5}{c:}{\underbrace{\hspace{6cm}}_{a}} & 
\end{array}\right) \tag{15}
$$

We can see that the last m - a elements are unrelated to the result of equation (13). Let $y = y_a = [y(1)\ y(2) \cdots y(a)\ 0\ 0 \cdots 0]^T$. Thus, equation (13) can be simplified as

$$
\begin{aligned}
f &= H^{RO}y + (I_m - H^{RO}H)y_a \\
&= f_0 + f_a
\end{aligned} \tag{16}
$$

The physical significance of the above equation is very obvious. The first term $f_0$ is the special solution of the vector matrix equation (9), which is the basic image. The first a image elements of the basic image are 0. This is a result of choosing the blurred image g as the blurring of a specific part of the original image outside the frame with some zero elements. The second

term $f_a$ represents the correction of the basic image based on an estimated value $y_a$ for the part outside the frame when that part is not zero. It is called the correction image. Because the basic and correction images are separated, it is possible to estimate the portion outside the frame according to different criteria to conduct an interactive restoration. Notice that the elements of $H^{RO}$ and $(I_m = H^{RO}H)$ only include 0 and +1, it is possible to avoid matrix multiplication when using equation (16) in the computation. Simple addition and subtraction can be used directly to drastically reduce the work load.

## 4. Experimental Results and Discussion

This method was simulated on a microprocessor. A FORTRAN subroutine was used to display the image as a gray toned image given by a conventional printer. Different characters are overlapped to print out different tones of gray. The results are shown in Figure 1. Figure (a) shows the initial image and the length of the image is 64 image elements. (b) shows the blurred image created by the uniform motion. The image shift distance is seven image elements. It is no longer possible to recognize the content of the original image based on this figure. (c) shows the result restored by using the method introduced in this work.

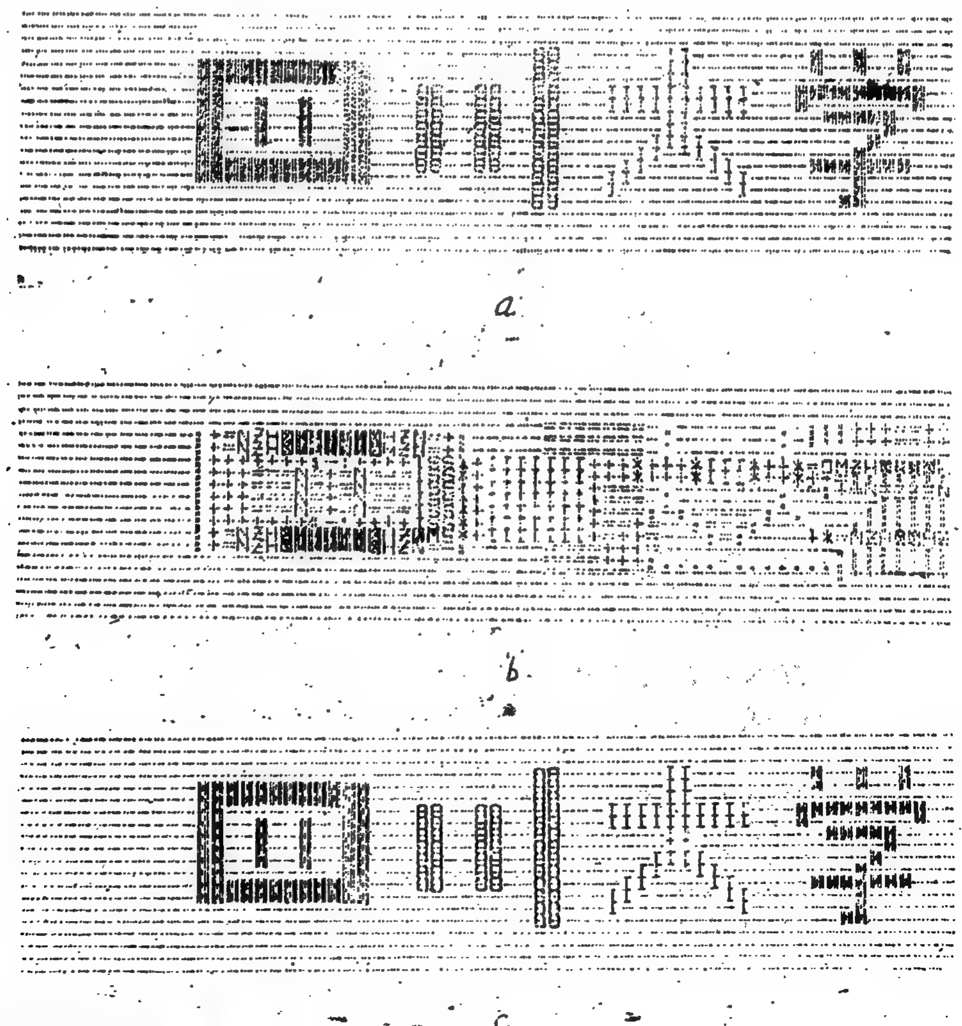




Figure 1

As for estimating the portion outside the frame, different criteria may be adopted. The simplest criteria are the average criterion and the equal grayness criterion in neighboring areas. The former gives an estimation based on the mean value of the blurred image and the latter gives an estimation based on the average of the blurred image in the frame and the adjacent area outside the frame. There are other methods. The pseudoinverse restoration method based on adding a correction image to the basic image will facilitate the use of various criteria to restore the image.

REFERENCES

1. Gonalez, R.C. and Wintz, P., "Digital Image Processing," Addison-Wesley, London, 1977.

2. Liu Zhizhen [0491 2748 2823], et al., MECHANICAL CONTROL, Beijing, Qinghua University Press, 1981.

3. Pratt, W.K., "Digital Image Processing," John Wiley and Sons, Inc., New York, 1978.

12553/9365
CSO: 4008/1074

SCIENTISTS AND SCIENTIFIC ORGANIZATIONS

## FUJIAN MATERIALS STRUCTURE INSTITUTE DESCRIBED

Beijing HUAXUE TONGBAO [CHEMISTRY] in Chinese No 7, 18 Jul 85 pp 58-59

[Article by Wu Dingming [0702 7844 6900]]

[Text] The Fujian Materials Structure Institute of the Chinese Academy of Sciences (FMSI hereafter) is located at the western suburb of Fuzhou on the banks of the Min Jiang. Situated at the foot of a hill and beside a stream, it commands magnificent views. It was established in 1960 by consolidating the six institutes--Technological Physics, Applied Chemistry, Electronics, Mathematical Mechanics, Automation and Rare Metals--earlier planned and established by the Fujian branch of the Chinese Academy of Sciences. In September 1961, it was further consolidated and reorganized into the Institute of Physical Sciences in accordance with the then enacted Eight Character Policy. In January 1962, it was renamed Huadong Materials Structure Institute and was subordinate to the Huadong branch of the Chinese Academy of Sciences. Its name was changed to the Institute No 7701 of the Office of Defense Industry, Fujian Province in 1970 and was finally settled in 1973 as the Fujian Materials Structure Institute of the Chinese Academy of Sciences.

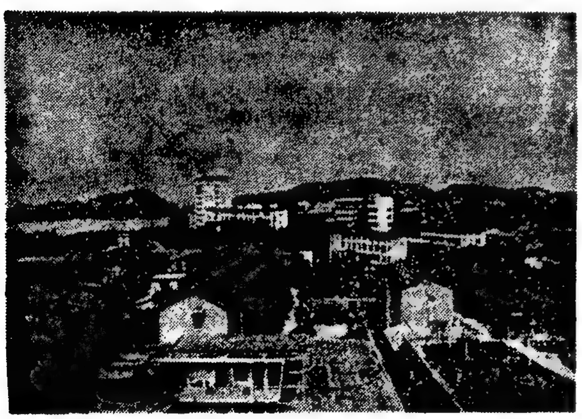

Ourdoor scene of FMSI

Professor Lu Jiaxi looking up literature

Through 20 some years of development, FMSI's own characteristic research emphasis has gradually evolved. They include, within the area of structural

chemistry, the exploration of the relationship between the macroscopic properties (chemical and physical) and the crystal and molecular structure of new type compounds; systematically carrying out the basic and applied research aiming at transition metal complexes (particularly atom cluster compounds), biological macromolecules and crystals as primary targets; properly probing structure research methodologies and raising research standards; development of catalysts, new technology crystals and the applied and developmental research on metal corrosion and its prevention in light of the economic construction needs; and emphasizing the combination of theory and practice, chemistry and physics as well as structure and property in order to build step-by-step a prominent, integrated research institute of structural chemistry.

Based on its developmental goals and research responsibilities, FMSI has set up laboratories in the areas of structural chemistry, new technology crystals; complex catalysis, analytical chemistry and the Shamen Sea Water Corrosion Experimental Station. There are also research supporting units such as computer station and books and information service. Furthermore, there are the small-scale production workshop of new technology crystals that have been through the research stage, the machine shop to meet the scientific research needs and a general service system that serves the whole institute. The institute currently employs more than 570 people, including over 370 research and technical personnel, in which 13 are senior researchers and over 200 are research assistants and engineers. Current director of the institute is Liang Jingkui [2733 2417 7608], a research fellow.

Lu Jiaxi [4151 0857 6932], the renowned structural chemist and the president of the Chinese Academy of Sciences, is the founder of FMSI and was its director until 1984 when he stepped down and served as its honorary director. Professor Lu studied at the London University of England in his early years and obtained a PhD. From 1939 to 1945, he was engaged in research at the California Institute of Technology and the University of California of the United States and published several papers on radiation chemistry and structural chemistry. He returned in 1945 and was involved in teaching, scientific research and the leadership role in the teaching body at the Shamen and Fuzhou University. He has trained for the country a number of talents in chemistry and physics, many of whom have become the key members in scientific research and teaching. In 1960, he started FMSI and poured in a tremendous amount of effort for the planning, construction, development and growth of the institute. Now he is still in charge of and cares about all aspects of the institute. He also directs the key research projects of the academy such as the structural model study of the active center of nitrogen fixation in nitrogenase and synthesis of its analogs and the synthetic chemistry and structural chemistry of molybdenum, iron and Mo-Fe cluster compounds (particularly the sulfur containing cluster compounds).

FMSI has all kinds of modern research tools and testing capability of structural chemistry. There are large precision instruments such as the PDP-11/70 computer, FTS-20E/D-V Fourier-transformed Infra-red spectrophotometer, PSM-50L ultraviolet spectrophotometer, PE-306 atomic absorption spectrophotometer, G.P3.5-D high-frequency ionic emission spectrophotometer,

Model 1106 elemental analyzer, Finnigan-MAT 312 mass spectrometer, FT-80A nuclear magnetic resonance spectrometer, B-ER 420 electron paramagnetic resonance spectrometer, CAD4-SDP34C bicircular diffractometer, 200mA rotating anode x-ray machine, D/MAX-YA rotating target x-ray machine, AD-1 automatic low-light densitometer, DX-3A scanning electron miscroscope, CA25 4096 channels pulse analyzer, OCD circular dichroism spectrometer, and the home-made Mossbauer spectrometer, positron annihilation spectrometer, magnetic balance, Model 41 differential precision thermobalance, etc. These instruments not only help accomplish the key projects of the institute but also provide services for the assay and examination of various natural chemical substances, crystals and chemical products as well as information for product analysis, property clarification and analog synthesis.

Since its establishment, FMSI has claimed over 120 scientific and technological accomplishments, 22 of them have won the significant scientific and technological achievement award of the National Science Meeting and of the Chinese Academy of Sciences. Examples are the study on the simulation of the nitrogen fixation active center of nitrogenase, the attempted synthesis of the "Fuzhou Model II" model compounds, the improvement of the catalyst for the synthesis of butanol by the Reppe carbonylation, the exploration of new materials and the functional group model of nonlinear optical materials, the study of yttrium aluminate (YAP) laser crystal and high power continuous laser, Ti-$PbO_2$ electrode with sandwiched micro layer of platinum, introduction of aldehyde functional groups to vinylon, and stainless steel equipment and monitor technology. Many optical crystals that have been successfully developed include the electrophoto and nonlinear optical crystal of ammonium dihydrogen phosphate (ADP), potassium dihydrogen phosphate (KDP) and deuterated potassium dihydrogen phosphate (DKDP), the yttrium aluminate laser crystal with single dopant (neodymium) or double dopants (neodymium, chromium) (Nd, Nd+Cr, YAP), the x-ray diffraction crystals such as potassium hydrogen phthalate (KHP), Pentaerythritol (PET), lead stearate (LS) and lead cerotate (LCer), and the crystal growth of the protein from Trichosanthes kirilowii and its crystal cell coordinates and low resolution structure determination (in collaboration with the Shanghai Organic Chemistry Institute and the Institute of Biophysics). There are also the new nonlinear optical crystal, the low-temperature phase-polarized barium borate, that has been discovered and successfully grown after many years of efforts. In recent evaluation by the academy, this is regarded as a successful development in the research of new technology crystals solely by our own scientific and technical personnel through combining theory with practice and physics with chemistry and one that has left our mark for the first time on the frontier of material science. It is believed to have significant impact on the advancement of laser technology.

Besides bringing the key research projects of the state and the academy to completion, FMSI also actively exploits its technical expertise to serve the application needs of Fujian provincial government and other production departments. Several technical accomplishments have been achieved and related production departments have derived varied degrees of economic benefits from them. Commendations and awards from the provincial government and Fuzhou city as well as many other related departments have been given us for this feat.

FMSI has been authorized by the Academic Degrees Committee of the State Council to accept and train doctoral and master degree students and to award degrees in physical chemistry and solid-state physics. At the moment, there are 20 masters degree candidates and 2 doctoral candidates.

FMSI has also actively pursued academic exchange with foreign countries in many forms such as tour of investigation in foreign country, engaging in advanced studies, attending international academic meetings, studying for degrees, collaborative research, short courses of technical training, inviting foreign scholars and experts to visit, give lectures, work for short term or set up and test instruments and equipment. In recent years, we have sent over 50 times all sorts of scientific and technical personnel abroad and have received on more than 130 occasions visiting experts, which have positively helped in maintaining a lively scientific atmosphere and raising the academic standard within the institute. For example, Professor Lin Weizhen [2651 1983 2823], a physical chemist from the University of British Columbia, Canada, was first invited in 1976 to teach and work for a short term. In 1979, it was approved by the Academy of Sciences to offer him the honorary research professorship at the institute. Mr Lin has made significant contributions on the aspects of research guidance and classroom lectures during his many short visits to FMSI in the past years. With the sponsorship of the academy, he gave lecture series at FMSI on "Basic Quantum Chemistry and the Ligand Field Theory" and "The Irreducible Tensor Method" in 1978 and 1979 that greatly benefited our institute and our sister organizations in the training of research and teaching staff.

In order to present new advancements, new achievements and new directions in each research area and to exchange scientific results and experience, FMSI started a new journal STRUCTURAL CHEMISTRY in 1982 on the foundation of its sporadically published FMSI NEWSLETTER. It includes as special issue the English edition Crystal Structure Report and is distributed publicly. Also, many monographs and collected papers on structural chemistry have been edited, translated and published in recent years.

Currently, FMSI is actively implementing the guiding ideology that scientific research be geared toward the needs of economic construction and carrying out the policy of "greatly strengthening applied research, actively and selectively participating in developmental work and paying continued attention to basic research." We have enthusiastically carried out reform in order to make new contributions in answering the needs of the four modernizations drive and producing more achievements and talents.

12922/9365
CSO: 4008/1086

SCIENTISTS AND SCIENTIFIC ORGANIZATIONS

## FIFTY YEARS OF ISOTOPE CHEMISTRY RESEARCH RECOUNTED

Beijing HUAXUE TONGBAO [CHEMISTRY] in Chinese No 7, 18 Jul 85 pp 51-57

[Article by Zhang Qinglian [1728 7230 5571] (Footnote) (About the author: Professor Zhang Qinglian was born at Changshu, Jiangsu in 1908. He studied at the graduate school of Qinghua University from 1931 to 1934 and obtained his PhD from Berlin University of Germany in 1936. The positions he has held include chemistry professor at the Southwestern Consolidated University and Qinghua University; professor and chairman of the Chemistry Department of Beijing University; deputy director of the Chemistry Department, Chinese Academy of Sciences; head of Stable Isotope Division, State Scientific and Technological Commission; member of the standing committee, the Chinese Chemical Society; chairman of the Chinese Mass Spectroscopy Society and member of the Committee on Atomic Weight and Isotope Abundance of IUPAC. Professor Zhang specializes in inorganic chemistry and has long been involved in the teaching and research in this area. Since 1953, he has been working on isotope chemistry and heavy water research and taken part in the research and development of various light isotopes)]

[Text] The need of new nuclear materials for the modern science and technology of nuclear energy has mandated the probe of isotopes of each element as a further step beyond the study of chemical elements. As a result, the borderline discipline of isotope chemistry is advancing rapidly. The isotope chemistry studies the chemical effect that is linked to the change of electron energy levels due to the difference in number of neutron within the nucleus of the same element. The area of utmost importance in this field is the separation of isotopes. It has pushed forward the study of such chemical effect as exchange, equilibrium and kinetics as well as the applications of analytical and tracer methodologies.

Since 1935, the author has corroborated with nearly 50 colleagues on several research projects. Brief summaries of works at each stage can be found in many reviews.[11,17,21,22,38,41,42,61]

On this occasion of the 50th anniversary, though the work continues, it seems appropriate to sum up my experience. What follows is my attempt to outline the four areas of my work.

## I. The Physical Properties of Isotopic Compounds

### 1.1 The Density and Heat Expansion of Heavy Water at 25°C

The density of heavy water at 25°C is an important physical constant in isotope chemistry, the accurate measurement of which has been continued for half a century. Only after the hydrogen and oxygen isotopes in water are accurately measured by mass spectrometry can the density of heavy water be accurately determined. In the 1970's, determinations to seven significant figures started to appear. Based on the density maximum of standard mean ocean water (SMOW), namely 999.975 $kg/m^3$, the author and co-workers had made two accurate determinations on three heavy water samples.[56,67] The four most recent determinations of the density at 25°C of the heavy water that have the same composition of oxygen isotopes as in SMOW are listed in Table 1. The results from three labs agree well with one another and show that the most reliable data so far for the density of heavy water at 25°C is the following:

$$d^{25}_{D_2O_{SMOW}} = 1104.467(5)\ kg/m^3$$

In 1941, we measured the heat expansion of heavy water and extended the temperature range to 50°C,[15] which was later further extended to 100°C in 1949.[26,27,31] Among the internationally accepted data of heat expansion, so far the best ones in the range of 85° to 100°C are those determined by the author and co-workers (G.S. Kell, 1977).

Table 1.

| Year | Authors | Method | Sample number | $kg/m^3$ |
|---|---|---|---|---|
| 1975 | Babeliowsky, Brulmans | Large magnetic float | 2 | 1104.475(3) |
| 1975 | Ceccaldi, Girard, Menache, Riedinger | Archimedes principles | 2 | 465(3) |
| 1983 | Nan Chunbo, Qian Qiuyu, Zhang Qinglian | Precise pycnometry | 2 | 467(9) |
| 1984 | Qian Qiuyu, Zhang Qinglian | " " | 1 | 466(9) |

### 1.2 The Temperature and Freezing Point Depression at the Density Maximum of Heavy Water

By using a 16ml quartz pycnometer, the temperature at the density maximum of heavy water was determined in 1941 as 11.21±0.05°C.[14] Again in 1948, we determined, using heavy water solutions of different acetone concentrations, the molar freezing point depression constant of heavy water as 2.00±0.01°C.[19]

## 1.3 The Vapor Pressure, Heat of Vaporization, Critical Constant and State Diagram of Heavy Water

Using a quartz differential barometer and a paraffin oil bath, we determined in 1936 the vapor pressure difference of $H_2O$ and $D_2O$ in the temperature range of 21.8° to 232.6°C and observed that the largest difference of 83 torr occurred at 170°C and that their vapor pressure was the same at 225°C and the $D_2O$'s became greater than the $H_2O$'s beyond this temperature.[3] This verifies the phenomenon that the critical temperature of $D_2O$ is lower than that of $H_2O$ as determined by the quartz capillary tube method in 1935. The critical temperature $t_c$ of $D_2O$ and $H_2O$ mixtures follows the empirical formula below[1,2]:

$$t_c = 374.2 - 2.7n$$

where n is the mole fraction of $D_2O$.

Comparative determinations of the critical pressure $p_c$ and the critical density $d_c$ have also been made and the data are listed in Table 2.

Table 2.

| Compound | $t_c$, °C | $p_c$, atm | $d_c$, g/cm$^3$ |
|---|---|---|---|
| $H_2O$ | 374.2 | 218.5 | 0.325 |
| $D_2O$ | 371.5 | 218.6 | 0.363 |

Within the temperature range of approximately 360° to 374.2°C, 40 density readings were obtained that enabled us to plot the density-temperature diagram of $H_2O$ and $D_2O$.

Take the vapor pressure data of $H_2O$ and $D_2O$ within the temperature range of 3.8° to 230°C and plot lg $(p_{H_2O}/p_{D_2O})$ versus 1/T, the difference in heat of vaporization can be calculated from the slope of the curve. Some of the data are listed in Table 3.

Table 3.

| °C | $H_2O$ Heat of vaporization cal/mole | $D_2O$ Heat of vaporization cal/mole | Ratio of heat of vaporization $D_2O/H_2O$ |
|---|---|---|---|
| 3.8 | 10703 | 11109 | 1.038 |
| 50 | 10255 | 10517 | 1.026 |
| 100 | 9719 | 9919 | 1.021 |
| 150 | 9101 | 9257 | 1.017 |
| 200 | 8353 | 8465 | 1.013 |
| 230 | 7808 | 7894 | 1.011 |

The difference in heat of vaporization ($D_2O$-$H_2O$) reduces from 406 cal/mole at 3.8°C to 86 cal/mole at 230°, thus disproves what was believed in the literature at that time that the difference was constant between 20° and 90°C.

## 1.4 Solubility in Heavy Water and the Distribution Constant of Solute Between Two Phases

In 1948/49, we determined and compared the solubility of various potassium salts in light and heavy water at 25°C. The results are listed in Table 4, in which S = moles of salt/55.51 moles of water.[23,24,25] It can be seen that the smallest difference in solubility is only 5 percent whereas the largest is 25 percent. Also, the percentage difference of potassium halide KX solubility increases with increasing radius of halide ion. $KXO_3$ also behave similarly.

Table 4.

| Potassium salt | $S_{D_2O}/S_{H_2O}$ | Potassium salt | $S_{D_2O}/S_{H_2O}$ |
|---|---|---|---|
| $KClO_4$ | 0.947 | $KBrO_3$ | 0.895 |
| $KClO_3$ | 0.935 | KBr | 0.888 |
| $K_2C_2O_4$ | 0.932 | KI | 0.884 |
| KCl | 0.906 | $KIO_3$ | 0.833 |
| $KReO_4$ | 0.900 | $K_2SO_4$ | 0.795 |
| $K_3Fe(CN)_6$ | 0.897 | $K_2Cr_2O_7$ | 0.745 |

Because the solubility ratios of $K_2Cr_2O_7$ and $CdI_2$ deviate substantially from unity, their solubilities Sn[32,34] in a mixture of light and heavy water at 25°C have been determined as follows:

$$K_2Cr_2O_7 \quad Sn = 0.5024 - 0.1467n + 0.017n^2$$
$$CdI_2 \quad Sn = 2.347 - 0.7046n + 0.068n^2$$

where n is the mole fraction of $D_2O$. The phase diagram of the $K_2Cr_2O_7$-$H_2O$-$D_2O$ three-component system at 25°C has also been drawn. Similar study has also been done on NaCl[12]:

$$NaCl \quad Sn = 6.145 - 0.334n$$

In 1950, the solubility of thallous nitrate in heavy water in the range of 5° to 50°C were measured[30] and the results disprove the occurrence of phase change between 25° and 28.4°C as recorded in the literature.

When a substance is dissolved in two immiscible phases, there exists a distribution constant. A typical example is that the distribution constant of iodine in $H_2O$ and $CCl_4$ at 25°C is 1:85.4, the concentrations in both phases being presented in grams of iodine/liter of solution. In 1944, the author used semi-micro method to determine the distribution constant of iodine in $D_2O$ and $CCl_4$ as 1:103.[18]

## 1.5 Thermodynamic Properties of Heavy Water Hydrates

By treating anhydrous manganese sulfate, zinc sulfate and cobalt sulfate with slight excess of heavy water with 99.9 atom percent D, three new heavy water hydrates were prepared: $MnSO_4 \cdot 4D_2O$, $ZnSO_4 \cdot 7D_2O$ and $CoSO_4 \cdot 7D_2O$.[65,66,72] The $^1$H-NMR was used to determine the isotope grade of the products. The differential thermal/thermogravimetric analysis showed that the dehydration initiation temperature at each stage generally was about 6-7°C higher than the corresponding light water counterpart and in certain stages the activation energy of dehydration was higher by about 2-5 kcal/mole. All these support that the heavy water hydrates are more stable than their light water counterparts.

## 1.6 The Vapor Pressure, Heat of Vaporization and Boiling Point of Partial Heavy Water

In 1936, we evaporated at 100°C the water containing 0.0347 percent HDO and measured the total enrichment of HDO and $H_2{}^{18}O$ in the residual water by the float method. Then the $H_2{}^{18}O$ content was determined by $H_2S$ balance method and the difference was HDO content. By the Rayleigh evaporation equation, the ratio of vapor pressure $HDO/H_2O$ at 100°C was calculated: $p_{HDO}/p_{H_2O} = 0.9734$. From this, it can be derived that the boiling point of HDO is 100.7°C. Using the known data for lower temperatures, we derived the empirical formula for 11° to 100°C range as follows:

$$p_{HDO}/p_{H_2O} = 1.16e^{-130/(RT)}$$

Hence, the average difference of heat of vaporization between HDO and $H_2O$ was calculated as 130 cal/mole.[4]

## 1.7 The Vapor Pressure, Heat of Vaporization, Boiling Point, Heat Expansion and IR Spectrum of Heavy Oxygen Water

In the above mentioned experiments, we also measured the vapor pressure of $H_2{}^{18}O$ at 65°, 80° and 100°C. Combining this with the known data for lower temperatures, the following can be obtained:

$$p_{H_2{}^{18}O}/p_{H_2O} = 1.013e^{-13/(RT)}$$

This is also applicable from 11° to 100°C. It can be seen that the average heat of vaporization of $H_2{}^{18}O$ is lower than that of $H_2O$ by 13 cal/mole. Table 5 lists some physical constants of the isotopic species of water. The vapor pressure data of $D_2O$, HDO and $H_2{}^{18}O$ measured by the author and coworkers have been applied in the technology of heavy water and heavy oxygen water productions.

Table 5.

| Isotope substituted water | $H_2O$ | HDO | $D_2O$ | $H_2{}^{18}O$ |
|---|---|---|---|---|
| Freezing point, °C | 0 | 2.11 | 3.80 | 0.3 |
| Boiling point, °C | 100 | $100.7_0$ | 101.40 | $1001.1_3$ |
| Vapor pressure at 20°C, Torr | 17.535 | $16.2_7$ | $15.2_4$ | $17.3_7$ |
| Vapor pressure at 100°C, Torr | 760 | 739.7 | 722.2 | 756.5 |
| Heat of evaporation at 100°C, cal mol | 9719 | 9849 | 9919 | 9732 |

Besides, in 1964, we took a water sample with 32.47 atom percent $^{18}O$ and treated it with hydrogen containing 0.003 atom percent D in the presence of Pt/C catalyst to normalize the hydrogen in the sample to 150ppmD. The heat expansions of this $H_2{}^{18}O$ water sample were measured by pycnometry, which were extrapolated to 100 percent $H_2{}^{18}O$. Using the known specific gravity value of heavy oxygen water at 25°C, an empirical formula for the heat expansion of $H_2{}^{18}O$ valid at the range of 5° to 90°C was derived[45]:

$$d_t^t = 1.11254 + 4.16 \times 10^{-6}t - 9.6 \times 10^{-9}t^2$$

Using a Nicolet 7199B FTIR spectrophotometer, the IR absorption peaks of $H_2{}^{18}O$ and $D_2{}^{18}O$ liquids were observed for the first time and were listed below in $cm^{-1}$:

| $H^{18}O$ | $D^{18}O$ | $H_2{}^{18}O$ | $D_2{}^{18}O$ |
|---|---|---|---|
| 3394 | 2488 | 1639 | 1202 |

Further measuring the IR absorption peaks of a 1:1 mixture gave the $\nu^2$ of $HD^{18}O$ as $1452 cm^{-1}$.

## 1.8 The Boiling Point and Density of Heavy Ethanol

In 1947, we prepared $C_2H_5OD$ by hydrolysis of sodium ethoxide and aluminum ethoxide with the heavy water containing 99.5 atom percent D and measured its properties. Their comparisons with those of $C_2H_5OH$ are listed in Table 6.[20]

Table 6.

| Isotopic compound | b.p., °C | Density at 25°C, g/ml |
|---|---|---|
| $C_2H_5OH$ | 78.32 | 0.78506 |
| $C_2H_5OD$ | 78.8 | 0.801 |

## 1.9 The Shifts in IR Spectra of Lithium Isotopic Compounds

The perchlorates of lithium isotopes, $^6Li_{0.905}{}^7Li_{0.095}ClO_4$ and $^7Li_{1.000}ClO_4$ and their crown-4, crown-5, crown-6, and crown-8 complexes were prepared. Their IR absorption spectra from 100-500cm$^{-1}$ were studied with a Nicolet 7199B FTIR spectrophotometer. Among the 16 pairs of absorption peaks with isotope shift, the differences in wave number of 10 pairs were 4.0-6.8 percent, which is roughly equal to the relative difference of the square roots of the mass of $^6$Li--O and $^7$Li--O, i.e., 5.5 percent.[62] From the mid-range IR spectra of the crown-5 and crown-6 complexes of $^6$Li and $^7$Li salts that contain water molecules, the water absorption peaks of lithium isotope shift by as much as 9cm$^{-1}$ in the region of 3436-3599cm$^{-1}$.[63]

# II. The Kinetic Effect and Isotope Separation of Isotopic Compounds

## 2.1 The Reaction Rates in Heavy Water

Three reactions were studied in heavy water. We designed a semimicro method in which 1 ml of reaction solution was put in a tiny crucible inside a constant temperature water bath. Heavy water of different concentrations were used and the data were extrapolated to 100 percent $D_2O$ medium. At 20°C, the reaction rate of $D_2O_2$ and $I^-$ in $D_2O$ was observed to be only 60 percent of that of the corresponding $H_2O_2$ and $I^-$ in $H_2O$.[13]

Next, we studied the reaction rate of $D_2O_2$ and $MnO_4^-$ in acidic $D_2O$ at 20°C. In $D_2O$, the autocatalysis of $Mn^{2+}$ ion in the presence of $D_3O^+$ is faster than the corresponding reaction in $H_2O$ in the presence of $H_3O^+$ while the rate that $D_2O_2$ and $MnO_4^-$ react is only 15 percent that of the $H_2O_2$ and $MnO_4^-$ reaction in $H_2O$.[16]

Also the Landolt reaction was studied at 25°C. The rates that $SO_3^{2-}$ reduces $IO_3^-$ in $H_2O$ and $D_2O$ were compared. Interestingly, it was observed that the rate constant ratio $k_D/k_H$ was 1.2 at 0.01 molar of hydrogen ion and was increased to 3.7 at 0.5 molar.[28]

## 2.1 The Electrolytic Coefficient of Protium and Deuterium

The classical method of producing heavy water is by electrolysis, which was later used only for high concentration solutions. We studied the change of electrolytic coefficient $\alpha$ at high current density in 1949, $\alpha$ being the relative evolution rate of protium. A 1 percent solution of $D_2O$ was examined at room temperature. It was made basic with NaOH. Using a platinum wire with a diameter of 1 mm as cathode, the experiment was carried out from 1 to 13 amp/cm$^2$. It was found that $\alpha = 6.5 \pm 0.5$ under 10 amp/cm$^2$ and dropped noticeably in the range of 10 to 13 amp/cm$^2$.[29]

In 1982, the fabrication of the electrolytic cell was improved and precise chromatographic method was used to measure deuterium so that the precision of $\alpha$ measurement reached ±0.1. An electrolysis experiment was done with a 1 percent $D_2O$ solution, made basic by $K_2CO_3$. A regular steel plate of 0.22 percent carbon content was used as cathode and the current density from 22 to

421 mA/$cm^2$ was applied. The $\alpha$ value was observed to increase from 7.8 to 10.1 (at approximately 250 mA/$cm^2$) and then dropped to 9.5.[53]

Later, the $\alpha$ values of the high concentration heavy water were measured. Under similar condition but with 197 mA/$cm^2$ and constant temperature of 23.5°C, the $\alpha$ was constant at 9.1 ± 0.1 when the electrolytic solution contained 91.8 to 99.5 atom percent D.[64] This result may have implications in heavy water production technology.

## 2.3 The Overall Distribution Constant of Deuterium in the Girdler-Sulfide Process

The overall distribution constant of deuterium $\beta$ in the GS process, a popular method for heavy water production, was determined in 1965. A teflon-sealed stainless steel exchange chamber of 500 ml capacity and sampling chambers for both gas and liquid phases were fabricated. The heavy water containing 1.5 atom percent D and the hydrogen sulfide gas of 98.6 percent purity were reacted at 20 atm for 5 hours to establish equilibrium under various temperatures. The $H_2S$ saturated aqueous phase and the water vapor saturated $H_2S$ gas phase were sampled and converted into pure water, which were then analyzed with precise density measurements. The experimentally-determined $\beta$ values were accurate to ±0.02 and were in good agreement with the generally accepted calculated values as shown in Table 7.[49]

Table 7.

| Temperature pressure, kg/$cm^2$ | 30<br>18 | 30<br>20 | 35<br>18 | 35<br>20 | 130<br>20 | 135<br>20 |
|---|---|---|---|---|---|---|
| $\beta$, obs. | $2.29_2$ | $2.33_5$ | $2.27_2$ | $2.26_0$ | $1.65_0$ | $1.58_6$ |
| $\beta$, calc. | $2.29_3$ | $2.28_9$ | $2.25_8$ | $2.25_4$ | $1.62_3$ | $1.58_4$ |

## 2.4 Attempts To Enrich Heavy Water by Fractional Crystallization

In 1936, a copper tube of 20 mm diameter with sealed bottom end was fashioned in such a way that the bottom section, 15 cm in length, was bent at 135° angle and was loaded with dry ice. The tube was spun in 0°C water so that ice formed was quickly pulled down. But no enrichment of heavy water in ice was observed even at a sedimentation speed of 1.5 m/sec. In fact, we were limited by the precision of the flotation method of analysis. Recently, deuterium enrichment in ice was observed with $\alpha$ = 1.02

# III. Analysis Methods for Stable Isotopes and the Preparation of Isotope Reference Samples

## 3.1 The Float Method

The heavy water concentration of a water sample, expressed in terms of atom percent D, can be measured by suspending a hollow borosilicate glass

or quartz float, about 15mm high, in the heavy water of certain concentration at a specific temperature. It is a better way to measure the rising and falling velocity of the float beyond and below the flotation temperature $t_0$ and then intrapolates to $t_0$. By using the density data of regular water and heavy water at various temperatures and the expansion coefficient of the float, the heavy water concentration in a water sample can be calculated.

In 1956, the velocity-temperature relationship of the float was studied and it was found that linear relationship only existed within certain temperature range.[33] Four types of float were later studied and compared and the spindle-shaped float was found to be most satisfactory.[40] With temperature kept constant to within ±0.0005°C, the accuracy of the measurements reached ±0.2 $\gamma$, where $\gamma$ = mg/l. At 25°C, $\gamma/0.1074$ = ppmD and $\gamma/0.1123$ = ppm$^{18}$O.

When analyzing high concentration heavy water, samples are degassed and re-dissolving of air should be avoided during measurement. Therefore, a flotation tube with a ground glass stopper and a capillary tubing within has been designed.[57] This is suitable for the testing of heavy water products. After $K_2CO_3$ is added, a product with about 99.8 atom percent D was subjected to electrolysis, using iron cathode ($\alpha$ = 9.1) and gold anode ($\alpha$ = 1.005 for $^{16}O/^{18}O$). When 1/4 of the liquid remained, D was enriched to 99.999 atom percent. This enriched sample was distilled out and compared with the product by the new type flotation tube. The accuracy reached ±0.01 atom percent D. This result was checked in four labs and also checked by mass spectrometric method. They all agreed within the error range. Taking into account the errors in heavy water density data, the accuracy was determined to be ±0.02 atom percent D. In 1964, when mass spectrometers were not readily available, this was adopted by the Ministry of Chemical Industry as a temporary standard method.

In order to extend the analysis to a wider range of concentrations and to shorten measuring time to an hour, a temperature-pressure flotation method was devised[58] and items measured are listed in Table 8. When checked by the specific gravity bottle method, it was found that the mean deviation was ±0.0005 atom percent D for heavy water samples of 0.11 to 0.83 atom percent D.

Table 8.

| Item | Reference water | Sample water |
|---|---|---|
| Thermostat temperature, Beckmann, °C | $t_1'$ | $t_2'$ |
| Pressure coefficient at flotation temperature, °C/torr | $K_1$ | $K_2$ |
| Flotation pressure, deviation from 760 torr | $p_1$ | $p_2$ |
| Normal flotation temperature, °C | $t_1 = t_1' - K_1p_1$ | $t_2 = t_2' - K_2p_2$ |

## 3.2 The Crystal Flotation Method

We studied the LiF crystal flotation method for measuring the abundance of lithium isotopes. The redistilled bromoform was mixed with n-pentanol and n-hexanol to get three mixtures of different compositions that were suitable for measuring different abundances. Their densities varied from 2.63 to 2.65 g/cm$^3$ at temperatures from 25.7° to 28.8°C and their stabilities were examined.

A furnace was made with platinum wire that could be heated to 980°C. A platinum crucible with a capacity of either 1 or 5 ml was used to hold the molten LiF, from the surface of which single crystals were produced by using a platinum needle 1 mm in diameter, which was soldered to a platinum tubing 3 mm in diameter. Outside the tubing was another soldered platinum tubing 6 mm in diameter. Inside the platinum tubing was a small glass tubing through which the cooling water flowed to the bottom and was directed to exit at the top to provide cooling for the needle. The tubing was fitted with a sliding mechanism.

The single crystals were dome-shaped with 2 mm in diameter. The flotation of the crystal was actually measured by the temperature convergence method. By using the Beckmann thermometer, temperatures were measured with an accuracy of ±0.002°C and ±0.004°C for repeated measurements. A depleted waste product from Russia was determined to contain 3.13±0.09 atom percent $^6$Li. The result was confirmed by the mass spectrometric determination, which gave 3.10±0.05 atom percent $^6$Li.[51]

## 3.3 The Gradient Tube Method

In 1960, we improved the gradient tube method by using new media, p-dimethylbenzene and bromobenzene. p-Dimethylbenzene was carefully poured on top of the bromobenzene layer inside the gradient tube and was allowed to diffuse for 50-60 hours at 25°C to form density gradient. Tiny 1 μl drops of heavy water, whose concentrations were known, were suspended in the gradient. By plotting the relative height vs D concentration, standard curves were obtained for two concentration ranges of 0-1.2 and 0-12. The D concentrations of testing samples were then determined from the curve by their heights.[40] The accuracy is about the same as that of the falling drop method.

## 3.4 The Falling Drop Method

In 1957, we measured the density of pure o-fluorotoluene from 14° to 30°C and designed a horizontal liquid transfer tube to produce drops whose volume variations were within 0.3 percent. The temperature of the thermostat was controlled to within ±0.0005°C. The accuracy of heavy water analysis by this method was improved. When a one atom percent D heavy water sample was analyzed, the relative accuracy was improved to ±0.3 percent from ±1 percent attained at that time.[35,36]

Two years later, taking advantage of the property that organic liquids have far greater heat expansion than water, we used a mixture of

α-chloronaphthalene and kerosene distillate as medium in conjunction with a multiple temperature method, namely at 15°, 20°, 25°, and 30°C, so that the falling drop method was useful for analyzing heavy water of an entire concentration range with an accuracy of 0.02-0.05 atom percent D.

For low concentration heavy water samples, we used a new medium, n-butyl benzoate, and studied the effect of the residual liquid at the tip of the tube during "drop making." The tube was treated with $SiHCl_3$ so that no residual liquid stuck to the tip. We also studied the wall effect and memory effect and confirmed that there was an optimal value of r/R, the ratio of drop radius r and the radius of the falling drop tube R, when the drop falling velocity was plotted against the drop volume. The drop falling velocity changed very little at the vicinity of this optimum. The optimum determined for n-butyl benzoate was 0.426 and for o-fluorotoluene 0.439.[43,44,59] Therefore, it is much more convenient to use the popular "microsampler" to inject sample drops of 10.00±0.02 μl.

Later, a mixture of α-chloronaphthalene and n-butyl benzoate was used to analyze samples of high concentration heavy water with 97 to 100 atom percent D. An r/R value of 0.430 was chosen. The reproducibility of the drop falling velocity was 0.2 percent (relative) and the accuracy of the determinations reached ±0.04 atom percent D.[60]

### 3.5 The Total Isotope Analysis of Water by the Density Method

When mass spectrometer is not available, the density method is often employed to determine the total content of $D_2O$ and $H_2{}^{18}O$. Then D and $^{18}O$ are normalized and one of them measured. The difference is attributed to the other. In 1936, a hydrogen isotopes normalization method using $H_2S$ was studied[4] and a $CO_2$ normalization of oxygen isotopes was used in 1959.[40] Later, the oxygen isotopes normalization was done over $MnO_2$ catalyst at 600°C using compressed oxygen. The cold trap and saturator on both sides of the horizontal reaction chamber were of the same shape so that one forward-reverse operation was enough to normalize the unusually high concentration of oxygen isotopes in natural water to within the error range of measurement.[48] Since the 1970's, the mass spectrometry has been used for determining D, $^{17}O$ and $^{18}O$ separately.

### 3.6 The Mass Spectrometric Analysis of Hydrogen Isotopes

The deuterium concentration of a heavy water product was examined by using a MAT-CH5 mass spectrometer. In actual practice, one measured the ratio of peak height, $HD^+/DD^+$. In order to compensate for the mass discrimination factor, a reference sample of 145.7 ppmD was used for dilution. We compared the high temperature platinum wire method and the $PtO_2$ catalysis for the preparation of gas samples and found the latter more convenient. When calculating molecular weights, the contents of $^{17}O$ and $^{18}O$ have to be taken into consideration. The results showed the purity of the sample was 99.939±0.003 atom percent D.[55] This sample was also sent to the labs in Japan and France to confirm our results and the data were in agreement. The mass spectrometry has been used for the preparation of second and third batches of standard sample series so

that a standard curve can be obtained for production departments to test their products by simple infra-red measurement.

### 3.7 The Reiteration Method in the Mass Spectrometric Analysis of Lithium Isotopes

In conjunction with the research on Lithium-6, we studied the mass spectrometric analysis of lithium isotopes in 1964.[50] A MИ-1305 mass spectrometer was used. As an ion source, a tantalum strip, after being applied a $LiNO_3$ solution, was dried on hot plate to form a solid layer of 600 $\mu g/cm^2$. When vaporized at 900°C, the lithium salt emitted $^6Li^+$ and $^7Li^+$ ions and $R_{7/6}$ was measured.

After being purified by crystallization, carbonates of natural and enriched lithium were examined for impurities and found to be mainly potassium, sodium, calcium, and iron. An intermediate sample was obtained by dissolving and thorough mixing of these two samples which were accurately weighed. By comparing the calculated and spectrometrically determined $R_{7/6}$ values of the intermediate sample, a first-approximation correction factor $K_{calc./exp.} = 0.9944$ was obtained. Through four reiterations, the values 0.9926, 0.9920, 0.9918, and 0.9918 were obtained successively. By using this converged K value to do corrections, the Li-6 concentrations in natural, mixed, and enriched lithium were found to be 7.5, 49.2, and 90.0 atom percent $^6Li$, respectively. The standard deviation was ±0.1 atom percent $^6Li$. The enriched sample was a Russian-made reagent. The $^6Li$ concentration of the mixed sample was also checked by the crystal flotation method to be 49.2±0.1 atom percent $^6Li$, which was in total agreement.

### 3.8 The Elimination of Memory Effect in the Boron Trifluoride Method for Mass Spectrometric Analysis

In connection with running a pilot plant for enriching B-10, we studied the $BF_3$ method in 1965.[52] Because the memory effect in this method is mainly attributed to the contamination of the line, the $BF_3$ samples were adsorbed to pure microcrystalline $CaF_2$ at 155° to form complexes. A tantalum or nickel crucible containing 10 mg of $BF_3 \cdot 3CaF_2$ was inserted into the ion source inside a Russian-made MИ-1305 mass spectrometer and heated to generate $BF_3$ gas, which was then bombarded with electrons to form $^{10}BF_2^+$ and $^{11}BF_2^+$ ions. The $R(^{11}B/^{10}B)$ values were determined. The memory effect was not observed when high and low concentration $^{10}B$ samples were alternated in the analysis sequence. The interference of other ions was discussed and their total influence on the R value would not exceed 1 percent. An enriched sample was examined by this method and found to have 82.2±0.1 atom percent $^{10}B$, which was in total agreement with results from the borax method. The system error correction was not made because only relative measurements were made for samples taken from each section of the separation column.

### 3.9 The Analysis of Reference Samples of Nitrogen Isotopes by Mass Spectrometry

Through mass discrimination correction, the $^{15}N$ abundances of three ammonium sulfate reagents were accurately determined by using a MAT-251 mass

spectrometer. Their purities were also determined and listed in Table 9. These reagents can serve as reference samples for the preparation of intermediate abundance samples useful for calibrating mass spectrometers and other instruments.[69] We also prepared a set of eight low $^{15}N$ reference samples for agricultural applications. The abundance ranges from 0.366 to 12.6 atom percent $^{15}N$.[68]

Table 9.

| Reference sample | Purity, percent | Atom percent $^{15}N$ |
|---|---|---|
| I | 99.77 | 0.366±0.001 |
| II | 99.28 | 98.35±0.02 |
| III | 99.93 | 99.88±0.01 |

### 3.10 The Preparation of C-13 Reference Samples and the Mass Spectrometric Analysis of Oxygen Isotopes

Like the nitrogen isotope project, the preparation of reference samples of carbon isotopes is also on the agenda of the State S&T Commission. A 99.95 percent pure barium carbonate reagent was treated with 100 percent $H_3PO_4$ to get $CO_2$ sample gas in 98.9±0.3 percent conversion. The $R_{13/12}$ was measured with a MAT-251 mass spectrometer. In actual practice, three peaks at 44, 45, and 46 were measured (the other three minor peaks were ignored) and corrected by the $^{17}O$ and $^{18}O$ content calculations to get $R'_{13/12}$. The mass discrimination factor can be calculated by using the PDB reference samples for comparison with the $\delta_{13/12}$ and $\delta_{18/16}$ values obtained for compressed $CO_2$, from which the true value of $R_{13/12}$ can be figured out. We obtained the result of 1.095±0.0001 atom percent $^{13}C$. The oxygen isotope contents were also determined, i.e. 0.0375±0.0001 atom percent $^{17}O$ and 0.2032±0.0008 atom percent $^{18}O$.[71]

Later, a high C-13 barium carbonate reagent was measured and its isotope abundance of 88.54±0.03 atom percent $^{13}C$ was determined after the correction for mass discrimination factor was made. The O-18 in the reagent was depleted to 0.223 atom percent $^{18}O$. We also found a reagent containing 98.11±0.03 atom percent $^{13}C$.

## IV. The Natural Abundance of Hydrogen and Oxygen Isotopes

### 4.1 The Distribution of Deuterium in the Precipitation, Surface and Underground Waters

At the end of 1935, four snow samples were collected in Northern Europe[6] and the change in the overall content of D and $^{18}O$ measured by the float method. In comparison with ocean water, the density difference ranges from −3.7 to −4.9γ and the difference is −4.2γ when compared with the vapor from evaporation of ocean water at 0°C.

In 1959, we collected all kinds of water samples from all over the country including waters from sea, river, lake, underground spring, hot spring, plateau lake, salt lake, and oil brine, a total of 50 samples. The total content of D and $^{18}O$ was analyzed by the float method while the content of D and $^{18}O$ of a few samples were determined by the $CO_2$ balance method.

The more obvious results were that ocean water was heavier than surface water, plateau lake water heavier than plain lake water, and waters of salt lake and oil brine were even heavier. This can generally be explained by the vapor pressures of $H_2O$, HDO, and $H_2{}^{18}O$.[37]

Between 1956 and 1983 we collected six batches of samples from the Chang Jiang (Wuhan, Nanjing, and Shanghai), the Zhu Jiang (Guangzhou), and the Qian Tang Jiang (Hangzhou). The waters were collected for 12 consecutive months. Reduction with magnesium powder produced hydrogen gases for precise chromatography. The results showed that deuterium content was highest in May and lowest in September, the difference being about 4-5 ppmD. This was consistent with previous results. The difference is due to the fact that river water comes from precipitations, which are gathered from vapors evaporized at different temperatures. At higher temperature, the ratio of vapor pressure $HDO/H_2O$ (less than 1 itself) deviates less from unity.

Between 1974 and 1983 we collected the deep well waters of the Beijing University, including the 12 months samples of 1978 and 1981-82. The deuterium contents were measured as 145.7±0.2 ppmD, an indication that it was constant within the error range of the determination in a 9-year span.[70]

In the 1970's, we measured the hydrogen and oxygen isotopes distribution of snow and ice samples in the high altitude area of Mt. Qomolangma.[46-48] The density method for the analysis of total isotopes and the mass spectrometry were used and some data are listed in Table 10. These samples were collected between 21-27 April 1975.

Table 10.

| Attitude, m | Precipitation | $\delta D$ (‰) | $\delta^{17}O$ (‰) | $\delta^{18}O$ (‰) |
|---|---|---|---|---|
| 7450 | Granular snow | - 62.0 | - 5.25 | - 9.43 |
| 7600 | Ice | - 22.3 | - 1.86 | - 4.31 |
| 8100 | Granular snow | - 82.2 | - 6.23 | -12.57 |
| 8600 | Surface snow | -136.2 | - 9.17 | -18.79 |
| 8848 | New snow | -208.8 | -13.82 | -26.99 |

### 4.2 The Regularity in the Distribution of Hydrogen and Oxygen Isotopes on Earth

In 1936, we proposed that oxygen and hydrogen isotopes recycled in nature in the form of water based on the fact that the vapor pressures of HDO and $H_2{}^{18}O$ are lower than that of $H_2O$. Water vaporizes and rises to form cloud, which in turn condenses or freezes and descends in the form of rain and snow. Part

of the vapors from ocean water precipitate on land and surface waters flow one-way into the ocean, hence forms a cycle and D and $^{18}O$ are enriched in ocean waters (on average, surface water contains 148 ppmD and 1970 ppm$^{18}O$ whereas ocean water 156 ppmD and 2000 ppm$^{18}O$). At the same time, land animals also enrich heavy isotopes from the water they drink through surface evaporation. Plants, due to their larger volume of evaporation, have greater enrichment (the crystallization water of minerals also has enrichment effect comparing with ocean water). In conclusion, the evaporation formulas of HDO and $H_2{}^{18}O$ can be used to roughly explain the distribution of D and $^{18}O$ on earth, although there are other secondary factors.[7,8,9]

### 4.3 The Effect of the Fluctuation of Hydrogen and Oxygen Distribution on the Units of Volume and Temperature

In 1936, we discussed the problem of such metric standards as volume and temperature[10] and pointed out that, in measuring 1 liter standard volume by water, the source of the regular water and its purification method should be specified. It is still impractical to use the ideal $^1H_2{}^{16}O$ as the standard material. The fluctuation of hydrogen and oxygen isotopes has smaller effect on temperature measurements. With the new international definition of $1l \equiv 1dm^3$, this problem is solved.

Looking back on my 50 years of experience in scientific research, I spent the early years on basic research, the results of which have been applied to separation and analysis methodology. After the Liberation, in adjusting to the demands of our socialist construction, I turned to applied research, which was focused on the study of chemistry and analysis of stable isotopes of light elements with an aim for their production and development. Half century of efforts is just like a drop in the bucket. But its path truly reflects the direction the surging torrent of new China's S&T development is heading.

## REFERENCES

1. Riesenfeld, E.H., Zhang Qinglian, Z. PHYSIK. CHEM., B28, 408-409 (1935).

2. Ibid., B30, 61-68 (1935).

3. Ibid., B33, 120-126 (1936).

4. Ibid., 127-132.

5. Riesenfeld, E.H., Zhang Qinglian, BER. DTSCH. CHEM. GES., 69, 1302-1305 (1936).

6. Ibid., 1305-1307.

7. Ibid., 1308-1310.

8. Riesenfeld, E.H., Zhang Qinglian, NATURWISS., 24, 616-618 (1936).

9. Riesenfeld, E.H., Zhang Qinglian, EMSCHAU WISS. TECHNIK, 40, 621-623 (1936).

10. Riesenfeld, Zhang Qinglian, PHYSIK, Z., 37, 690-692 (1936).

11. Zhang Qinglian, "The Isotope Chemistry of Water," Diss. Univ. Berlin, 50 pages, Neuenhahn, Jena, 1936.

12. Zhang Qinglian, Zhu Jinchang, Z. PHYSIK. CHEM., A184, 411-415 (1939).

13. Zhang Qinglian, Wei Yuzhi, ZHONGGUO HUAXUEHUI HUIZHI [JOURNAL OF THE CHINESE CHEMICAL SOCIETY], 7, 138-143 (1940).

14. Zhang Qinglian, Qian Renyuan, Ibid., 8, 74-75 (1941).

15. Zhang Qinglian, Qian Renyuan, J. AM. CHEM. SOC., 63, 1709-1711 (1941).

16. Zhang Qinglian, Wei Yuzhi, KEXUE JILU [SCIENTIFIC RECORDS], 1, 132-134 (1942).

17. Zhang Qinglian, SCIENCE, 100, 29-30 (1944).

18. Zhang Qinglian, J. AM. CHEM. SOC., 66, 1940-1941 (1944).

19. Zhang Qinglian, Zhu Jinchang, QINGHUA DAXUE LIKE BAOGAO [PHYSICAL SCIENCES REPORT, QINGHUA UNIVERSITY], A4, 361-362 (1947).

20. Zhang Qinglian, Wei Yuzhi, Ibid., A4, 451-452 (1947).

21. Zhang Qinglian, ZHONGGUO KEXUE JISHU [CHINESE SCIENCE AND TECHNOLOGY], 1, 109-110 (1948).

22. Zhang Qinglian, "Studies on Heavy Water," the 50th Anniversary Commemorative Publication of Beijing University, The School of Physical Sciences, 129-142 (1948).

23. Zhang Qinglian, Xie Yuyuan, QINGHUA DAXUE LIKE BAOGAO [PHYSICAL SCIENCES REPORT, QINGHUA UNIVERSITY], A5, 252-259 (1948).

24. Zhang Qinglian, Xie Yuyuan, ZHONGGUO HUAXUEHUI HUIZHI [JOURNAL OF THE CHINESE CHEMICAL SOCIETY], 16, 10-13 (1949).

25. Ibid., 65-71.

26. Zhang Qinglian, Dong Luhe, NATURE, 163, 737 (1949).

27. Zhang Qinglian, Dong Luhe, ZHONGGUO WULI XUEBAO [ACTA PHYSICA SINICA], 7, 230-240 (1949).

28. Zhang Qinglian, Dong Luhe, ZHONGGUO HUAXUEHUI HUIZHI [JOURNAL OF THE CHINESE CHEMICAL SOCIETY], 16, 1-9 (1949).

29. Zhang Qinglian, Wang Jinhua, Ibid., 59-64.

30. Zhang Qinglian, Zeng Yinglun, KEXUE JILU [SCIENTIFIC RECORDS], 3, 101-105 (1950).

31. Zhang Qinglian, ZHONGGUO KEXUE [SCIENTIA SINICA], 2, 185-190 (1951).

32. Zhang Qinglian, Zhang Rongsen, HUAXUE XUEBAO [ACTA CHIMICA SINICA], 21, 320-327 (1955); ZHONGGUO KEXUE [SCIENTIA SINICA], 4, 555-561 (1955).

33. Zhang Qinglian, Gao Zi, Huang Chunhui, Ibid., 22, 234-240 (1956).

34. Zhang Qinglian, Wang Kechang, Ibid., 22, 414-416 (1956).

35. Zhang Qinglian, Cheng Zhixiang, Xu Huibi, KEXUE JILU [SCIENTIFIC RECORDS, NEW EDITION], 1, 383-384 (1957); English Edition, 411-413 (1957).

36. Zhang Qinglian, Cheng Zhixiang, Xu Huibi, "Production of Isotopes, etc." IZV AN SSSR, 59-66 (1958), paper, Conference on Isotope Applications, Moscow, April 1957.

37. Zhang Qinglian, Yin Zhao, Zhang Xianlu, KEXUE JILU [SCIENTIFIC RECORDS, NEW EDITION], 3, 402-404 (1959); English Edition, 495-498 (1959).

38. Zhang Qinglian, "Studies on the Heavy Water Analysis," Higher Education Publication, p 22 (1959).

39. Huang Ailun, Guo Dezhu, Jiao Rangjie, Cheng Zhixiang, Zhang Qinglian, KEXUE JILU [SCIENTIFIC RECORDS, NEW EDITION], 3, 189-191 (1959); English Edition, 239-245 (1959).

40. Zhang Qinglian, KERNENERGIE, 3, 892-896 (1960), paper, Conference on Isotope Applications, Leipzig, December 1959.

41. Zhang Qinglian, "The Physical Properties of Heavy Water and Heavy Hydrogen," document, 820 Professional Meeting, p 34, September 1960.

42. Zhang Qinglian, "Methods for Heavy Water Analysis," Ibid., p 29.

43. Jin Deqiu, Zhang Qinglian, ZHONGGUO KEXUE [SCIENTIA SINICA], 12, 147-148 (1963).

44. Jin Deqiu, Zhang Qinglian, HUAXUE XUEBAO [ACTA CHIMICA SINICA], 29, 266-276 (1963).

45. Zhang Qinglian, Gu Zhennan, ZHONGGUO KEXUE [SCIENTIA SINICA], 13, 688-689 (1964).

46. Zhang Shen, Yu Weixin, Zhang Qinglian, Huang Chunhui, Zhang Rongsen, Gu Zhennan, Wei Qingong, Xie Zichu, Zeng Qunshu, ZHONGGUO KEXUE [SCIENTIA SINICA], 16, 430-433 (1973); English Edition, 560-564 (1973).

47. Zhang Shen, Zhang Qinglian, Xie Zichu, "Report of Scientific Survey in Mt. Qomolangma Area (1966-1968), Modern Glaciers and Geomorphology," Science Publication, 71-76 (1975).

48. Zhang Qinglian, KEXUE TONGBAO [MONTHLY JOURNAL OF SCIENCE], English Edition, 25, 208-212 (1980), paper, 27th IUPAC Congress, Helsinki, August 1979.

49. Zhang Qinglian, Huang Hantong, SEPAR. SCI. TECHN., 15, 397-403 (1980), abstracts, p 3, Separation Science and Technology Symposium, Gatlinburg, October-November 1979.

50. Zhang Qinglian, Wang Guanghui, Zhuan Yahui, KEXUE TONGBAO [MONTHLY JOURNAL OF SCIENCE], English Edition, 26, 897-900 (1981), paper, Gordon Conference on Isotope Chemistry and Physics, Ventura, February 1981.

51. Zhang Qinglian, Shen Dixin, Ibid., 26, 995-1000 (1981).

52. Wang Guanghui, Zhang Qinglian, Ibid., 27, 986-988 (1982); English Edition, 968-972 (1982), 12th British Conference of Mass Spectroscopy, Cambridge, September 1981.

53. Zhou Xihuang, Xu Dagang, Xu Wenrui, Zhang Qinglian, HUAXUE TONGBAO [CHEMISTRY], (9), 568-569 (1982).

54. Zhou Xihuang, Li Ping, Yang Guomin, Zhang Qinglian, Ibid., (6), 17-18 (1983).

55. Yu Jianguo, Ni Baoling, Zhang Qinglian, KEXUE TONGBAO [MONTHLY JOURNAL OF SCIENCE], 28, 405-407 (1983); English Edition, 29, 776-779 (1984).

56. Nan Chunbo, Qian Qiuyu, Zhang Qinglian, ZHONGGUO KEXUE [SCIENTIA SINICA], English Edition, B26, 449-453 (1983).

57. Huang Chunhui, Zhang Qinglian, HUAXUE TONGBAO [CHEMISTRY], (8), 11-12 (1983).

58. Ibid., 12-13.

59. Wang Shouguo, Zhang Qinglian, Ibid., (9), 17-18 (1983).

60. Ibid., 18-19.

61. Zhang Qinglian, "Stable Isotopes Research at the Beijing University," paper, Saclay Atomic Nucleus Research Center Workshop, August 1983.

62. He Shaoqi, Wu Jinguang, Zhang Qinglian, REV. CHIM. MINTR., 20, 737-744 (1983).

63. He Shaoqi, Wu Jinguang, Zhang Qinglian, HUAXUE XUEBAO [ACTA CHIMICA SINICA], 42, 1183-1187 (1984).

64. Zhou Xihuang, He Xihua, Zhang Qinglian, HUAXUE TONGBAO [CHEMISTRY], (1), 14-15 (1984).

65. Qian Qiuyu, Wang Mei, Li Hong, Zhang Qinglian, KEXUE TONGBAO [MONTHLY JOURNAL OF SCIENCE], 29, 402-403 (1984); English Edition, 897-899 (1985).

66. Qian Qiuyu, Qian Jiuxin, Wang Baiyang, Zhang Qinglian, Ibid., 785-788.

67. Qian Giuyu, Zhang Qinglian, Ibid., 1058-1061.

68. Yang Yuemei, Jin Deqiu, Zhang Qinglian, Ibid., 1504-1506.

69. Yang Yuemei, Jin Deqiu, Zhang Qinglian, "Proceeding of Sino-Japanese Mass Spectroscopy Symposium," English Edition, Tokyo, 1985.

70. Zhou Xihuang, Jiang Shihe, Zhang Qinglian, HUAXUE TONGBAO [CHEMISTRY], (1), 13-14 (1985).

71. Li Wenjun, Qian Qiuyu, Zhang Qinglian, Ibid., (7), 23 (1985).

72. Qian Qiuyu, Qian Jiuxin, Ye Yijun, Zhang Qinglian, Ibid., (6), 23 (1985).

12922/9365
CSO: 4008/1086

JPRS-CST-85-040
20 November 1985

AUTHOR: WANG Shuozhong [3769 2592 0022]

ORG: Institute of Acoustics, Chinese Academy of Sciences

TITLE: "An Application of Diffraction Theory to Echo Formation"

SOURCE: Beijing SHENGXUE XUEBAO [ACTA ACUSTICA] in Chinese Vol 10 No 5, Sep 85 pp 302-318

TEXT OF ENGLISH ABSTRACT: Diffraction theory is applied to treat echo-formation problems in this paper. This overcomes some drawbacks of the previously accepted image pulse theory. The new approach provides a comprehensive physical interpretation for the mechanism of echo formation. It predicts different echo behavior for objects made of different materials, and gives correct results for problems of echo formation by smoothly curved surfaces. In these aspects, the previous theory breaks down. In principle, the diffraction approach can tackle any echo-formation problem so long as there exists a solution to the relevant configuration of diffraction. The method is strongly supported by experimental results.

AUTHOR: ZHANG Junjie [1728 0193 2638]

ORG: China University of Science and Technology

TITLE: "Calculation of $(\partial V^E/\partial p)_s$ and Ultrasonic Velocities in Seven Ternary Liquid Mixtures"

SOURCE: Beijing SHENGXUE XUEBAO [ACTA ACUSTICA] in Chinese Vol 10 No 5, Sep 85 pp 319-323

TEXT OF ENGLISH ABSTRACT: The formula for sound velocity in a mixture of weak interactives is used to calculate the sound velocities in seven ternary systems. The results show that the agreement between the calculated and experimental values of sound velocity is quite good. The results illustrated in this article show that the large negative value of excess isentropic compressibility does not always indicate a large positive value of $(\partial V^E/\partial p)_s$.

9717
CSO: 4009/3

JPRS-CST-85-040
20 November 1985

AUTHOR: TANG Minzhong [0781 2404 0022]

ORG: Harbin Aerodynamic Research Institute

TITLE: "The Experimental Investigation of Kármán Vortex Street in the Supersonic Wake"

SOURCE: Mianyang KONGQIDONGLIXUE XUEBAO [ACTA AERODYNAMICA SINICA] in Chinese No 3, 1985 pp 1-8

TEXT OF ENGLISH ABSTRACT: A Kármán vortex street was observed in the wake of a rough flat plate at M = 2.2. The supersonic vortex flow was investigated by optical methods. Flow velocity and velocity fluctuations were recorded with a laser doppler anemometer (LDA). The flow was visualized by schlieren and interferometer methods, and the density distribution in the wake was measured with a Mach-Zehnder interferometer in connection with a high speed camera. The frequency of vortex shedding was determined with a laser interferometer.

The width of the wake is larger and base pressure of the plate is lower when compared with a fully turbulent wake behind a smooth flat plate under the same flow conditions. The ratio h/l of the vortex street is about 0.37, i.e., higher than that in the incompressible flow behind a cylinder. The Strouhal number of the vortex street shedding is about 0.22. The influence of the boundary conditions on the vortex street and the interaction of the vortex street with an oblique shock are discussed in the paper.

AUTHOR: YAN Hengyuan [0917 1854 0337]

ORG: Northwestern Polytechnic University

TITLE: "The Rolling Vortex-Damping of Supersonic Wing"

SOURCE: Mianyang KONGQIDONGLIXUE XUEBAO [ACTA AERODYNAMICA SINICA] in Chinese No 3, 1985 pp 45-53

TEXT OF ENGLISH ABSTRACT: Based on the separated vortex-field of the wing and vortex-lifting theory, the theoretical formulas of the supersonic wing's rolling vortex-damping due to the separated vortex of the low-aspect-ratio sharp-edged wings under the existence of the roll and attack angle are derived using supersonic linear theory. Two terms are contained in the roll vortex damping--one is proportional to the product of the attack angle and roll rate, and the other is proportional to the square of the roll rate. Then, the new theoretical calculation model of the roll damping is given.

From the theoretical results obtained, some figures of the rolling damping factor with various combinations of parameters of wing platforms are also given. In addition, some comparisons between this method and the prevalent potential theory are presented.

AUTHOR: LIN Bingqiu [2651 3521 4428]

ORG: Beijing Institute of Aerodynamics

TITLE: "A Calculating Method for the Breakdown Feature of the Leading-Edge Separating Vortex for Slender Delta Wings"

SOURCE: Mianyang KONGQIDONGLIXUE XUEBAO [ACTA AERODYNAMICA SINICA] in Chinese No 3, 1985 pp 63-71

TEXT OF ENGLISH ABSTRACT: A double layer mode was established, which is used here to describe the separating vortex flow over the delta wing leading-edge. The inner layer of this double layer mode is the vortex core and the outer layer is the irrotational potential flow. These provide the initial and outer edge conditions which are necessary for solving vortex core development. In incompressible flow this method can not only compute the initial breakdown angles of attack, but can also compute the breakdown points along the line of the root chord when the angles of attack are greater than the critical ones. The theoretical results agree well with the experimental measures and show that the breakdown points are insensitive to the Reynolds number.

AUTHOR: CAI Jinshi [5591 6855 3740]

ORG: China Aerodynamic Research and Development Center

TITLE: "On Rolling Resonance and Small Asymmetrical Aerodynamic Force of Re-entry Body"

SOURCE: Mianyang KONGQIDONGLIXUE XUEBAO [ACTA AERODYNAMICA SINICA] in Chinese No 3, 1985 pp 72-81

TEXT OF ENGLISH ABSTRACT: In this paper, the problems in flight mechanics and aerodynamics of rolling resonance of the re-entry body are discussed; the mechanism of the divergence of the angle of attack of the re-entry body is also analyzed. It is shown that rolling resonance is a primary hazard of the re-entry body in the divergence of the angle of attack. Research results of the rolling resonance and small asymmetrical aerodynamic force as well as existential problems relating to the re-entry body are emphatically described. It is shown that the determination of the random ablative configuration and the corresponding mathematical expectation and the variance of small asymmetrical aerodynamic coefficients is the key problem in predicting the rolling resonance probability of the re-entry body. Flight testing is the primary method for solving this difficult problem.

9717
CSO: 4009/6

JPRS-CST-85-040
20 November 1985

AUTHOR: FENG Changgen [7458 7022 2704]
SCOTT, S.K.

ORG: SCOTT of the School of Chemistry, University of Leeds, United Kingdom

TITLE: "Thermal Explosion of Dispersed Media: Criticality for Discrete Reactive Particles in an Inert Matrix"

SOURCE: Beijing BINGGONG XUEBAO [ACTA ARMAMENTARII] in Chinese No 3, Aug 85 pp 1-10

TEXT OF ENGLISH ABSTRACT: In the present paper, theoretical interpretations are developed which explore the criteria for safe storage of explosive masses in the situation in which a number of centers of reaction are embedded in an inert, but not perfectly conducting, matrix. The simplest case is that in which the temperature of the matrix is uniform, but temperature distributions within the reactive zones are also considered. Finally different applications of model propellant systems are discussed.

AUTHOR: WU Xiong [0702 7160]

ORG: None

TITLE: "Detonation Properties of Condensed Explosives Compacted with the VLW Equation of State"

SOURCE: Beijing BINGGONG XUEBAO [ACTA ARMAMENTARII] in Chinese No 3, Aug 85 pp 11-20

TEXT OF ENGLISH ABSTRACT: A simplified virial equation of state based on Lennard-Jones 6-12 potential, called VLW EOS, is proposed for detonation products. The detonation properties of explosives composed of CHNO, CNO, HNO, NO, HN, CHNOF and CHNF have been calculated with this equation, and the results are compared with those of BKW EOS and LJD EOS. The principal feature of this approach is that the third and fourth virial coefficients can be conveniently obtained from the well known second one. It is shown that the agreement between the predicted detonation parameters and the experimental data is reasonably satisfactory.

AUTHOR: YANG Daren [2799 1129 0117]

ORG: None

TITLE: "Design of Linear Prismatic Scanner with High Accuracy"

SOURCE: Beijing BINGGONG XUEBAO [ACTA ARMAMENTARII] in Chinese No 3, Aug 85 pp 32-38

TEXT OF ENGLISH ABSTRACT: This paper presents the design of a high accuracy linear scanner used in laser beam scanning systems for automatic inspection of object size by means of a rectangular prism and correct selection of the rotation center. The transmitted laser beam scans in the direction precisely parallel to the outlet direction. For prismatic glass with a refraction index of about 1.9 and a measurement region of up to 43.74 mm, the maximum linear error is less than ±20 nm. When the measurement region is limited to within 39 mm, the maximum linear error is less than ±6 nm.

AUTHOR: WANG Cenghui [3769 2582 6540]
TIAN Deyu [3944 1795 0151]
LI Guozhen [2621 0948 6966]
XU Liqing [1776 7787 3237]

ORG: None

TITLE: "Synthesis and Properties of 2,3,5,6-Tetranitrato-1,4-Dinitropiperazine"

SOURCE: Beijing BINGGONG XUEBAO [ACTA ARMAMENTARII] in Chinese No 3, Aug 85 pp 60-63

TEXT OF ENGLISH ABSTRACT: A new energetics compound, 2,3,5,6-tetranitrato-1,4-dinitropiperazine (TN), is synthesized and its properties are determined. The method for preparing intermediate disodium 2,3,5,6-tetrahydroxypiperazine-1,4-disulphonate (SP) and 2,5-diacetoxy-3,6-dinitrato-1,4-dinitropiperazine (DN) for TN has been improved.

9717
CSO: 4009/7

## Computers

AUTHORS: ZHOU Chongjing [0719 1504 4842]
HOU Daqing [0186 1129 1987]

ORG: Northeast Institute of Technology

TITLE: "Design and Microprocessor-Implementation of QMF Used for SBC"

SOURCE: Shenyang DONGBEI GONGXUEYUAN XUEBAO [JOURNAL OF NORTHEAST INSTITUTE OF TECHNOLOGY] in Chinese No 3, Sep 85 pp 107-112

ABSTRACT: Using the prevailing and low-priced microprocessors, a quadrature mirror filter (QMF) system is designed and implemented for subband coder (SBC). Methods are proposed to improve the low precision and processing speed of the microprocessor, such as the distributed algorithm, additional hardware logic and multimicroprocessor structure. A sampling frequency up to 9000 Hz is attained by the use of a 32 tap FIR filter and a Z80A CPU if the resolution of intermediate stored value is 16-bit and that of input signal 12-bit. It is sufficient to meet the requirement of real-time speech signal processing. (Paper received 24 October 1984)

### REFERENCES

〔1〕 Crochiere R. E., Webber S. A., and Flanagan J. L., *Bell Syst. Tech. J.*, 55 (1976) №8, pp. 1069~1085.
〔2〕 Estaban. D. and Caland C., Proc. 1977 IEEE Int. Conf. *ASSP, Harford CT. May* 1977 pp 191~195.
〔3〕 Little, W.D., *IEEE Trans. Computer*, (C23) (1974), №5, pp. 466~469.
〔4〕 Johnson J.D., *Proc. IEEE Int. Conf. ASSP, April* 1980, pp291~294
〔5〕 Tan B.S. and Hawinkins G.J., *IEEE Proc.E*, 128 (1981), №3, pp 85~94.
〔6〕 周崇经，现代通信选论，东北工学院印刷厂， 1983 年。
〔7〕 周明德，微型计算机软件、硬件及应用，清华大学出版社，1982 年。

/9365
CSO: 4009/1015

Computers

AUTHORS: ZHOU Chongjing [0719 1504 4842]
ZHANG Zhenchuan [1728 2182 1557]

ORG: Northeast Institute of Technology

TITLE: "Design and Microprocessor-Implementation of ADPCM Encoder for SBC"

SOURCE: Shenyang DONGBEI GONGXUEYUAN XUEBAO [JOURNAL OF NORTHEAST INSTITUTE FOR TECHNOLOGY] in Chinese No 3, Sep 85 pp 113-119

ABSTRACT: Designs and implements an adaptive differential pulse-code-modulation (ADPCM) system for encoding and decoding in the sub-band (SBC) system of speech based on a Z-80 microprocessor. At the transmitting end, the 16-bit binary digital signals are compressed as 3 or 4-bit codewords by an encoder, and then at the receiving end, a decoder is used to recover these codewords. With optimal parameters selected, the system offers a dynamic range of 40 db and the process signal-to-noise ratios attainable are 25 and 33 db, respectively, for the 3 and 4-bit codings. Implementing with no more than 20 IC chips and taking a Z-80 CPU which operates at 4 MHz clock frequency as the ALU, the encoder can process each sample value in a duration about from 3000 to 3200 CPU clock cycles with an acceptable input signal frequency greater than 1200 Hz. The system is thus available to the real-time coding of speech at 8 sub-bands (with sampling frequency 8000 Hz). With the addition of multiplier hardware, the processing speed of encoder can be increased in so much that the acceptable input signal sampling frequency is greater than 4000 Hz and the system can thus be used for the real-time coding of speech at two sub-bands. Discusses in detail the algorithm design, step-size parameters and IC implementation and analyzes the microcomputer simulation. (Paper received 22 October 1984)

REFERENCES

〔1〕 Crochiere, R.E.; Webber, S.A.; Flanagan, J.L.;B.S.T.J, 55(1976), *p* 1069.
〔2〕 Flanagan,J.L.; Schroeder, M.M.; Atal, B.S. et al,*IEEE Trans. Commu.* 27(1979), №4, *p* 710
〔3〕 周崇经，滤波理论与语音编码，辽宁科技出版社，正在出版中。
〔4〕 Cummiskey, P.; Jayant, N.S.; Flanagan, J.L.; *B.S.T.J*, 52(1973), *p* 1105.
〔5〕 Boddie, J.R., *B.S.T.J*, 60(1981), *p* 1547.
〔6〕 Goodman, D.J.; Wilkinson, R.M.; *IEEE Trans. Commu.*, 23(1975), *p* 1362

/9365
CSO: 4009/1015

AUTHOR: LIU Jishun [0491 4949 5293]
ZHANG Qishan [1728 1477 1472]

ORG: Fushun Petroleum Institute

TITLE: "The Application of a Microprocessor in the Steam Flow Measuring System"

SOURCE: Shanghai ZIDONGHUA YIBIAO [PROCESS AUTOMATION INSTRUMENTATION] in Chinese Vol 6, No 9, 20 Sep 85 pp 28-32, 46

TEXT OF ENGLISH ABSTRACT: In the process of steam flow metering, more and more attention has been devoted to the compensation of temperature and pressure. A metering system consisting of TP801 single-board processor has been described and its functions and working principle are discussed. The strategy of the recommended system has been field tested and proven to be practical and feasible.

AUTHOR: SHEN Xiyu [3088 6932 3768]
JI Linhong [1323 2651 4767]

ORG: Automation of Instruments and Meters Research Institute of the Shanghai Bureau of Industries

TITLE: "An Operator Panel for a Microcomputer Control System"

SOURCE: Shanghai ZIDONGHUA YIBIAO [PROCESS AUTOMATION INSTRUMENTATION] in Chinese Vol 6, No 9, 20 Sep 85 pp 33-35, 27, 32, 46

TEXT OF ENGLISH ABSTRACT: An operator panel is the window for the operator to monitor and run the process as well as the process of man-machine interface between the operator and the computer. A functional key panel for process control system is presented with detailed descriptions of its functions and key-controlled service program.

12949
CSO: 4009/1013

AUTHOR: SHENG Shouhua [3932 1108 5478]

ORG: Research Institute 608 of the Ministry of Aeronautics

TITLE: "Miniature Eddy-Current Displacement Transducer Series"

SOURCE: Shanghai ZIDONGHUA YIBIAO [PROCESS AUTOMATION INSTRUMENTATION] in Chinese Vol 6, No 9, 20 Sep 85 pp 11-14, 18, 46

TEXT OF ENGLISH ABSTRACT: A miniature eddy-current transducer based on high frequency eddy-current effect is described. The diameter of the probe is only 2.2-7 mm, which makes it especially suitable for measuring the displacement and vibration of minute parts. The construction, working principle and main technical data of the transducer are discussed in full detail. Brief examples of some applications are given.

12949
CSO: 4009/1013

AUTHOR: QIAO Yunzhi [0829 0336 5347]

ORG: None

TITLE: "Radon and Dust Reduction and Environmental Protection at Uranium Open-pit Mine"

SOURCE: Beijing YOU KUANG YE [URANIUM MINING AND METALLURGY] in Chinese Vol 4, No 3, Aug 85 pp 6-12

TEXT OF ENGLISH ABSTRACT: At a certain uranium open-pit mine, the sources of dust and radon have been investigated since its establishment. In places where dust and radon are found, a series of safety measures and safeguards has been adopted to reduce dust and radon emission and ensure workers' health in uranium mining. Mine water and waste have been treated appropriately for the goal of environmental protection. It follows that the surroundings and natural environment of the uranium mine have not yet been appreciably polluted by radioactive fallout.

AUTHOR: XIAO Meiwen [5135 5019 2429]

ORG: None

TITLE: "Mineral Processing for Some Uranium Ore of Sedimentary Deposit Containing High Carbonates and Sulphides"

SOURCE: Beijing YOU KUANG YE [URANIUM MINING AND METALLURGY] in Chinese Vol 4, No 3, Aug 85 pp 13-18


TEXT OF ENGLISH ABSTRACT: Either carbonate leaching or acid leaching of the uranium ore of some sedimentary deposit containing high carbonates and sulphides could not give satisfying technical and economical performances. Thus a flotation-leaching process was proposed and described therewith in this paper.

First of all, the selective flotation of the pyrite in alkaline medium by isopropyl xanthate was conducted. The sulphide concentrate containing 39.1 percent S with the S recovery of 80.98 percent was obtained. Subsequently, the flotation of the carbonaceous matter by pine oil-kerosene was carried out. Finally, the thickened reground tailings were further treated by flotation with oxidized paraffin soap as the collecting reagent for carbonates. The floated carbonates containing 0.013~0.015 U could be rejected. The uranium containing sulphide concentrate and the mixed concentrates were separately treated by acid leaching with the consumption of 66 kg sulfuric acid per ton of the ore subject to mineral processing, and the overall uranium extraction of 90.73 percent could be attained.

AUTHOR: XIE Chaoyan [6043 2600 3508]

ORG: The Beijing Research Institute of Uranium Ore Processing

TITLE: "Studies on Dissolution Kinetics of Pitchblende in Dilute Sulphuric Acid Medium"

SOURCE: Beijing YOU KUANG YE [URANIUM MINING AND METALLURGY] in Chinese Vol 4, No 3, Aug 85 pp 19-25

TEXT OF ENGLISH ABSTRACT: Based on the research work of dissolution rate of $UO_2$ in various systems of $MnO_2$-$UO_2$-$H_2SO_4$-$H_2O$, $MnO_2$-Fe(III)-$UO_2$-$H_2SO_4$-$H_2O$ and $UO_2$-Fe(III)-$H_2SO_4$-$H_2O$ with $MnO_2$ as the oxidant, the relationship is explored between the oxidation-dissolution rate of $UO_2$ and the dissolution rate of ferric active complex formed on the $MnO_2$ surface, and the electron pair quantity of Fe(III)/Fe(II) in the solution as well.

It is believed that dissolution rate of $UO_2$ is dominated by that of ferric active complex on the $MnO_2$ surface. In the fixed conditions of leaching temperature and acidity with high total ferroferric concentration, the dissolution rate of primary uranium mineral is mainly dependent on the Fe(III) concentration in leaching solution and bears no important relation redox potential. If the total ferroferric concentration in leaching solution is over 5g/1 (Fe(III)/Fe(II)=1), the redox potential as low as -400 mV or even somewhat lower is still adequate to be the oxidative requirement for leaching of uranium ore. However, if the total ferroferric concentration in leaching solution is relatively low, the dissolution rate of primary uranium mineral is mainly dependent upon the ratio of Fe(III)/Fe(II), i.e., the redox potential of the leaching solution. For example, when the total ferroferric concentration is 1g/1, the primary uranium mineral can be well dissolved only if the Fe (III)/Fe(II) in the leaching solution is maintained at $\geqslant 10$, i.e., the redox potential is all along maintained at $< -400$ mV.

AUTHOR: WANG Zhengyuan [3769 2973 0337]
TAO Dening [7118 1795 1337]
et al.

ORG: The Beijing Research Institute of Uranium Ore Processing

TITLE: "The Technological Parameters of Counter-current Ion Exchange in Multi-stage Agitating Tanks and Their Effects on U Adsorption"

SOURCE: Beijing YOU KUANG YE [URANIUM MINING AND METALLURGY] in Chinese Vol 4, No 3, Aug 85 pp 26-32

TEXT OF ENGLISH ABSTRACT: In this paper the effects of the main influential technological parameters on uranium adsorption process in the multi-stage agitating tanks are described. These parameters are resin-saturation, resin-residence time, residence time of processed solution and uranium concentration of the feed solution. The relationship among these parameters is presented in the expression of material balance equation.

1. Effects of uranium concentrations of the feed solutions. The test data indicated that the variant uranium concentrations of the feed solutions, i.e., at the range of 0.12~0.50g/1U, did not make a numerical difference to the number of adsorption stages required, however, the specific equipment capacity $\Upsilon$ and the specific adsorption rate $\omega$ increased with the increase of the uranium concentration of feed solutions in question.

2. Effects of residence time of processed solution. At the range of residence time from 5 to 30 minutes, the increase of residence time had almost no effect on $\omega$ and the number of adsorption stages, but the $\Upsilon$ increased with decrease of the residence time of the processed solution.

3. Effects of resin-residence time. As the resin-residence time was set at 40, 70, 100 and 200 minutes, the longer the resin-residence time, the less the adsorption stages needed and the $\omega$ , however, the higher the $\Upsilon$.

4. Effects of resin-saturation. The tests showed that the higher the resin saturation, the more the adsorption stages required and the lower the $\Upsilon$ and the $\omega$ .

AUTHOR: WEI Shiliang [7614 1102 5328]

ORG: None

TITLE: "Design Principle for Mixed-phase Ports of Box-type Mixer-settlers"

SOURCE: Beijing YOU KUANG YE [URANIUM MINING AND METALLURGY] in Chinese Vol 4, No 3, Aug 85 pp 43-51

TEXT OF ENGLISH ABSTRACT: There has been no design principle so far available or found in the literature for engineering design. Thus, a practical and useful design principle for the mixed-phase ports of box-type mixer-settlers is urgently needed for extraction processes. In this paper, hydraulic behaviors taking place in some mixed-phase ports on condition that hydrostatic balance had been established between the mixer and the settler were analyzed, and also the rule of distribution of hydrostatic pressure difference along the vertical direction in the mixed-phase ports was revealed. The causes of recycle in mixed-phase ports were explained, and the equations for design of calculating size were derived for various cases. It was quantitatively shown that the mixed-phase ports should be designed for a long horizontal opening, when pressure drop might be negligible and there was not any recycle.

12649
CSO: 4009/15

END